Russian Original Vol. 30, No. 5, May, 1971

Translation published November, 1971

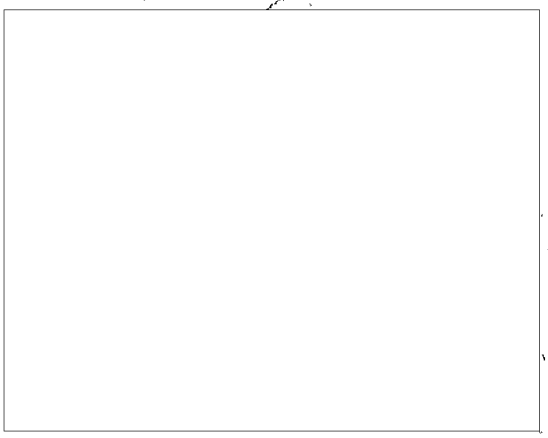

ILLEGIB

SOVIET ATOMIC ENERGY

АТОМНАЯ ЭНЕРГИЯ
(ATOMNAYA ÉNERGIYA)

TRANSLATED FROM RUSSIAN

CONSULTANTS BUREAU, NEW YORK

SOVIET ATOMIC ENERGY

Soviet Atomic Energy is a cover-to-cover translation of *Atomnaya Énergiya*, a publication of the Academy of Sciences of the USSR.

An arrangement with Mezhdunarodnaya Kniga, the Soviet book export agency, makes available both advance copies of the Russian journal and original glossy photographs and artwork. This serves to decrease the necessary time lag between publication of the original and publication of the translation and helps to improve the quality of the latter. The translation began with the first issue of the Russian journal.

Consultants Bureau journals appear about six months after the publication of the original Russian issue. For bibliographic accuracy, the English issue published by Consultants Bureau carries the same number and date as the original Russian from which it was translated. For example, a Russian issue published in December will appear in a Consultants Bureau English translation about the following June, but the translation issue will carry the December date. When ordering any volume or particular issue of a Consultants Bureau journal, please specify the date and, where applicable, the volume and issue numbers of the original Russian. The material you will receive will be a translation of that Russian volume or issue.

Subscription
$67.50 per volume (6 Issues)
2 volumes per year
(Add $5 for orders outside the United States and Canada.)

Single Issue: $30
Single Article: $15

CONSULTANTS BUREAU, NEW YORK AND LONDON

227 West 17th Street
New York, New York 10011

Davis House
8 Scrubs Lane
Harlesden, NW10 6SE
England

Second-class postage paid at Jamaica, New York 11431.

SOVIET ATOMIC ENERGY

A translation of *Atomnaya Énergiya*
Translation published November, 1971

Volume 30, Number 5 May, 1971

CONTENTS

CONTENTS

(continued)

The Russian press date (podpisano k pechati) of this issue was 4/13/1971. Publication therefore did not occur prior to this date, but must be assumed to have taken place reasonably soon thereafter.

INCREASING THE CAMPAIGN OF THE FIRST UNIT OF THE NOVO VORONEZH ATOMIC POWER STATION BY REDUCING THE POWER BEFORE RECHARGING THE FUEL

F. Ya. Ovchinnikov, L. I. Golubev, and S. F. Gaivoronskii

UDC 621.311.2:621.039

It is well known that reactors of the water-cooled, water-moderated type have a negative power effect in relation to their reactivity (the Doppler effect). On reducing the power the degree of xenon poisoning is also reduced. When the reserve of reactivity falls to zero at the end of a campaign, it may thus well be possible to increase the depth of burn-up of the fuel and reduce the net cost of 1 kW/h of production by gradually reducing the power of the reactor and thus releasing a certain amount of additional reactivity.

Under these conditions (spontaneous reduction in power), the critical state of the reactor is preserved by:

1) The increase in the breeding factor, following the reduction in power, arising from the Doppler effect ($d\rho_N$), the reduction in the temperature of the heat carrier ($d\rho_T$) and the reduction in xenon poisoning ($d\rho_{Xe}$).

2) The reduction in the breeding factor arising from the burn-up of the fuel and the accumulation of slags ($d\rho_{bu}$).

Thus the overall balance of reactivity may be written in the following manner:

$$d\rho_{bu} = d\rho_N - d\rho_T - d\rho_{Xe}. \quad (1)$$

The reactivity effects associated with the changes in power, heat-carrier mean temperature, and operating time of the reactor (amount of power developed) may in turn be written as follows:

$$d\rho_N = -\alpha(N)\,dN; \quad (2)$$

$$d\rho_T = -\beta(T)\,dT; \quad (3)$$

$$d\rho_{Xe} = -\varepsilon(N)\,dN; \quad (4)$$

$$d\rho_{bu} = -K(t)\,dW = -K(t)\,N(t)\,dt, \quad (5)$$

where the quantities $\alpha, \beta, \varepsilon$, and K are usually known from calculations and experiments made when starting the reactor.

TABLE 1. Composition of the Fourth Fuel Charge in the First Unit of the Novo Voronezh Atomic Power Station in Relation to the Build-Up of Slags in the Fuel Cassettes

Initial enrichment with U^{235}, %	Number of fuel cassettes with a build-up of slag γ_{sl}, kg/ton U			
	$\gamma_{sl} = 0,0$	$2,0 < \gamma_{sl} \leqslant 5$	$5,0 < \gamma_{sl} \leqslant 3,0$	$3,0 < \gamma_{sl} \leqslant 13$
2,0	84	54	93	61
1,5	—	9	24	—
0,714	—	3	6	9

TABLE 2. Composition of the Fifth Fuel Recharging of the First Unit in the Novo Voronezh Atomic Power Station in Relation to the Build-Up of Slags in the Fuel Cassettes

Initial enrichment with U^{235}, %	Number of fuel cassettes with a build-up of slag γ_{sl}, kg/ton U				
	$\gamma_{sl} = 0,0$	$1,7 < \gamma_{sl} \leqslant 5,0$	$5,0 < \gamma_{sl} \leqslant 8,0$	$8,0 < \gamma_{sl} \leqslant 13$	$\gamma_{sl} > 13$
2,0	130	33	48	114	3
1,5	3	—	—	3	—
0,714	—	—	—	3	—
3,0	6	—	—	—	—

Translated from Atomnaya Énergiya, No. 5, pp. 419-422, May, 1971. Original article submitted June 12, 1970; revision submitted August 24, 1970.

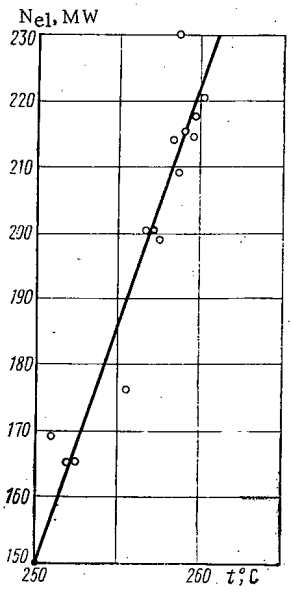

Fig. 1

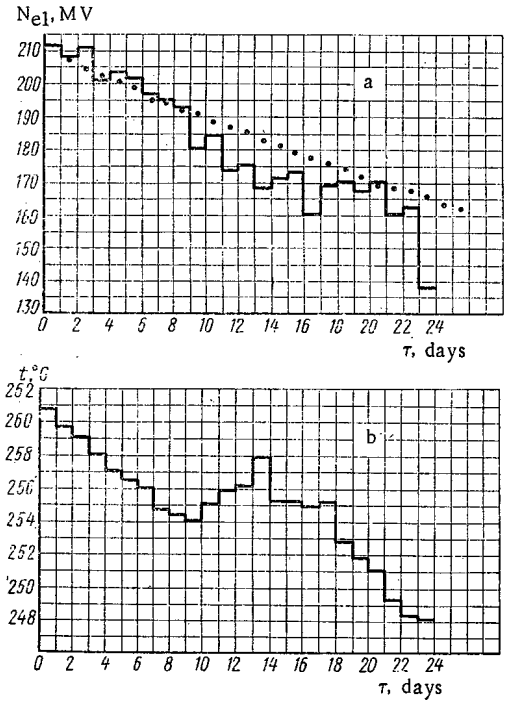

Fig. 2

Fig. 1. Dependence of the electrical power of the first unit of the Novo Voronezh Atomic Power Station on the mean temperature of the heat carrier in the first circuit, the experimental points (○) being analyzed by the method of least squares.

Fig. 2. Change in the mean daily electrical power N_{el} (a) and mean daily temperature of the water in the first circuit t° (b) in the period of operation of the first unit in Novo Voronezh Atomic Power Station during the fall in power before the recharging of the fuel in the fourth campaign (● calculated change in the electrical power for τ = 96 days).

After experimentally determining the mutual relationship between the temperature of the water in the first circuit and the electrical power of the atomic power station with the throttle valves of the turbines fully open (Fig. 1)

$$dT = \gamma(N)\, dN, \tag{6}$$

we may solve Eq. (1) with due allowance for Eqs. (2)-(6), i.e., we may find the dependence of the electrical power of the atomic power station on the period of working after exhausting the reserve of reactivity in burn-up.

For the reactor of the first unit of the Novo Voronezh Atomic Power Station the reactivity coefficients (converted to electrical power, assuming constant efficiency), we have the following values: $\alpha = 9.05 \cdot 10^{-5}$ MW^{-1}; $\beta = 1.5 \cdot 10^{-4}°C^{-1}$ in the temperature range 220-260°C; $\varepsilon = 2.5 \cdot 10^{-5}$ MW^{-1} for powers of 60-100% of the nominal power N_0 = 210 MW (electrical); $K = 5.95 \cdot 10^{-8}$ MW/h, for a reactor operating time of more than 150 effective days. The quantity γ was determined experimentally during the fourth campaign of the reactor.

Experiment showed that over the power range 160-220 MW (electrical) the mutual relationship between the electrical power and the average temperature of the heat carrier was satisfactorily approximated by the equation $T = \gamma N + b$ with γ = 0.142°C/MW; b = 228.7°C.

Solving Eq. (1) with due allowance for the assumptions made and the values of the reactivity coefficients presented, we have

$$N(t) = N_0 e^{-\frac{t}{\tau}}, \tag{7}$$

where $\tau = (\alpha + \beta\gamma + \varepsilon)/K \approx 96$ days is the time for the power to fall by a factor of e; N_0 = 210 MW (electrical).

TABLE 3. Some Parameters Characterizing the Operation of the First Unit in the Novo Voronezh Atomic Power Station Using the Reactivity Power Effect in the Fourth and Fifth Campaigns

Characteristic	Fourth campaign		Fifth campaign	
	beginning of operation in the power effect	end of operation in the power effect	beginning of operation in the power effect	end of operation in the power effect
Electrical power, MW	210	163	210	142
Mean temperature of first-circuit heat carrier, °C	260.8	248.0	258.2	244.5
Steam pressure in steam generator, kg/cm^2	30.0	26.0	30.0	23.5
Output of electrical energy as a result of the reactivity power effect, MW/h	-	99,448	-	158,110
Period of operation in the power effect, effective days	-	20	-	31
Efficiency, %	28.2	26.2	26.07	25.0

Using formula (7), we may make an approximate estimate of the power of the atomic power station in order to predict the amount of electrical energy developed and aid in planning the operation of the power system.

The possibility of using the reactivity power effect in order to increase the period of the campaign was discussed earlier [1]. An experimental verification of the mode of operation involving a spontaneous reduction in power was carried out for the first time in the first unit of the Novo Voronezh Atomic Power Station at the end of the fourth campaign (April-May 1968) and repeated at the end of the fifth campaign (March-April 1969) [2].

The duration of the campaign based on the fourth fuel charge (composition indicated in Table 1) was calculated by means of a special computer program [3] and equaled 230 effective days (i.e., 230 days continuous operation of the atomic power station at the nominal power of 210 MW).

Actually, when working at full power, the reactivity fell to zero in 228 effective days, the electrical energy produced during this period being E_0 = 1,115,468 MW/h.

The zero reserve of reactivity with the station working at full power was reached on April 17, 1968; at this time all the cassettes of the control sections lay in the top position. However, for various reasons it became necessary to prolong the operation of the station to May 10. It was therefore decided to continue the operation of the atomic power station in the mode of spontaneous power fall-off. This mode may be achieved in two ways:

1) The reactor power may be reduced by lowering the control-rod absorbers into the active zone; as the fuel burns up, the control devices again assume the top position, after which the power is reduced again, and so on.

2) All the control devices may be left in the top position; as a result of the spontaneous control effect the reactor power will then fall by itself.

The second method is the more reasonable, since it gives a greater development of electrical energy for the same period of operation of the atomic power station than the first method. The second method, involving a spontaneous reduction in the power with all the control units drawn fully out, was accordingly the one selected. It should nevertheless be noted that, in the period between 10 and 18 days of operation of the atomic power station with reduced power (Fig. 2), the power was controlled by automatic regulation.

In practice, over this period the Novo Voronezh Power Station operated in the mode of spontaneous power fall-off for up to 24 days. The actual change in the electrical power of the station is shown in Fig. 2, which also indicates the change in the mean temperature of the water in the first circuit. The experimental value of τ, determined by analyzing the power fall-off curve equaled 85 days.

The actual electrical power fall-off curve and the curve representing the fall in the mean temperature of the heat carrier agreed satisfactorily with the calculated relationships for τ = 96 days, γ = 0.142°C/MW and b = 228.7°C.

The deviations of the actual values from the calculated values in the period between 10 and 18 days (Fig. 2) may be explained by the special operating conditions of the station (change in the number of circulating pumps of the first circuit in operation, dispatch graph, etc.). At the end of the fifth campaign the experiment was repeated. The composition of the fifth fuel charging is indicated in Table 2.

During the operation of the Novo Voronezh Atomic Power Station with reduced power in the fifth campaign, the experimental value of τ was 107 days. The other parameters characterizing the operation of the atomic power station in this period are presented in Table 3.

During the period of operation of the first unit of the Novo Voronezh Atomic Power Station involving the spontaneous reduction of power, no unstable processes were observed in the reactor. The increased duration of the campaign of the first unit in the Novo Voronezh Atomic Power Station resulting from the release of additional reactivity by reducing the power of the reactor enabled the fuel constituent of the net cost of 1 kW/h of electrical energy to be considerably reduced.

In the case in which a fraction $\eta \approx 1/3$ of the cassettes were recharged, the fall in the fuel component of cost ΔC_T may be estimated [4] from the equation

$$\frac{\Delta C_T}{C_T} = \frac{\Delta E \frac{2\eta}{1+\eta}}{E_0 + \Delta E \frac{2\eta}{1+\eta}}, \tag{8}$$

where E_0 and ΔE are the outputs of electrical energy before reducing the power and during the power reduction, respectively. For the fourth campaign the reduction in the fuel component was ~4% and for the fifth 5.5%.

The experience thus achieved in working with reduced power before recharging the fuel should help in planning the extended operation of the station in subsequent campaigns.

LITERATURE CITED

1. L. Ya. Kramerov et al., At. Énerg., 17, 427 (1964).
2. F. Ya. Ovchinnikov et al., ibid., 27, 270 (1969).
3. A. N. Novikov et al., Fuel Burn-Up Predictions in Thermal Reactors, Vienna, IAEA (1968).
4. Yu. I. Mityaev, At. Énerg., 30, 243 (1971).

MONITORING THE FIELDS OF ENERGY EVOLUTION BY REFERENCE TO THE RELATIVE EFFICIENCY OF THE CONTROL RODS

I. Ya. Emel'yanov, B. G. Dubovskii,
Yu. V. Evdokimov, L. V. Konstantinov,
I. K. Pavlov, V. V. Postnikov,
E. I. Snitko, and G. A. Shasharin

UDC 621.039.51

The charging of the active zone in the reactors of the Beloyarsk Atomic Power Station [1] comprises a number of evaporating channels with 1.5, 2, and 3% degrees of enrichment (relative to U^{235}), used for the preheating and partial evaporation of the water (gravimetric vapor content at the outlet ~25%), together with steam-heating channels in which the steam is superheated to a working temperature of around 520°C.

Compensation for the reactivity of the cold reactors at the onset of the campaign is achieved by means of 64 (first unit) and 78 (second unit) manual control rods, together with several rods forming a system of two-position rod compensators.

Monitoring the power of the evaporating channels by ordinary thermotechnical methods requires the measurement of the steam content of each individual channel, and this necessitates the use of complicated and expensive sensors. A simplified method has therefore been developed in Beloyarsk in order to monitor the fields of energy evolution; this is based on measurements of the relative efficiency of the manual control rods.

It is well known [2] that for "large" uranium–graphite reactors the following relationship holds

$$N(\mathbf{r}) = \text{const}\sqrt{\Delta\rho}, \tag{1}$$

where $N(\mathbf{r})$ is the unperturbed neutron density at the point $\mathbf{r}$, and $\Delta\rho$ is the reactivity due to the introduction of an absorber at the point $\mathbf{r}$.

Equation (1) is infringed wherever substantial inhomogeneities occur, and at the boundary between the active zone and the reflector. Calculations showed that the presence of three zones with different proportions of graphite, uranium, and construction materials in the reactor of the first unit of the Beloyarsk Atomic Power Station only led to slight deviations from Eq. (1), not exceeding 2% at distances of more than 0.5 m from the reflector.

In determining the radial fields of energy evolution $W(\mathbf{r})$ by the method here described, we use the concept of the "macrofield" of energy evolution of the fuel channels, together with the "microstructure" of the field, in the same way [3] as proposed earlier for neutron-density distributions [4]. The "macrofield" $W_M(\mathbf{r})$ is the arbitrary name given to the radial distribution of the power of fuel channels of specified type, integrated over the whole reactor, these channels having exactly the same degree of burn-up and lying at a distance greater than the arbitrary "influence" distance $r_{inf} = 0.5$ m from the inserted control rods, empty sites, or other local inhomogeneities (nonuniformities).

By the "microstructure" of the field of energy evolution $\varphi(\mathbf{r})$ we understand the distribution describing the relative changes in the power of the fuel channels in the neighborhood of local inhomogeneities, so that

$$W(\mathbf{r}) = W_M\varphi(\mathbf{r}). \tag{2a}$$

Translated from Atomnaya Énergiya, No. 5, pp. 422-425, May, 1971. Original article submitted September 12, 1970.

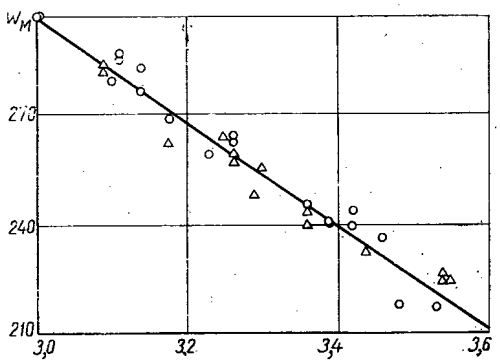

Fig. 1. Relative variation in the macrofield W_M at the periphery of the active zone, measured by reference to the residual γ activity of the fuel channels in the stopped reactor: ○) evaporation channels with an enrichment of 2%; △) evaporation channels with an enrichment of 3%.

It is here considered that

$$\varphi(\mathbf{r}) = \xi_T(\mathbf{r}) \prod_i \xi_i(|\mathbf{r} - \mathbf{b}_i|), \tag{2b}$$

where $\xi_T(\mathbf{r})$ is a coefficient depending solely on the construction, the original enrichment, and the burn-up of the uranium in the fuel channel situated at the point $\mathbf{r}$; $\xi_i(|\mathbf{r} - \mathbf{b}_i|)$ is a coefficient allowing for the local inhomogeneity situated at the point $\mathbf{b}_i$. For $|\mathbf{r} - \mathbf{b}_i| \geq r_{inf}$ we have $\xi_i = 1$.

By using an approach of this kind, the problem of the discrete monitoring of the fuel-channel power distributions may be reduced to that of determining the values of the macrofield at individual points, interpolating these values, and then introducing corrections to allow for the microstructure of the field associated with every individual fuel channel.

It was found experimentally that the assumption used in formulating this approach led to a mean square error of no more than 2% in determining the power of the fuel channels.

During the initiation and service of the reactors in the Beloyarsk Atomic Power Station, we studied the relation between the macrofield $W_M(\mathbf{r})$ obtained by means of Eqs. (2a) and (2b) and the relative distribution of the quantities $\sqrt{\Delta\rho(\mathbf{r})}$. The mean square deviation between these distributions never exceeded 2% if, on moving a manual control rod, the change in its efficiency was less than $(15\text{-}20)\cdot 10^{-3}\,\beta_{eff}$, while the distance from the site of the control rod to the boundary of the zone with the reflector was greater than 50 cm. The presence of an empty site or a fuel channel of a different type or degree of enrichment close to the manual control rod then led to no deviations from Eq. (1) outside the specified limits. For carrying out our calculations by the proposed method, we therefore used the values of $\sqrt{\Delta\rho(\mathbf{r})}$ in order to characterize the macrofield at the points accommodating the manual control rods.

During the measurements we tended in general to use manual control rods lying in the extreme positions, these being moved in turn through the same distances and subsequently returned to their original position.

Experience in the use of the two reactors showed that not more than 20-30% of the manual control rods usually occurred in the intermediate position. For the completely inserted (or extracted) manual control rods, we measured the quantities $\Delta\rho_i$ (ins) or $\Delta\rho_i$ (extr), i.e., the relative efficiencies of identical sections of the rods on moving these from the original positions by an amount corresponding to 10-15% of their total efficiency; this was done by using one of the two automatic power controls to produce overcompensation. The values of the relative macrofield at the sites of the completely-extracted manual control rods were calculated from the formula

$$W_M^{rel} = \sqrt{\Delta\rho_{i\,(extr)}}, \tag{3}$$

and for the completely-inserted control rods from

$$W_M^{rel} = m\sqrt{\Delta\rho_{i\,(ins)}}, \tag{4}$$

where m is a coefficient normalizing the distribution of $W_M^{rel}(\mathbf{r})$ for the inserted rods to the analogous distribution for the completely-extracted rods.

As a method of interpolating the values of W_M^{rel} measured at the sites of the control rods, we applied correlation analysis to the distribution of the global field of energy evolution, considered as a nonstationary, random field [5]. We found that linear interpolation was best. For carrying out the interpolation, the whole of the active zone, except for the region between the peripheral manual control rods and the lateral reflector, was arbitrarily divided into triangles with vertices at the sites of the manual control rods. Within the limits of each triangle the values of W_M^{rel} for the fuel channels were calculated by plane interpolation from the values of W_M^{rel} at the vertices of the triangles. The values of W_M^{rel} for the periphery of the active zone were calculated from the values of W_M^{rel} on the lines joining the peripheral manual control rods, and from

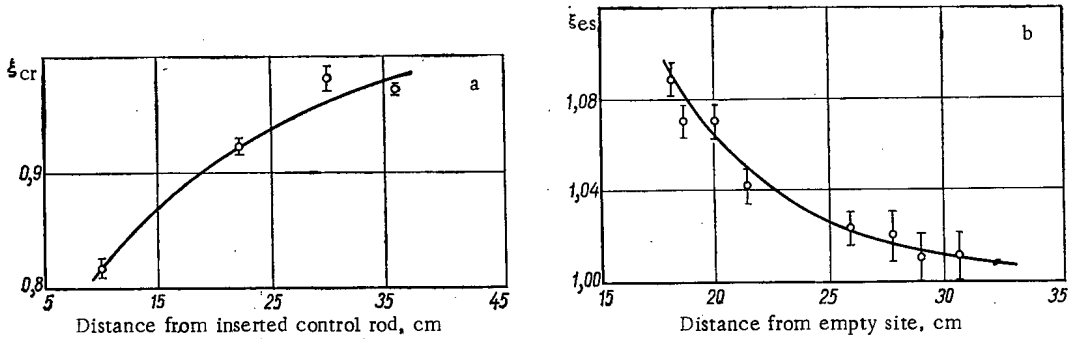

Fig. 2. Relative distribution of energy evolution in fuel channels of similar types close to a completely-extracted manual control rod ξ_{cr} (a) and close to an empty site ξ_{es} (b). Mean square error of the experiments indicated.

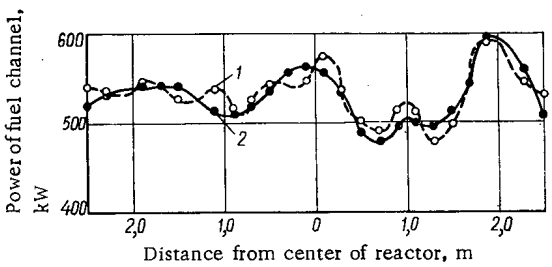

Fig. 3. Distribution of energy evolution along one of the diametral directions of the reactor, as obtained by measuring the residual γ activity of the fuel channel (1), and also as obtained by the method here described (2).

the gradient of the macrofield measured by other methods on the reactor periphery. Repeated measurements, based on thermotechnical determinations of the power of the evaporating channels in the nonboiling mode of operation of the reactor, show that the radial variation in the macrofield at the periphery of the active zone is accurately described by a linear law and has hardly any angular dependence at all (within the limits of 2-3%), despite the complicated shape of the boundary between the active zone and the reflector (Fig. 1).

These results were confirmed by measuring the activation of a steel wire in a horizontal experimental channel working at nominal power, and also by measuring the neutron-density distribution by means of small fission chambers in the initial stages of reactor operation [3].

Experience in using the Beloyarsk Atomic Power Station showed that the relative radial dependence of the macrofield at the periphery of the active zone depended very little (within 1-2%) on the rechargings of the fuel channels of various types, and remained constant over the whole period of operation (i.e., since 1964).

The values of the coefficients ξ_i and ξ_T were obtained on the basis of measurements carried out both on a physical test-bed and also on the reactor at low and nominal power levels [3]. These coefficients were determined by comparing the energy-evolution distributions before and after the introduction of the perturbation. The values of ξ_i and ξ_T were also obtained by the method of least squares, with due alllowance for the minimum error in determining the power of the fuel channels by means of Eq. (2). The coefficients obtained by the two methods agreed to within the limits of experimental error. The distributions of $\xi_i(|\mathbf{r}-\mathbf{b}|)$ for the principal local nonuniformities are presented in Fig. 2a, b. The coefficients ξ_T determined by the form of the fuel channels depended very little on nonuniformities in the active zone, the values for the fresh channels being 0.91, 1.09, 1.00, and 1.27 respectively for the fuel channels of the first unit (with an enrichment of 1.5 and 2%) and for the fuel channels of the second unit (with an enrichment of 2 and 3%). During the operation of the reactor, the variation in ξ_T for each fuel channel was taken into account by calculating the dependence of ξ_T on the energy production of the channel in question.

It should be noted that the values of the coefficients ξ_i were obtained as quantities averaged over various possible compositions of the active zone at the point of introduction of the perturbation. The difference of the averaged values from the real ones was only slight (1-2%).

The method here described is used periodically in order to determine the distribution of the absolute powers of the fuel channels $W(\mathbf{r})$ by normalizing the relative distribution obtained to the total power of the reactor. The calculation of $W(\mathbf{r})$ from the measured values of $\Delta\rho$ is carried out by means of a special computer program. Operative monitoring of the relative changes in the fields of energy evolution in the two units of the Beloyarsk Atomic Power Station is effected by recording the relative changes in the incremental heat content of the steam in individual steam-superheating channels.

The error in the periodic monitoring of the power of the fuel channels by the method here described arises from a number of factors, the most important being as follows.

1. The infringement of Eq. (1) due to: a) a difference in the neutron-density distribution of the active zone from the rated distribution; b) the use of relatively strong absorbents in the measurements; c) a difference in the relative neutron-density distributions with respect to the height of the reactor at different distances from the axis.

2. Errors in the assumptions made when representing the power distribution over the reactor in the form of Eqs. (2), and errors in the interpolation of the macrofield.

3. The error due to the method chosen for calculating the macrofield at the periphery of the active zone, using the experimentally-obtained radial dependence of the relative macrofield near the boundary between the zone and the reflector.

4. Errors in determining the microstructural coefficients ξ_i and ξ_T.

5. Errors in measuring the quantities $\Delta\rho$ by overcompensation with the help of the automatic control rods.

6. A possible difference in the original absorbing properties of the manual control rods, or errors committed when allowing for their degree of burn-up.

7. Errors in measuring the total thermal power of the reactor.

The complex interaction of the errors due to these various factors impedes any attempted estimation of the resultant error of the method based on the individual components. In our experimental study of the monitoring principles under consideration, we therefore made a special point of determining its metrological characteristics by comparing with distributions obtained in other ways. The mean square relative error of the method σ was determined from the equations:

$$\begin{aligned}
&\frac{1}{n-1}\sum_{i=1}^{n}\left[\frac{W_i}{W_{\mathrm{I}i}}\left(\frac{\overline{W_{\mathrm{I}i}}}{W_i}\right)-1\right]^2=\sigma^2+\sigma_{\mathrm{I}}^2;\\
&\frac{1}{n-1}\sum_{i=1}^{n}\left[\frac{W_i}{W_{\mathrm{II}i}}\left(\frac{\overline{W_{\mathrm{II}i}}}{W_i}\right)-1\right]^2=\sigma^2+\sigma_{\mathrm{II}}^2;\\
&\frac{1}{n-1}\sum_{i=1}^{n}\left[\frac{W_{\mathrm{I}i}}{W_{\mathrm{II}i}}\left(\frac{\overline{W_{\mathrm{II}i}}}{W_{\mathrm{I}i}}\right)-1\right]^2=\sigma_{\mathrm{I}}^2+\sigma_{\mathrm{II}}^2,
\end{aligned}\qquad (5)$$

where n is the number of fuel channels in which the power was measured by the method described (W_i) and by two other independent control methods (W_{Ii} and W_{IIi}); σ_I and σ_{II} are the mean square relative error of the other (control) methods.

Experiments showed that the error in the method described was distributed in accordance with a normal law and that σ equaled ~4%. By way of control methods, we used measurements of the relative activity of the extracted fuel channels, the activation of steel wires placed in horizontal experimental channels, thermotechnical measurements in the evaporating channels for nonboiling modes of operation of the channels, and so on.

For comparison, Fig. 3 illustrates the diametral distribution of the energy evolution obtained by the method described and also by measuring the γ activity of the fuel channels in the stopped reactor of the second unit.

The main advantage of our simplified method lies in the fact that it requires no special sensors to be installed for monitoring the distribution of energy evolution in the active zone; standard control rods may be used.

The method enables us to carry out measurements over the whole range of powers envisaged, starting from the minimum level to be monitored.

The method here described may find applications in large graphite reactors equipped in such a manner as to facilitate the operative monitoring of changes taking place in fuel-channel powers (for example, by measuring the temperature of the single-phase heat carrier at the outlet from individual channels) for making periodic measurements of the fields of energy evolution.

In conclusion, the authors wish to thank A. Ya. Evseev, I. M. Kisil', and M. E. Minashin for help in carrying out this work and for useful critical comments.

LITERATURE CITED

1. N. A. Dollezhal' et al., At. Énerg., 5, 223 (1958).
2. A. D. Galanin, Theory of Nuclear Reactors Using Thermal Neutrons [in Russian], Atomizdat, Moscow (1957), p. 151.
3. B. G. Dubovskii et al., Report No. 29 to the International Conference of Physical Problems Involved in Designing Thermal Neutron Reactors [in Russian], London (1967).
4. A. M. Weinberg, in: Theory of Nuclear Reactors [Russian translation], T. Birkhoff and E. Wigner (editors), Gosatomizdat, Moscow (1963), p. 22.
5. E. S. Wentzel, Theory of Probabilities [Russian translation], Nauka, Moscow (1964).

THE METHOD OF SUBGROUPS FOR CONSIDERING THE RESONANCE STRUCTURE OF CROSS SECTIONS IN NEUTRON CALCULATIONS

M. N. Nikolaev, A. A. Ignatov,
N. V. Isaev, and V. F. Khokhlov

UDC 621.039.51.13

In the first part [1] of the present paper we presented the basic propositions of the method of subgroups; an algorithm for the analytic method of subgroup calculations of reactors, cells of heterogeneous lattices, and for the solution of problems involving the transmission of neutrons in the diffusion approximation was given; the equations were written for calculating the shielding in the (x, μ)-geometry by the method of subgroups.

Below we describe the devices used to formulate the subgroup constants, and examples are used to demonstrate the possibilities of the method.

Obtaining the Subgroup Constants

The complexity of obtaining the subgroup constants consists in the optimal partitioning of the group interval into subgroups in which the total cross section and the cross sections of the various processes would vary weakly (i.e., the effects of resonance self-screening in a subgroup would be negligible).

Let us consider two methods of obtaining the subgroup constants. In the first of them we shall start from the conservation of the total and partial transmission functions in the transition to the subgroup representation of the resonance structure of the cross sections:

$$T(t) = \frac{1}{\Delta u}\int_{\Delta u} e^{-\sigma_t(u)\rho t}\,du; \tag{1a}$$

$$T_x(t) = \frac{\int_{\Delta u}\sigma_x(u)\,e^{-\sigma_t(u)\rho t}\,du}{\int_{\Delta u}\sigma_x(u)\,du}, \tag{1b}$$

where t is the thickness of the sample; σ_t, σ_x are the total and partial microscopic cross sections; ρ is the density of the nuclei of the samples; Δu is the group lethargy interval.

The subgroup representation of the transmission function has the form

$$T(t) \approx \sum_{j=1}^{n} a_j e^{-\sigma_{t_j}\rho t}; \tag{2a}$$

$$T_x(t) \approx \sum_{j=1}^{n} a_j \frac{\sigma_{x_j}}{\langle\sigma_x\rangle} e^{-\sigma_{t_j}\rho t}; \tag{2b}$$

$$\langle\sigma_x\rangle = \frac{1}{\Delta u}\int_{\Delta u}\sigma_x(u)\,du \approx \sum_{j=1}^{n} a_j\sigma_{x_j}, \tag{2c}$$

where a_j is the fraction of the subgroup j in the interval Δu; σ_{t_j}, σ_{x_j} are the total and partial cross sections in the subgroup j; n is the least number of subgroups describing the functions T(t) and $T_x(t)$ in the range $t \leq t_{max}$ with a stipulated accuracy.

Translated from Atomnaya Énergiya, No. 5, pp. 426-430, May, 1971. Original article submitted March 12, 1970; revision submitted August 7, 1970.

In order to obtain the subgroup constants $a_j, \sigma_{t_j}, \sigma_{x_j}$ one can use the method of least squares for which conditions (2) are fulfilled with an accuracy of up to errors of the left sides of these approximate equations. This accuracy likewise determines the minimum number n of subgroups required for the approximation. In turn, the total and partial transmission functions can be taken from experiments [2, 3] or can be calculated according to detailed energy plots of the cross sections [4].

It should be noted that the transmission functions must be measured or calculated in a fairly wide range of thicknesses in order for these functions to reflect both the cross sections at the resonances, whose major contribution takes effect at small thicknesses, and interresonance cross sections whose contribution takes effect at larger thicknesses.

At present the transmission functions are being processed on an electronic computer in order to obtain the subgroup constants, but the shortage of experimental and calculated information prevents a complete subgroup system of constants from being obtained on the basis of the method given. Therefore, for practical calculations by the method of subgroups a subgroup system of constants [5, 6] was obtained on the basis of the 26-group system of constants [7].

The self-screening coefficients given in this paper, by means of which the following quantities were determined within the limits of the group interval for various "dilution cross sections" [7]:

$$\left\langle \frac{1}{\sigma_t+\sigma_0} \right\rangle, \left\langle \frac{1}{(\sigma_t+\sigma_0)^2} \right\rangle, \left\langle \frac{\sigma_c}{\sigma_t+\sigma_0} \right\rangle, \left\langle \frac{\sigma_f}{\sigma_t+\sigma_0} \right\rangle$$

were used as the initial information on the resonance structure of the cross sections. In the subgroup representation these quantities will have the form:

$$\langle 1/(\sigma_t+\sigma_0)\rangle \approx \sum_{j=1}^{n} a_j/(\sigma_{t_j}+\sigma_0); \tag{3a}$$

$$\langle 1/(\sigma_t+\sigma_0)^2\rangle \approx \sum_{j=1}^{n} a_j/(\sigma_{t_j}+\sigma_0)^2; \tag{3b}$$

$$\langle \sigma_x/(\sigma_t+\sigma_0)\rangle \approx \sum_{j=1}^{n} a_j\sigma_{x_j}/(\sigma_{t_j}+\sigma_0); \tag{3c}$$

$$\langle \sigma_t\rangle \approx \sum_{j=1}^{n} a_j\sigma_{t_j}; \tag{3d}$$

$$\langle \sigma_x\rangle \approx \sum_{j=1}^{n} a_j\sigma_{x_j}, \quad x \equiv c, f. \tag{3e}$$

The "dilution cross section" σ_0 is understood to mean the total cross section of all the remaining elements of the medium which corresponds to one atom of the element considered.

Equations (3) are the complete set of conditions which must be satisfied by the subgroup parameters in order for the information on the structure of the cross sections contained in the tables for the dependence of the self-screening coefficients on σ_0 to be reflected.

The quantities $a_j, \sigma_{t_j}, \sigma_{x_j}$ satisfying these conditions with an accuracy of up to errors in determining the left sides of Eqs. (3) were found by the method of least squares according to a special CSPC program. The subgroup constants ($a_j, \sigma_{tj}, \sigma_{cj}, \sigma_{fj}$) found by this method for those groups and elements for which the resonance effects have essential significance are given in [5]. Just as in [7], it is assumed that there is no self-screening of the inelastic scattering; i.e., $\sigma_{in_j} = \langle \sigma_{in} \rangle$. The elastic-scattering cross section is defined uniquely by the equation

$$\sigma_{e_j} = \sigma_{t_j} - \sigma_{c_j} - \sigma_{f_j} - \sigma_{in}. \tag{4}$$

For practical calculations the subgroup system of constants obtained should be complemented by the cross sections for the exchange of neutrons between subgroups.

Let us consider the exchange cross sections connected with elastic scattering. If the energy loss as a result of elastic scattering exceeds the distance between resonances or the average width of the resonances, and under these conditions the distribution of the distances between levels is close to being random (this is almost always fulfilled in the region of forbidden resonances), then for the condition that the group contains a large number of resonances the cross section for transfer from the subgroup p belonging to the

group n to the subgroup q belonging to the same group may be represented in the form [5]

$$\sigma_{e,\ n}^{p\to q} = \sigma_{e,\ n}^{p} a_q s_n, \tag{5}$$

where $\sigma_{e,n}^{p}$ is the cross section for elastic scattering in the subgroup p of the group n; a_q is the fraction of the subgroup q; s_n is the probability that a neutron will not depart beyond the limits of the group n after scattering. If the neutron flux averaged over the resonance singularities has a Fermi form, then

$$s_n = 1 - \frac{\xi}{\Delta u_n},$$

where ξ is the average lethargy increment per elastic collision.

If the subgroup q belongs to the group m and the assumption made above is fulfilled for both groups, then the exchange cross section can be represented in the form

$$\sigma_e^{p(n)\to q(m)} = \sigma_e^{p(n)} (1 - s_n) a_{q(m)}. \tag{6}$$

Analogously, the exchange cross sections for inelastic scattering can be calculated, since for inelastic scattering the assumption made is always fulfilled*:

$$\sigma_{in,\ n}^{p(n)\to q(n)} = a_{q(n)} \sigma_{in}^{n\to n}; \tag{7a}$$

$$\sigma_{in,\ n}^{p(n)\to q(m)} = a_{q(m)} \sigma_{in}^{n\to m}. \tag{7b}$$

If this assumption is not fulfilled (i.e., the number of resonances in the group is small, for example, two-three, or they have a width comparable with the energy loss), then one should consider the distribution of the subgroups in the group according to the known energy plot of the cross sections and calculate the neutron-exchange cross sections in each specific case. In this case the CPIS program is used to calculate the exchange cross sections.

Using the method expounded above and the self-screening factors [7], collections of subgroup parameters corresponding to various temperatures of the medium were calculated.

It turned out that the approximation of the temperature dependences of the subgroup parameters

$$a_j(T) = a_j(T_0) + \Delta a_j (\sqrt{T/T_0} - 1); \tag{8a}$$

$$\sigma_{t_j}(T) = \sigma_{t_j}(T_0) + \Delta\sigma_{t_j} (\sqrt{T/T_0} - 1); \tag{8b}$$

$$\sigma_{x_j}(T) = \sigma_{x_j}(T_0) + \Delta\sigma_{x_j} (\sqrt{T/T_0} - 1), \tag{8c}$$

(T_0 = 300°K) guarantees a description of the dependence of the self-screening factors on temperature in the 300-2100°K range with the same accuracy as that with which they are determined in [7]. Therefore, the temperature corrections Δa_j, $\Delta\sigma_{t_j}$, and $\Delta\sigma_{x_j}$ are more expediently determined simultaneously with the determination of the basic subgroup parameters according to the CSPC program. The results of the calculations are presented in [5].

The macroscopic subgroup constants of the medium can be calculated in terms of the microscopic subgroup cross sections as follows.

Assume that N elements are present in the medium, each of which has n_i subgroups in the group considered; then the resonance structure of the macrocross-section of the medium can be represented in the form of the superposition of K subgroups, where

$$K = \sum_{i=1}^{N} n_i. \tag{9}$$

The subgroups of the macrocross-section are formed via various combinations of subgroups of the elements. Each such combination will contain N subgroups (one subgroup from each element of the medium). Evidently, the total number of such combinations will be equal to K. If in the group considered all elements of the medium which have a resonance structure of the cross section contain a large number of resonances, then by virtue of the independence of the energy plot of the cross sections of various elements the fraction of macrocross-section subgroups will be equal to the product of the fractions of the subgroups forming the given macrocross-section subgroups; i.e.,

*The subgroup system of constants [5, 6] was calculated for the use of the approximation considered.

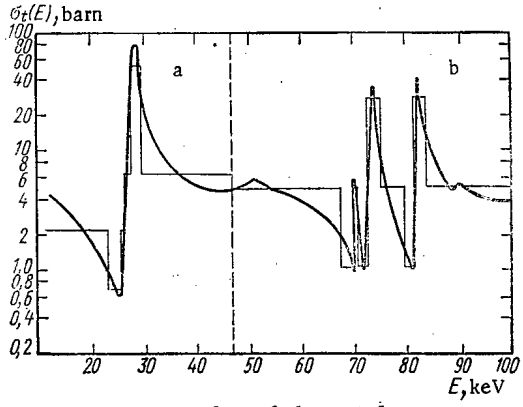

Fig. 1. Energy plot of the total cross section of iron and its subgroup representation: a) the tenth group is approximated by four subgroups (σt_I = 51.3 barn; σt_{II} = 6.68 barn; σt_{III} = 2.10 barn; σt_{IV} = 0.694 barn); b) the ninth group is approximated by nine groups which form three subgroups (σt_I = 29.0 barn; σt_{II} = 4.96 barn; σt_{III} = 1.04 barn).

$$a_r = \prod_{i=1}^{N} a_{p_i}(r), \tag{10}$$

where $p_i(r)$ is the number of the subgroup of the i-th element in the combination forming the r-th subgroup of the macrocross-section. The subgroup macrocross-sections of some process x are defined as the sum of the corresponding subgroup macrosections of the elements:

$$\Sigma_{x,r} = \sum_{i=1}^{n} \rho_i \sigma_{x,i}^{p_i(r)}. \tag{11}$$

As a rule, a medium consisting of several resonant elements has a less pronounced structure of its cross sections than does each of these elements. In order to reduce the number of subgroups and to determine their optimal number one may use the method already described for obtaining subgroup constants from transmission functions. The total and partial transmission functions of the medium may be calculated by means of the subgroup constants of the individual elements and approximated by the method of least squares using the least number of subgroups.

For the case in which several elements having one-two resonances in a group are included in the medium, it is necessary to consider the mutual placement of the subgroups in order to obtain the fractions of the macrocross-section subgroups.

The Use of the Subgroup Approach in Calculating the Group Constants

In [7] the resonant structure of the cross sections is considered by means of the self-screening factors, which are represented as functions of the "dilution cross section" and the temperature, in averaging group constants.

Such an approach is connected with the following additional simplifying assumptions: first, microscopic rather than macroscopic cross sections of the individual elements are averaged, the total cross sections of all other elements of medium being considered independent of energy (their sum forms a "dilution cross section" σ_0); second, the mutual positions of the resonances of the individual elements of the medium is not considered even in the case in which few resonances are in the group.

The subgroup approach allows these simplifications to be avoided and simultaneously allows the volume of initial information to be reduced relative to the volume used in [7]. On the assumption that the collision density is constant, the average group macrocross-sections of some process x may be expressed [7] by means of quantities of the type

$$\left\langle \frac{\Sigma_x(u)}{\Sigma_t(u)} \right\rangle, \quad \left\langle \frac{1}{\Sigma_t^n(u)} \right\rangle,$$

which can be calculated with sufficient accuracy via the subgroup constants. If the elements of the medium have a large number of resonances in the energy interval of the group, then these quantities can be calculated as follows:

$$\left\langle \frac{\Sigma_x(u)}{\Sigma_t(u)} \right\rangle = \sum_{p_1=1}^{n_1} \cdots \sum_{p_N=1}^{n_N} a_{p_1}^1 \cdots a_{p_N}^N \frac{\sigma_{x,\,p_1}^1 \rho_1 + \ldots + \sigma_{x,\,p_N}^N \rho_N}{\sigma_{t,\,p_1}^1 \rho_1 + \ldots + \sigma_{t,\,p_N}^N \rho_N}. \tag{12}$$

The quantities $\langle 1/\Sigma_t^n(u) \rangle$ are calculated analogously.

If the group contains a small (one-three) number of resonances, then it is required to know the mutual conditions of these resonances in order to calculate the group macrocross-sections (i.e., it is necessary to know the details of the energy plot of the cross sections within the limits of the groups). This information can be stipulated most economically and with a fair accuracy if for each such element the group is partitioned into several smaller groups in such a way that the average total cross section in the smaller groups

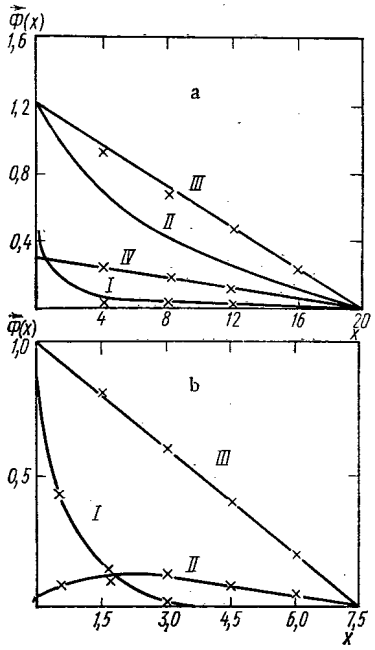

Fig. 2. The relative phase distribution of neutron fluxes as a function of the distance measured in mean free paths of the neutrons of the first subgroup (I-IV represent the numbers of the subgroups): a) for the tenth group: ——) represents the subgroup calculation; ×) represents the 30-group calculation; b) for the ninth group: ——) represents the subgroup calculation; ×) represents the nine-group calculation.

is equal to the total cross section of one of the subgroups. (In order to carry out such a procedure of "arrangement of subgroups" an AP program is written.) The ARAMAKO program, which calculates the 26-group macroconstants of media on the basis of the catalog of subgroup constants, has likewise been created.

Examples of Computation

It is well known that the consideration of the detailed structure of the cross sections in the resonance range can be carried out in principle with arbitrary accuracy within the framework of the group method, although under these conditions it is also required to introduce an extremely large number of groups. Based on this, it is valid to compare calculations carried out according to the subgroup method with multigroup calculations which consider all of the details of the resonance structure of the substance under study.

As an example, let us consider a certain group model for calculating a single resonance peak (the tenth group of iron [7]). The graph for the total cross section of this resonance and the partitioning into subgroups which allows the detailed structure of the cross sections to be considered are displayed in Fig. 1a. For a fairly reliable description of the absorption and moderating processes for this resonance it is necessary to take 30 groups or four subgroups.

In the other example the passage of neutrons through a plate having a thickness equal to 10 full mean free paths (according to the cross section of the resonance peak) was calculated for stipulated boundary conditions near the boundary of a plate source $\vec{\Phi}(0)$ and on the boundary with a vacuum $\vec{\Phi}(R) = 0$. Within the framework of the diffusion 30-group approximation the distribution of the neutron flux in the plate (Fig. 2a) was calculated. From the figure it is evident that the subgroup fluxes practically coincide with the results of the 30-group calculation (with preliminary convolution into subgroup packets).

Let us consider a more complex example in which the resonance region contains several resonances (for example, the ninth group of iron is the system of constants in [7]). Figure 1b shows the graph of the total cross section as well as the subgroup and detailed group partitioning of this resonance region. For a plate having a thickness equal to eight mean free paths (with respect to neutrons of the I subgroup) comparative calculations were carried out in the nine-group and three-subgroup representation of the problem of transmission of neutrons. The results of the calculations are displayed in Fig. 2b. The calculation with three subgroups was three times as short on the electronic computer as the calculation with nine groups.

From the examples presented the practical equivalence of the description of the resonance structure by the detailed-group and subgroup methods is evident. At the modern state of computer technology practical calculation with allowance for the detailed construction of the cross sections of substances using the method of groups is actually impossible due to their large number. At the same time consideration of the resonance structure by means of the screening factors [7] leads to substantial errors in the space–energy distribution of the neutrons. For comparison purposes the space–energy distribution of neutrons in an iron plate 12 cm thick was determined by the subgroup calculation and by means of the 26-group calculation with allowance for the self-screening factors for the resonance groups.

The energy spectrum of the neutrons on the plate–source boundary constituted a typical spectrum for a large power reactor (BN-250). Figure 3 shows the energy spectra of the neutrons emitted from the plate, as calculated by the methods indicated. The integral values of the neutron current emanating from the plate differ by ~40% in this example.

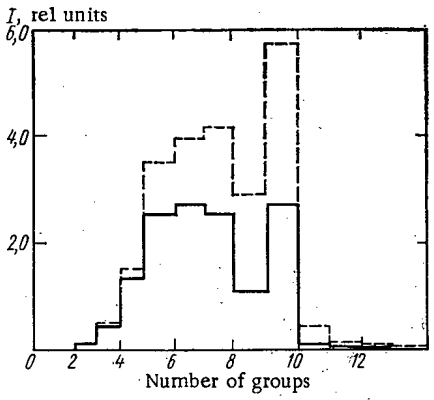

Fig. 3. Energy spectrum of neutrons emitted from an iron plate 12 cm thick: ——) represents the calculation by the method of subgroups; ---) represents the 26-group calculation.

The analytical method [8] ensures sufficient accuracy of the calculations only at distances of several tens of minimal neutron mean free paths. In this case the zero mean free path approximation is introduced at large distances from the source for subgroups having a large cross section, and the flux of a subgroup having a large cross section can easily be expressed in terms of the fluxes and constants of the group and subgroups having smaller cross sections.

LITERATURE CITED

1. M. N. Nikolaev et al., At. Énerg., 29, 11 (1970).
2. M. N. Nikolaev, "Softwear for neutron calculations by means of group constants, and the demand for nuclear data," Materials of the Comecon Symposium: The State and Prospects of Work on the Creation of Atomic Electric Power Stations with Fast-Neutron Reactors, Vol. 2, p. 5.
3. V. V. Filippov and M. N. Nikolaev, "Measurement of the structure of total neutron cross sections" [in Russian], Anglo-Soviet Seminar: Nuclear Constants for Reactor Design, Dubna (June 18-22, 1968).
4. L. P. Abagyan, M. N. Nikolaev, and L. V. Petrova, in: Information Bulletin of the Nuclear Data Center [in Russian], No. 3, Atomizdat, Moscow (1966), p. 418.
5. M. N. Nikolaev and V. F. Khokhlov, "The subgroup system of constants" [in Russian], Anglo-Soviet Seminar: Nuclear Constants for Reactor Design, Dubna (June 18-22, 1968).
6. M. N. Nikolaev and V. F. Khokhlov, in: Information Bulletin of the Nuclear Data Center [in Russian], No. 4, Atomizdat, Moscow (1967), p. 420.
7. L. P. Abagyan et al., Group Constants for the Design of Nuclear Reactors [in Russian], Atomizdat, Moscow (1964).
8. S. B. Shikhov, V. I. Davydov, and L. K. Shishkov, in: Engineering-Physics Problems of Nuclear Reactors [in Russian], Atomizdat, Moscow (1966), p. 67.

HIGH-TEMPERATURE EMBRITTLEMENT OF NEUTRON-IRRADIATED STEEL Kh15N35V3T

B. B. Voital', Sh. Sh. Ibragimov,
V. N. Shemyakin, A. N. Vorob'ev,
L. A. Syshchikov, and A. G. Vakhtin

UDC 621.039.553:669.15.194

Any material can be used for components of reactor cores only after study of its radiation stability, especially in connection with high-temperature embrittlement, which is observed in alloys with austenitic structures (see, e.g., [1-5]).

We have studied the effects of neutron irradiation on the mechanical properties and structure of dispersion-hardened austenitic steel of the type Kh15N35V3T (ÉI612). Specimens of the steel (fivefold breaking

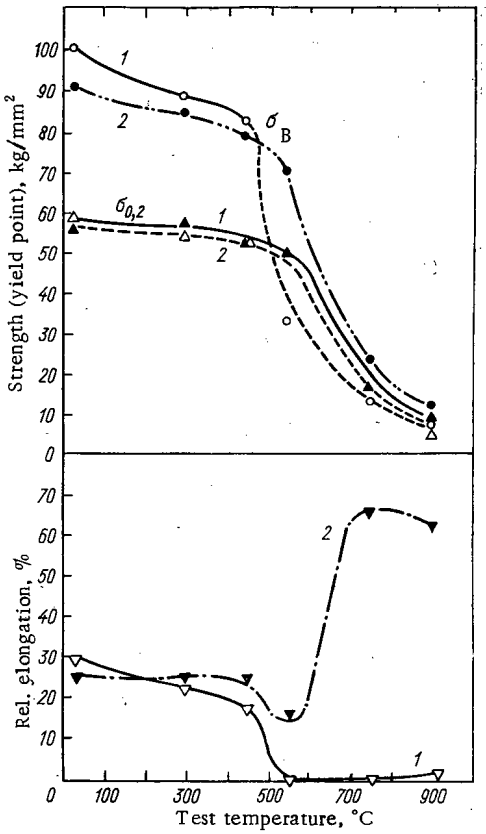

Fig. 1

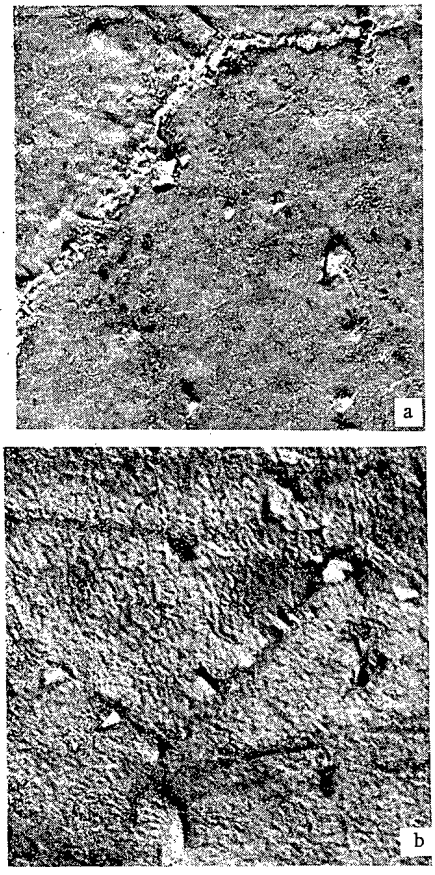

Fig. 2

Fig. 1. Temperature dependence of mechanical properties of steel (routine A). 1) Irradiated specimens; 2) control specimens.

Fig. 2. Microstructure of steel (routine A). a) Control specimens; b) irradiated specimens. Lacquer replica (×5400).

Translated from Atomnaya Énergiya, No. 5, pp. 430-433, May, 1971. Original article submitted March 20, 1970.

TABLE 1. Mechanical Properties of Steels

Test temperature, °C	Routine A						Routine B					
	control specimens			irradiated specimens			control specimens			irradiated specimens		
	σ_B, kg/mm^2	$\sigma_{0.2}$, kg/mm^2	δ_5, %	σ_B, kg/mm^2	$\sigma_{0.2}$, kg/mm^2	δ_5, %	σ_B, kg/mm^2	$\sigma_{0.2}$, kg/mm^2	δ_5, %	σ_B, kg/mm^2	$\sigma_{0.2}$, kg/mm^2	δ_5, %
25	91	57	25	100	59	29	98	65	24,5	100	68	21
450	79	53	25	82	53	17	82	55	23	84	56	17
550	69	50	16	33	—	0	75	53	19	44	—	0
750	23	17	66	13	—	0	25,5	22	62	28	25	4

Fig. 3

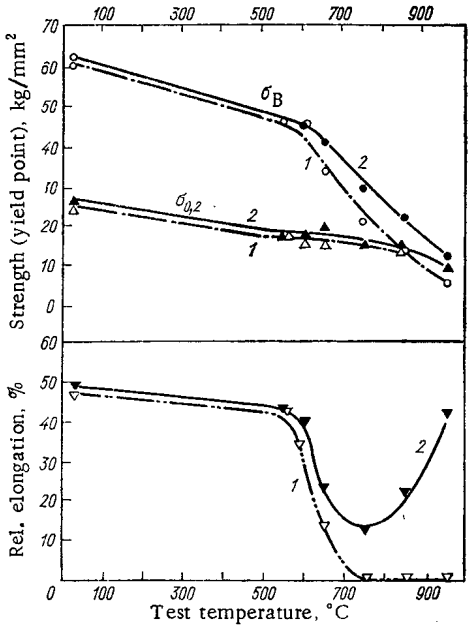

Fig. 4

Fig. 3. Intergrain rupture of control specimen of steel (routine A) for test temperature of 550°C (×300).

Fig. 4. Mechanical properties of steel after annealing at 950°C for 20 h. 1) Irradiated specimens; 2) control specimens.

with a working-section diameter of 3 mm) were first subjected to two heat treatment routines, as follows:

i) Treatment A. Quenching from 1080°C in water; tempering, 10 h at 850°C; 25 h at 750°C.

ii) Treatment B. Quenching from 1080°C in water; tempering, 25 h at 750°C.

The specimens were irradiated in the core of a BR-5 reactor at 450-500°C by an integral flux of $2.5 \cdot 10^{21}$ neutrons/cm^2 (irradiation time 2500 h; about 30% of neutrons with energies above 1 MeV). In addition, a control batch of specimens was kept at 500°C for 1500 h.

Tensile tests on the control and irradiated specimens was carried out in an UMD-5 remote-controlled machine at 25-950°C with a deformation rate of $4.4 \cdot 10^{-3}$ sec^{-1}. We studied the microstructure and the fracture type of the broken specimens. Lacquer replicas of metallographic sections were shadowed with chromium and inspected under the electron microscope.

According to Table 1, the strength characteristics of steel treated according to routine B were appreciably better than those of steel treated according to routine A; for irradiation under the above-stated conditions, the properties of the steel (up to 450-500°C) vary only very slightly.

In tests at 550-900°C we observe a marked high-temperature embrittlement of the irradiated steel and some decrease in the plasticity of the nonirradiated steel (Fig. 1). In contrast with the nonirradiated steel, in the irradiated steel the relief is apparently due to growth of disperse inclusions of a γ'-phase of the Ni_3Ti

type, which indicates some reaging of the material during irradiation (Fig. 2a, b). The type of fracture depends on the test temperature. At 25-450°C fracture of the steel occurs in the bodies of the austenite grains. At 450-550°C, at which we observe a fall in the plasticity of the steel (especially marked in the irradiated specimens), the fracture type changes from intragrain to preferentially intergrain. The specimens break by formation and development of wedge-shaped fractures along the grain boundaries (Fig. 3).

On further rise in test temperature, the shapes of the intergrain fractures in the control specimens change from wedge-shaped to rounded, and fracture is accompanied by marked plastic deformation of the material. Up to 950°C the irradiated specimens display brittle fracture. During high-temperature tests on the nonirradiated steel, grain-boundary migration and recrystallization also occur; this is not observed in the irradiated material.

The results of investigation of the properties and fracture type of the specimens under tension gives grounds to assert that, for steel ÉI612 treated by routines A and B, 500°C is the equicohesive temperature of demarcation between the regions of intergrain and intragrain fracture of the material. A rise in the plasticity of the control specimens at temperatures above 500°C is evidently due to thermal recrystallization of the grain body and to relaxation of stresses at the sharp ends of the cracks owing to plastic deformation of the surrounding material.

It appeared that the equicohesive temperature depends on the initial structure of the alloy. Control and irradiated specimens were annealed for 20 h at 950°C with the aim of elucidating the degree of restoration of the high-temperature plasticity of the steel; this led to an increase of about 150°C in the equicohesive temperature (see Figs. 1 and 4). The effect of high-temperature embrittlement due to irradiation remained unchanged. As a result of annealing we observed a decrease in the strength and an increase in the low-temperature plasticity of the alloy; up to 600°C the values of these characteristics were practically the same for the irradiated as for the nonirradiated steel.

In the microstructure of the annealed alloy there was a growth of austenite grains and an enlargement of the separations of γ'-phase; however, no clear difference was observed between the structures of the irradiated and the nonirradiated materials.

After annealing, fracture of specimens during tensile tests at 750°C occurs along the grain boundaries without marked deformation of those near the fracture. Above this temperature up to 950°C the irradiated specimens undergo brittle fracture while the fracture of the control specimens is of a mixed type and is accompanied by deformation of the austenite grains, formation of microcavities along the boundaries, and recrystallization of the material.

One can suppose that softening and rise in the low-temperature plasticity of the steel resulting from annealing in the above-stated conditions are due to processes of reaging of the material and annealing of radiation defects, while the shift in equicohesive temperature is probably due to a change in the ratio between the strengths of the bodies and boundaries of the grains [6].

Both before and after annealing, high-temperature embrittlement of the irradiated steel appears clearly at temperatures at which the grain boundaries play the principal role in deformation of the material. Therefore the absence of a rising branch on the plasticity–temperature curve for the irradiated steel (high-temperature embrittlement) can be explained only by a change in the state of the grain boundaries of the austenite, resulting from irradiation. This hypothesis agrees well, for example, with the results of Andre et al. [7], who show that the high-temperature plasticity of polycrystalline nickel specimens was reduced by neutron irradiation, whereas that of single crystals remained practically unchanged.

As possible causes of the change in high-temperature strength of the austenite grain boundaries we may cite the presence of gaseous fission fragments (in particular, helium) in the irradiated materials and the high vacancy concentration which leads to formation of micropores along the boundaries, which act as sources of fissures during high-temperature deformation of the alloys [8].

In addition, elements such as lithium, formed by reactor irradiation of the materials, change the surface energies of the grains and can thus promote development of intergrain fracture.

LITERATURE CITED

1. R. Roy and B. Solly, Z. Metallkunde, 58, 258 (1967).
2. H. Bohm, W. Dienst, and H. Hauck, ibid., 57, 352 (1966).

3. D. Harries, J. Brit. Nucl. Energy Soc., 5, 74 (1966).
4. Sh. Sh. Ibragimov and I. M. Voronin, At. Énerg., 20, 137 (1966).
5. S. Votinov et al., Proc. Intern. Conf. Strength of Metals and Alloys (Tokyo, 1967), Sendai (1968), p. 238.
6. M. G. Lozinskii and N. Z. Pertsovskii, Fiz. Metallov i Metallovedenie, 17, 903 (1964).
7. I. Andre et al., Dixieme Colloque de Metallurgie, Fragilite et Effets d'Irradiation, Saclay (1968), p. 199.
8. J. Holmes, Acta Metallurgica, 16, 955 (1968).

RADIATION DAMAGE OF BERYLLIUM DURING HIGH-TEMPERATURE IRRADIATION

Z. I. Chechetkina, V. P. Gol'tsev, V. A. Kazakov, G. A. Sernyaev, and V. G. Bazyukin

UDC 621.039.532.5

The radiation damage of beryllium during high-temperature irradiation is aggravated by the following fact. The helium and tritium atoms formed during the irradiation have a sufficient diffusion mobility to enable them to join together and form nucleating centers for gas bubbles, or during the later stages of irradiation, pores; under certain conditions these can lead to an appreciable swelling of the material and a change of its mechanical properties. The nature of the swelling of the beryllium is determined by both the structural state of the material and the irradiation conditions.

In the present paper we give the experimental results of a study of the physicomechanical properties of beryllium (hot-pressed obtained from a powder of grain size <60 and 600 μ and also single- and bicrystalline beryllium) after irradiation at different temperatures by a total dose of fast neutrons of $6 \cdot 10^{20}$ neutrons /cm^2. The investigated samples had a diameter of 6 mm and were 9 mm high. They were irradiated in an SM-2 reactor in a vertical channel in an atmosphere of helium of industrial purity. The flux density of the fast neutrons in the channel was $4 \cdot 10^{14}$ neutrons/cm$^2 \cdot$ sec^{-1} and that of thermal neutrons was $2 \cdot 10^{14}$ neutrons/cm$^2 \cdot$ sec^{-1}. High-temperatures were produced by the absorption of γ-rays by the irradiated samples. During the irradiation process the temperature was measured by means of Chromel–Alumel thermocouples. After the irradiation we investigated the density, strength, and plasticity of the samples under compression and also their microstructure.

In Fig. 1. we show the change in the density (determined by the hydrostatic method) of beryllium in different structural states irradiated by a fast neutron dose of $6 \cdot 10^{20}$ neutrons/cm^2 as a function of the irradiation temperature. The original density of the samples was 1.830-1.834 g/cm^3. As can be seen from Fig. 1, irradiation at 100-400°C did not change the density of the samples. At temperatures above 400°C a slight change in the density was observed; however, it was only at temperatures above 800°C that the density began to decrease appreciably.

For hot-pressed beryllium with grain size <600 μ (curve 1) at 580°C no change in the density was observed; however at 770°C the change was 0.5% and at 970°C it was 3%. The hot-pressed beryllium with grain size <60 μ (curve 2) under the same irradiation conditions had a swelling of 0.7% at 770°C and 1.7% at 970°C. The density of the single-crystal and cast beryllium (curve 3) did not change at any of the investigated irradiation temperatures.

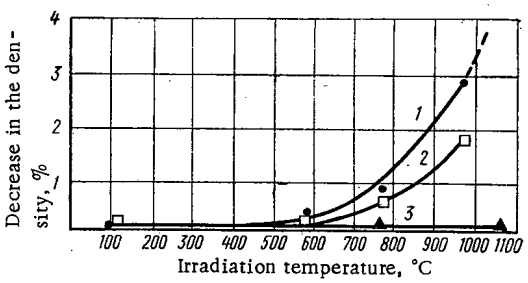

Fig. 1. Change in the density of beryllium as a function of the irradiation temperature.

Figure 2 shows the microstructures of the irradiated hot-pressed beryllium with grain size <600 μ.

At 580°C an enhanced porosity was observed in the beryllium (Fig. 2a). Basically, the pores were situated at the grain boundaries. Over the whole volume of the grain there were distributed "convexities"; when these were opened they revealed either segregated material surrounded by a cavity of a certain kind or individual pores.

Translated from Atomnaya Énergiya, No. 5, pp. 434-438, May, 1971. Original article submitted March 3, 1970.

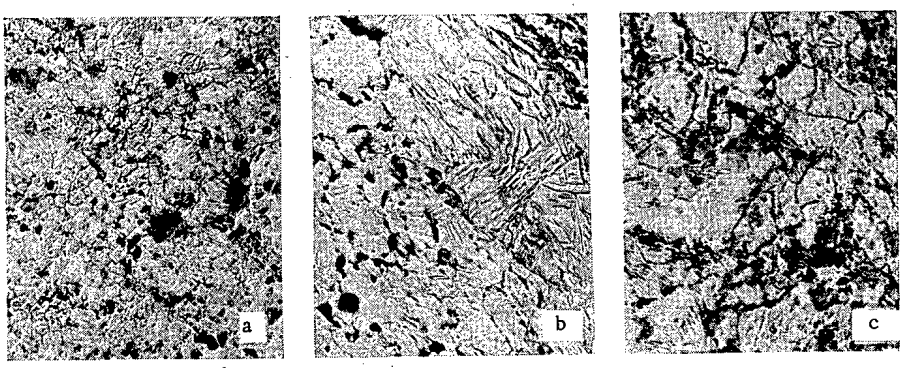

Fig. 2. Microstructure of hot-pressed beryllium after irradiation at different temperatures (×200): a) 580°C; b) 770°C; c) 970°C.

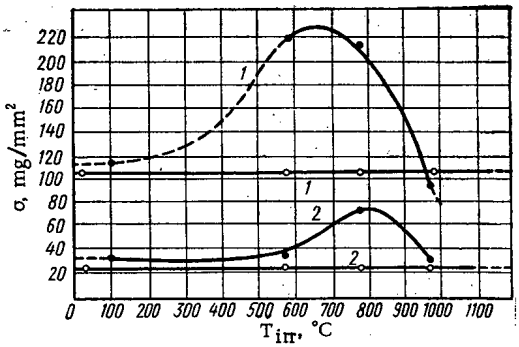

Fig. 3. Influence of high-temperature irradiation on the compressive strength (1) and yield point (2) of hot-pressed beryllium: •) after irradiation; ○) after annealing.

When the temperature was increased to 770°C, the number of such defects increased. These "convexities" formed continuous chains around the grain boundaries. In addition, the beryllium irradiated at this temperature had a large number of twins (Fig. 2b). A further increase in the irradiation temperature led to the appearance of pores that formed complete clusters at the position of inclusions, at block boundaries, and at different inhomogeneities of the microstructure (Fig. 2c). At the irradiation temperature 970°C we observed a large number of pores between sintered particles of the powder.

In the hot-pressed beryllium with grain size <60 μ we observed a similar change in the microstructure with increasing irradiation temperature; however, the pores had smaller dimensions and their concentration was greater.

In the microstructure of single- and bicrystals of cast beryllium irradiated at 580°C we detected fine pores of diameter 100 Å distributed uniformly over the whole volume of the grain. Larger pores were found at the boundaries. It should be noted that annealing for 260 h of nonirradiated beryllium (which corresponded to the effective irradiation time) at the given temperatures did not lead to any changes of the investigated properties. The microstructure of the comparison samples annealed at 580°C remained unchanged. After annealing at 770 and 970°C the grains became larger, their diameters lying in the range 100-300 μ. Electron-microscope investigations of the beryllium after annealing failed to reveal any change in its fine microstructure.

In Figs. 3-5 we give the values calculated from the data of the mechanical experiments for the compressive strength, the compressive yield point, the relative shortening under compression, and also the measured microhardness.

The compressive strength of the metal (curves 1, Fig. 3) increased as the irradiation temperature approached 800°C and then began to fall. The yield point (curves 2, Fig. 3) and the microhardness (see Fig. 5) exhibited a similar behavior. The mechanical properties of the comparison samples annealed at the same temperatures did not change.

Data on the changes in the physicochemical properties of beryllium under the influence of neutron irradiation at high-temperatures enables us to establish some features of the process of swelling and strengthening of beryllium under the influence of irradiation.

As can be seen in Figs. 3-5, irradiation at 580-770°C leads to an appreciable strengthening of the material and a decrease in its plasticity. The effect of radiation strengthening at temperatures above 800°C is absent. The electron-microscope investigation of the structure of beryllium irradiated at 580-770°C showed that the number of the pores in the material became appreciable, their diameters not exceeding 100 Å. Under these conditions the change in the density was less than 0.1%. After irradiation at 970°C the beryllium microstructure revealed a large number of pores of diameter 500-1000 Å and greater.

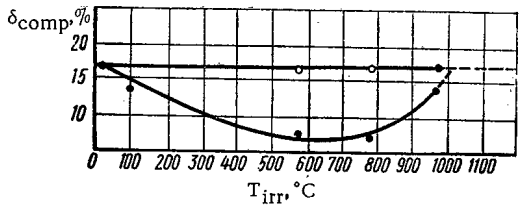

Fig. 4

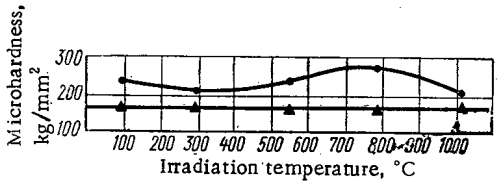

Fig. 5

Fig. 4. Influence of high-temperature irradiation on the relative shortening under compression of hot-pressed beryllium: ●) after irradiation; ○) after annealing.

Fig. 5. Influence of high-temperature irradiation on the microhardness of hot-pressed beryllium: ●) after irradiation; Δ) after annealing.

Figure 6 shows that the pores were distributed nonuniformly in the material. The largest pores were found at the boundaries of the particles of the beryllium powder, where the greatest number of inclusions (basically BeO) was observed; smaller pores were found at boundaries of grains and blocks. The changes in the beryllium density amounted to 1.7-3%. Under the same irradiation conditions finer pores were observed in the hot-pressed beryllium with smaller grain size (<60 μ) than in the coarse-grained beryllium (<600 μ). However, the pores were distributed in the same way.

In the single-crystal beryllium the pores were formed and distributed in a somewhat different manner. After irradiation at 580°C the pores that could still be detected were distributed relatively uniformly in the volume of the metal. After irradiation at 970°C gas pores in the single-crystal beryllium were virtually absent. A change in the density of the beryllium single-crystals was also not detected. The mechanical properties (microhardness) did not differ from those of the original material.

The results of the investigations enable us to explain the change in the properties of the beryllium by the state of the helium that accumulates in the beryllium and confirms the point of view according to which gaseous pores play a fundamental role in the process of strengthening and swelling of beryllium under the influence of neutron irradiation [1-4].

At low temperatures (<100°C) the helium formed in the nuclear reactions remains in the beryllium crystal lattice. With increasing temperature, the diffusion mobility of the helium also increases and this enables it to migrate in the bulk of the metal, accumulating at dislocations and other defect traps; in this way it forms pores. The formation of pores and their subsequent growth leads to two processes of radiation damage of beryllium. These are the hardening of the material as a result of the immobilization of dislocations by the gas pores and the swelling of the beryllium. Both of these processes depend qualitatively and quantitatively on the dimensions of the pores and their concentration distribution. The strengthening depends extremally on the dimensions and number of the gas pores formed. An increase in the pores leads to an appreciable swelling of the material.

Different authors have expressed different opinions about the influence of the grain size on the distribution of the gas pores. However, the majority assumption is that the principal factor responsible for the greater swelling is the migration of individual gas atoms and complete pores to the grain boundaries and other sources of vacancies. It follows that everything that hinders their movement must help to reduce the swelling.

An estimate of the importance of the structural state of beryllium on the process of swelling as a result of irradiation can be obtained by comparing the number and sizes of the helium pores in samples that have different grain sizes. The results of our investigations show that the grain boundaries and the phase boundaries are not only centers for the formation of pores, but also places at which they can stop during migration. Clearly, the most active centers of this kind are the metal-inclusion boundaries and cavities that arise as a result of the technical working.

Given the same amount of accumulated gas and a uniform distribution of the latter, the number of pores formed (and hence the swelling) will be less, the greater the concentration of the defects at which they can be formed and settle. At the same time great importance attaches to the diffusion velocity of helium in beryllium.

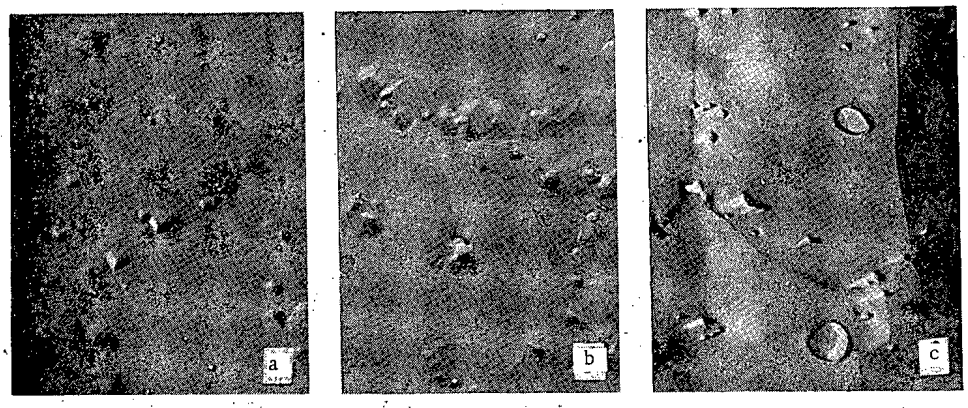

Fig. 6. Microstructure of hot-pressed beryllium at different temperatures (×10,000): a) 580°C; b) 770°C; c) 970°C.

If the diffusion mobility of the helium atoms in beryllium is so low that they do not reach the grain boundaries during the irradiation time, but remain within the grains, pores can be formed both at the grain boundaries and within the grains, i.e., at dislocations and other defect traps. Since the grain boundaries in beryllium are sources of vacancies, the helium pores will grow faster near the boundaries than within the grains. It follows that a material that contains an extensive system of boundaries has a greater number of centers of enhanced growth of pores and, consequently, will have a tendency to swell more.

Calculations show that the swelling of beryllium due to the formation of pores by this mechanism does not exceed ~0.01% at a dose of $6 \cdot 10^{20}$ neutrons/cm^2 at 580°C; this is appreciably less than the swelling detected experimentally.

It is evident that other factors must be more important; these would be the appearance of pores and cavities at the grain boundaries under the influence of stresses due to nonuniform swelling of individual grains. In a fine-grained material the pores formed by this method will then have smaller dimensions and be distributed more uniformly. This conclusion is typical for irradiation temperatures up to 600°C and is well confirmed by our results and those of other authors [5, 6].

As the temperature is further increased, the diffusion mobility of the helium atoms and the plasticity of the beryllium also increase; the probability for the formation of pores by the mechanisms described above therefore decreases.

If the diffusion mobility of the helium atoms (or gas pores) is sufficient to ensure that they reach the grain boundaries during the irradiation, an extended system of boundaries and dispersion of the inclusions will lead to a smaller amount of swelling. This is characteristic for temperatures of 800°C and higher, when the material has the greatest tendency to swelling.

It should be noted that at temperatures of 970°C and higher the diffusion velocity of helium atoms ensures that the gas can leave the grains. In this case the presence of different inclusions hinders the free diffusion of the gas, whereas a boundary, being a conductor for the gas, serves as the shortest path for the subsequent diffusion and removal of the gas. At these temperatures the most effective "traps" are inclusions and pores that arise during technical treatment. In the given temperature range the greatest radiation stability will be exhibited by cast or hot-pressed metal with finely dispersed inclusions that have a high concentration in the material.

From these considerations we can draw the following conclusions:

1. The radiation damage of beryllium is manifested in its swelling and its strengthening.

2. The amount of swelling of beryllium during the irradiation process depends largely on its structural state and on the irradiation temperature: a) cast material in the whole of the investigated temperature range does not undergo appreciable swelling; b) hot-pressed materials made of powders with particle sizes <60 μ and also <600 μ do not undergo appreciable swelling in the temperature range <600°C; c) the swelling of hot-pressed materials increases appreciably above 600°C and continues to increase with increasing irradiation temperature; d) a material hot-pressed from a powder of particle size <600 μ has a greater tendency to swelling than a material obtained from a powder with particle size <60 μ.

3. The strength properties (σ_B, $\sigma_{0.2}$, δ) of beryllium depend nonmonotonically on the irradiation temperature; for example, the greatest strengthening (the compressive strength is equal to 200 kg/mm^2) occurs at the temperatures 600-800°C. The minimum of the plasticity (2-3%) occurs at the same temperatures.

4. The electron-microscope investigation reveals that the changes in the properties of the material are well correlated with the behavior of the helium that accumulates in the material. In its turn, the behavior of the helium in materials prepared by different methods is largely determined by their structural state.

LITERATURE CITED

1. S. T. Konobeevskii, The Influence of Irradiation on Materials [in Russian], Atomizdat, Moscow (1967), p. 278.
2. R. Barns, Metallurgy of Beryllium, Chapman and Hall, London (1963), p. 372.
3. R. Barns et al., Nucl. Sci., Abstrs., 16, No. 2262 (1962).
4. I. I. Papirov and G. F. Tikhinskii, Physical Metallurgy of Beryllium [in Russian], Atomizdat, Moscow (1968), p. 411.
5. Materials of Moderators, Reflectors, and Regulating Devices (Reviews of the Bettla Institute) [Russian translation], D. M. Skorov (editor), Atomizdat, Moscow (1962).
6. J. B. Rich et al., J. Nucl. Mater., 4, 287 (1961).

RADIOLYSIS OF URANIUM HEXAFLUORIDE

V. A. Dmitrievskii and A. I. Migachev

UDC 541.15

Uranium hexafluoride is the only uranium compound with a relatively high vapor pressure, which places it among the promising compounds for use in various atomic installations.

UF_6 was first mentioned as a possible nuclear fuel in [1]. Since then many different plans for atomic installations using UF_6 have been published. A brief survey of the Soviet and foreign literature on the use of UF_6 as a nuclear fuel is cited in [2].

One of the difficulties in using UF_6 is the radiation breakdown of its molecules, chiefly under the action of the kinetic energy of fission fragments. The first data on such radiolysis of UF_6 were published in [3], devoted to an investigation of a bench reactor working on gaseous UF_6. In work of the reactor at an increased power level, a decrease in the gas pressure and reactivity was observed in it. On the assumption that the dissociation of UF_6 molecules proceeds according to the equation

$$UF_6 \rightsquigarrow UF_5 + \frac{1}{2}F_2, \qquad (1)$$

the rate of decomposition of UF_6 per unit power was determined. It proved equal to 0.32 mole/kW·h, which corresponds to a radiation chemical yield G = 0.8 molecules/100 eV. It was shown that, using a strong oxidizing agent (chlorine trifluoride) as the stabilizing impurity, radiation stability of the UF_6 molecules can be ensured.

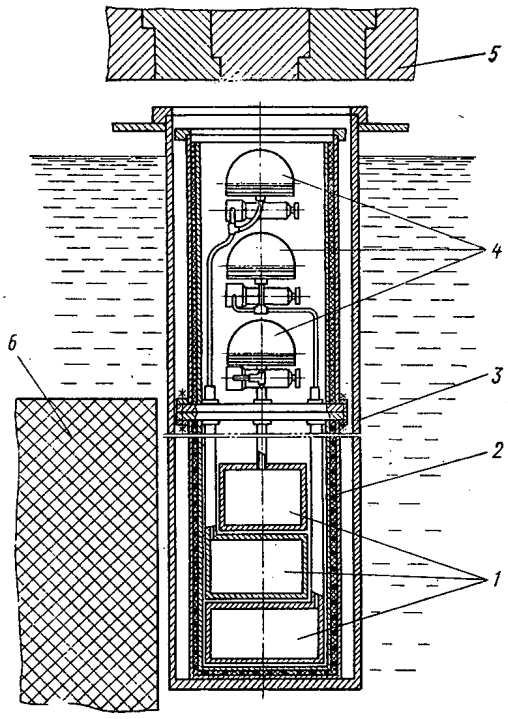

Fig. 1. Scheme of the experimental installation: 1) vessels with UF_6; 2) electric heater; 3) outer protective casing; 4) manometers; 5) shield of reactor; 6) active zone of reactor.

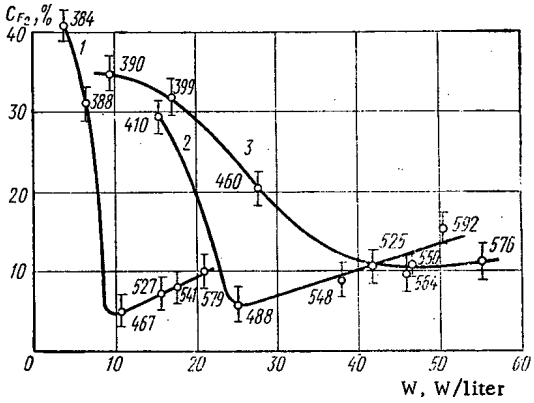

Fig. 2. Dependence of the equilibrium concentration of fluorine on the dose rate at an initial pressure (in mm Hg): 1) 150; 2) 204; 3) 272. The numbers indicate the values of the effective temperature of the gas in the ampoule (in °K).

Translated from Atomnaya Énergiya, No. 5, pp. 438-443, May, 1971. Original article submitted February 9, 1970.

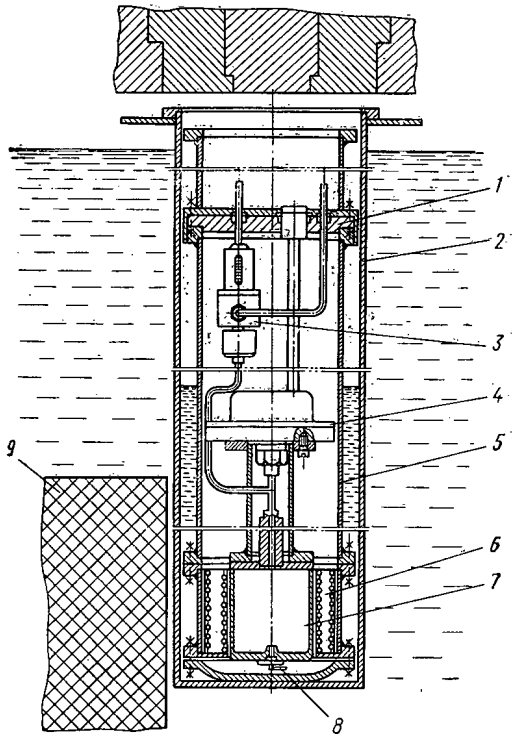

Fig. 3. Scheme of the experimental installation for high dose rates: 1) connecting flange; 2) reactor channel; 3) valve; 4) manometer; 5) protective casing; 6) steel rib; 7) ampoule with UF_6; 8) thermocouple; 9) active zone of the reactor.

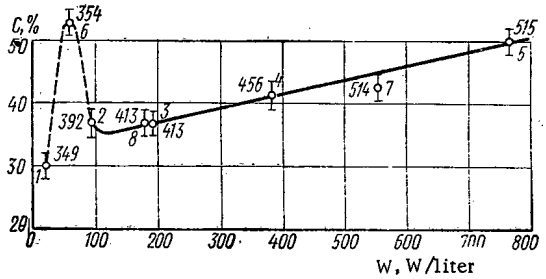

Fig. 4. Dependence of the equilibrium concentration of fluorine on the dose rate. The numbers indicate the sequence of the experiment and the average gas temperature in the ampoule (°K).

The radiation breakdown of uranium hexafluoride under the action of α particles was studied in [4]. A value G ≈ 1 molecule/100 eV was obtained.

A detailed study of the radiolysis of the uranium hexafluoride – fluorine system under the action of the kinetic energy of fission fragments was published by the authors in 1959 [5]. In this work it was shown experimentally that the dissociation of UF_6 proceeds according to Eq. (1). The rate of decomposition of uranium hexafluoride (without a fluorine impurity) is 0.21 mole/kW·h of energy liberated in the gas at the initial moment of time and decreases as free fluorine is accumulated in the ampoules. With the passage of time an equilibrium state is established. The values of the concentrations of UF_6 and its radiolysis products in the equilibrium state are determined by the dose rate, by the initial pressure and the temperature. If a mixture of UF_6 with fluorine, the concentration of which at the initial moment is higher than the equilibrium value, is irradiated, then the composition of the mixture does not change with time, i.e., such a mixture of gases is stable to neutron irradiation in the radiation chemical respect and can serve as a gaseous nuclear fuel.

In [6] the radiolysis of UF_6 and its decomposition products under the action of fast electrons was studied. The rate of the radiation chemical decomposition of UF_6 under the action of fast electrons proved to be negligible ($4.5 \cdot 10^{-3}$ mole/kW·h or $1.1 \cdot 10^{-2}$ molecules/100 eV). In the same work it was shown that the lower fluorides of uranium (UF_5 and UF_4) are fluorinated to UF_6 under the action of fast electrons in the presence of free fluorine. The rate of radiation fluorination obeys the equation

$$v = B_1 P_{F_2} \sqrt{\mathcal{J}}, \qquad (2)$$

where P_{F_2} is the fluorine pressure: $\mathcal{J}$ is the current of the electron beam. Since the dose rate W is proportional to the pressure,

$$v = B_1 \sqrt{W P_{F_2}}. \qquad (3)$$

From the form of the function (3) it follows that an important role in the formation of active particles is played by recombination processes (the square root of the dose rate) and collision with gas molecules (dependence on the pressure).

A study of the radiolysis of UF_6 under the action of the kinetic energy of fission fragments was continued chiefly to determine the dependence of the equilibrium concentrations on the initial pressure and the dose rate, as well as to refine the value of G. The method described in [5] was used. Three aluminum vessels (Fig. 1) with a volume of ~2 liters had dimensions significantly exceeding the range of U^{235} fission fragments at the pressure of UF_6 that existed in them. The vessels were filled with UF_6 90% enriched with respect to the isotope U^{235}. The initial UF_6 pressures were equal to 150, 204, and 272 mm Hg at 70°C.

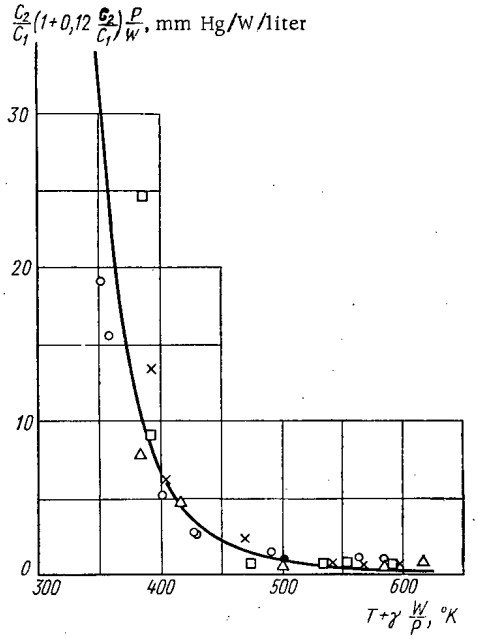

Fig. 5. Comparison of the experimental data with the calculated curve according to Eq. (13). The experimental points correspond to the initial pressures (in mm Hg): ○) 1112; □) 150; △) 204; ×) 272. The experimental point ● was taken from [5] on the assumption that it corresponds to the equilibrium state.

The pressure was measured with differential membrane manometers with a complete scale of 75 mm Hg according to a scheme with counter pressure. The pressure in the "zero" volumes of the manometers was determined with an absolute mercury manometer. The temperature of the walls of each vessel was measured with copper–constantan thermocouples. The vessels, manometers, and supply lines had electric heaters with a thermoregulator. Before the experiment the inner surfaces of the apparatus were treated first with fluorine, then with UF_6 of the natural isotopic composition at the temperature 250°C, until the corrosion losses were no longer appreciable within the limits of error of the measurement.

The apparatus was arranged in the vertical channel (190 mm in diameter) of the VVR reactor [7]. The electrical cables and tubes of the "zero" volumes of the manometers were brought out from under the upper shield of the reactor. The value of the neutron flux necessary for calculating the dose rate was found by averaging the known distribution of the neutron flux along the height of the channel. As has already been indicated, prolonged irradiation of UF_6 results in an equilibrium state. Therefore the experiment was conducted as follows. UF_6 (without fluorine impurity) was irradiated in a reactor at a constant value of the neutron flux until an equilibrium state was reached. These experiments aided in determining the value of G. Then, without changing the composition of the gas, irradiation was conducted at another value of the neutron flux, until an equilibrium state was reached, etc. To determine the value of G, the experimental dependences of the pressure change in the vessels on the time of irradiation (or dose) until the establishment of an equilibrium state was interpolated by the expression

$$P = P_\infty + (P_0 - P_\infty)\, e^{-\alpha t}, \qquad (4)$$

where P_0 is the initial pressure; P_∞ is the pressure corresponding to the equilibrium state; t is the time of irradiation.

The values of P_∞ and α found experimentally were used to determine the initial rate of change in the pressure of UF_6, when the partial pressure of fluorine was equal to zero, and to determine the value of G:

$$-\frac{dP_{UF_6}}{dt}\Big|_{t=0} = \frac{1}{1-\xi}\,\alpha\,(P_0 - P_\infty), \qquad (5)$$

where $\xi = 0.5$ is the stoichiometric coefficient of reaction (1).

The dose rate was calculated according to the value of the neutron flux and the pressure of $U^{235}F_6$. All the known values of G for UF_6 under the action of the kinetic energy of fission fragments are cited in Table 1. Within the limits of error of the measurement, the rate of radiolysis of UF_6 molecules does not depend on the pressure and dose rate and is 0.28 mole/kW·h of absorbed energy or (0.8 ± 0.1) molecule/100 eV. The dependences of the equilibrium concentrations of fluorine at various initial pressures on the dose rate are cited in Fig. 2. The curves show a pronounced minimum, which is shifted in the direction of higher dose rates with increasing pressure. Since the equilibrium concentration of fluorine at a dose rate equal to zero should also be equal to zero, the curves of C = f(W) should have a second extreme (maximum) in the region of low values of the dose rate.

A special experiment was conducted to investigate the dependence of the equilibrium concentrations of fluorine in the presence of large energy liberations. A cylindrical aluminum ampoule was used, along the generatrix of which six steel ribs were fastened, so as to maintain the necessary temperature gradient between the walls of the ampoule and the walls of the outer casing, immersed in the water filling the channel (diameter 190 mm), of the VVR reactor. Electric heaters were mounted in the space between the ribs to

TABLE 1. Values of the Radiation Chemical Yield for UF_6

Gas pressure, mm Hg	Temperature, °C	Dose rate, W/liter	G, molecules /100 eV	Literature cited
150	100	7,85	0,85	This work
204	100	18,8	0,64	The same
272	100	20,7	0,76	" "
1112	69	23,2	0,76	" "
Condensed state	8	2,9	0,64 *	[5]
1160	93	7,0	0,97 *	[3]

* In the cited works, the total energy of fission was considered in the calculation of G. Since the absorption of the energy of β and γ disintegration and neutrons in gas is negligible, the values of G cited in the table were obtained considering only the kinetic energy of the fission fragments.

heat the ampoule. The electric heaters were also equipped with a manometer, valve, and supply lines. The temperature was measured in 13 different points of the apparatus with copper–constantan thermocouples. The scheme of the apparatus is cited in Fig. 3. The manometer was prepared on the basis of a standard membrane-type differential manometer, in which the attachment of the dome of the "zero" volume was strengthened, and the membrane was sealed with a copper gasket. The range of measurement of the manometer was 200 mm Hg. The pressure in the "zero" volume of the manometer was measured either with a mercury manometer (for pressures below atmospheric) or with a standard sample manometer (for pressures above atomospheric).

Treatment of the inner surfaces of the apparatus and analysis of the composition of the gas mixture were performed according to the method described above. The dose rate was varied either by varying the reactor power or by the arrangement of the ampoule relative to the center of the active zone of the reactor. The ampoule was filled with UF_6, 90% enriched with respect to the isotope U^{235}, to a pressure of 1112 mm Hg at the temperature 70°C. At each level of reactor power, the gas was irradiated for 10-14 h, so that at the end of the period of irradiation, equilibrium concentrations of UF_6 and F_2 were established in the system. The temperature of the walls of the ampoule was kept comparatively low (it did not exceed 130°C). The value of G determined from this experiment is cited in Table 1. The dependence of the equilibrium concentration of fluorine on the dose rate takes qualitatively the same form as that obtained earlier (Fig. 4). In accord with the curves of Fig. 2, the minimum on the curve of $C = f(W)$ is even more shifted into the region of larger dose rates.

The experimental dependences obtained find a simple explanation. The lower nonvolatile fluorides of uranium, which are formed in the decomposition of UF_6 molecules, coagulate into large particles (sols). Since these particles contain a fissioning substance, their temperature is higher than the temperature of the surrounding medium by an amount

$$\Delta T = \frac{q\rho}{3k} \tag{6}$$

(for spherical particles), where ρ is the radius of the particle; q is the amount of heat liberated in a unit volume of sol; k is the coefficient of heat transfer.

If the dimensions of the reaction volume are sufficiently great, so that the rate of reduction of UF_6 on the walls can be neglected, and only its radiation synthesis on the surface of the sols can be considered, the equation for the loss of UF_6 molecules per unit volume can be written in the form

$$-\frac{dn_1}{dt} = GW\frac{aC_1}{aC_1 + bC_2} - Ze^{-\frac{Q}{R(T+\Delta T)}}, \tag{7}$$

where W is the dose rate in a unit volume of the gas mixture; C_1 and C_2 are the concentrations of UF_6 and F_2, respectively; Z is the density of collision of "active" fluorine with the surface of the sols; Q is the activation energy; T is the temperature of the gas.*

The factor $aC_1/aC_1 + bC_2$ considers the fraction of the total energy absorbed by UF_6. The coefficients a and b are determined by the stopping power of UF_6 and fluorine and are approximately proportional to the total number of electrons in the molecule. The value of Z is proportional to the total surface of the sol in a unit volume and the density of "active" fluorine molecules, which, in accord with (3), is equal to

$$n^* = B\sqrt{W\frac{bC_2}{aC_1 + bC_2}P}, \tag{8}$$

where $W(bC_2)/aC_1 + bC_2$ is the dose rate, liberated in fluorine.

*Henceforth it will not be considered that the temperature in the tracks of the fragments can be significantly higher than the temperature of the gas.

Let us determine the temperature of the sols. If the particles have a sufficiently large radius (in comparison with the free range of the molecules), then the coefficient of heat transfer can be determined (see, for example, [8]) from the Nusselt criterion:

$$\mathrm{Nu} = \frac{k \cdot 2\rho}{\lambda} = c\,(\mathrm{Gr} \cdot \mathrm{Pr})^n, \tag{9}$$

where λ is the coefficient of the thermal conductivity of the surrounding medium; Gr and Pr are the Grashof and Prandtl criteria. For particles with dimensions 1-100 μ, the exponent n = 1/8, while the coefficient c = 1.18. Substituting the expression for k into formula (6) and replacing the numbers Gr and Pr by their values, we can obtain an equation for the determination of ΔT. Omitting the computations, let us cite the final results:

$$\Delta T = \gamma \frac{(\Phi \cdot C_5)^{8/9}}{P^{2/9}}, \tag{10}$$

where Φ is the value of the neutron flux; C_5 is the concentration of U^{235}, γ is a constant coefficient. It is more convenient to determine the value of ΔT in terms of the dose rate absorbed by the gas mixture. Since the dose rate W is proportional to $P_0 \Phi C_5$,

$$\Delta T = \gamma \frac{(W)^{8/9}}{P^{2/9} P^{8/9}} \approx \gamma \frac{W}{P_0}. \tag{11}$$

(The values of the stationary concentrations of fluorine reach ~50% in individual experiments, which corresponds to an ~30% drop in the initial pressure. Since a qualitative description of the process is of interest, in formula (11) the quantity P is replaced by P_0.) Now Eq. (7) for the decrease in UF_6 can be written in the form

$$-\frac{dn_1}{dt} = G \cdot W \frac{aC_1}{aC_1 + bC_2} - BS_0 \sqrt{W \frac{bC_2}{aC_1 + bC_2}}\, P\, e^{-\frac{Q}{R\left(T + \gamma \frac{W}{P_0}\right)}}, \tag{12}$$

where S_0 is the specific surface of the suspended particles of lower fluorides of uranium, which can be considered for simplicity to be a constant; B is a constant coefficient.

In the equilibrium state $(dn_1/dt) = 0$, and we obtain an equation from which the value of the relative concentration of fluorine C_2/C_1 is determined:

$$\frac{C_2}{C_1}\left(1 + 0.12\,\frac{C_2}{C_1}\right) = \mathrm{const}\,\frac{W}{P} e^{\frac{2Q}{R\left(T + \gamma \frac{W}{P_0}\right)}}. \tag{13}$$

The function determined by Eq. (13) has two extremes for the dose rate:

$$W^* = \frac{P_0}{\gamma} \cdot \frac{Q}{R}\left[\left(1 - \frac{RT}{Q}\right) \pm \left(1 - 2\,\frac{RT}{Q}\right)^{1/2}\right]. \tag{14}$$

The minus sign corresponds to the maximum of the function, the plus sign to the minimum. In accord with the experimental curves (see Figs. 2 and 4), when the initial pressure is increased, the minimum concentration is shifted in the region of larger dose rates. Let us mention still another peculiarity of the experimental curves of Figs. 2 and 4. The temperature of the walls of the vessel (and, consequently, the temperature of the gas) increased monotonically with increasing dose rate. Moreover, it was noted that when the reactor power was rapidly turned off (dropping the rods), in the first moment a rapid drop in the presssure in the vessels was observed, caused by cutoff of the internal heat sources. The initial temperature of the gas in the case of a high dose rate differed substantially from the temperature of the walls of the vessel. Therefore, in a comparison of the experimental curves of C = f(W) with the calculated curves, it should be considered that in formula (13) the value of T is also a function of the dose rate. The average temperature of the gas in the ampoules was determined according to the value of the pressure "drop" when the reactor was turned off and is indicated in Figs. 2 and 4. At high dose rates, the average temperature of the gas reached ~300°C. At such a temperature, the thermal reaction of fluorine with lower fluorides of uranium should proceed at an appreciable rate, and a factor proportional to $S_0 P C_{F_2} e^{-Q_1/R(T+\Delta T)}$, must be added in the right-hand portion of Eq. (12), where Q_1 is the activation energy for this reaction. However, considering the fact that when this equation was written simplifying assumptions were made and the purpose was to obtain only qualitative agreement with the experiment, the thermal reaction can be neglected.

Figure 5 depicts a graph of the function (solid line) represented by Eq. (13) in a plot of $C_2/C_1(1 + 0.12 (C_2/C_1))P/W$ versus $T + \gamma (W/P)$. In these coordinates all the experimental points obtained at various pressures, temperatures, and dose rates should be plotted according to formula (13) on one curve. The following values of the constants were selected: $\gamma = 100$ (mm Hg · °K) /(W/liter); $(2Q/R) = 4200(1/°K)$; $A = 2 \cdot 10^{-4}$. All the experimental points were plotted on the same graph. From Fig. 5 it follows that Eq. (13), determining the value of the equilibrium concentration, is in satisfactory agreement with the experiment.

In conclusion, the authors would like to express their gratitude to I. K. Kikoin for his interest and attention to the work, to S. V. Kersnovskii who designed the apparatus, and to Yu. V. Boikov, who took part in certain experiments.

LITERATURE CITED

1. K. Goodman (editor), Scientific and Technical Bases of Nuclear Energetics [Russian translation], Izd-vo Inostr. Lit., Moscow (1948), p. 273.
2. V. A. Dmitrievskii, E. M. Voinov, and S. É. Tetel'baum, At. Énerg., 29, 251 (1970).
3. I. K. Kikoin et al., Report No. 2502 (USSR), Second Geneva Conference (1958).
4. H. Bernhard, W. Davis, and C. Shiflett, Report No. 522 (USA), Second Geneva Conference (1958).
5. V. A. Dmitrievskii and A. I. Migachev, At. Énerg., 6, 533 (1959).
6. A. I. Migachev and A. P. Senchenkov, At. Énerg., 16, 510 (1964).
7. Yu. G. Nikolaev, "Reactor Construction and the Theory of Reactors." First Geneva Conference on the Peaceful Uses of Atomic Energy [in Russian], Izd-vo AN SSSR, Moscow (1955), p. 91.
8. M. A. Mikheev, Fundamentals of Heat Transfer [in Russian], Gosénergoizdat, Moscow (1956).

GREEN'S FUNCTION OF THE NEUTRON TRANSPORT EQUATION FOR A MOVING MEDIUM

E. A. Garusov and Yu. V. Petrov

UDC 539.125.52

In the paper the system of eigenfunctions of the stationary neutron transport equation obtained in [1] is generalized to the case of nuclei of infinite mass that move with the same velocity **u** in a direction perpendicular to the plane of the source. It is assumed that the cross sections are independent of the energy and that the neutrons are scattered isotropically in the center of mass system.

The solution of the neutron transport equation for a moving medium [2]

$$w\mu \frac{\partial \Psi}{\partial Z} + \Sigma \,|\, \mathbf{w}-\mathbf{u} \,|\, \Psi = \int \Sigma_s \frac{\delta(|\,\mathbf{w}'-\mathbf{u}\,|-|\,\mathbf{w}-\mathbf{u}\,|)}{4\pi\,|\,\mathbf{w}-\mathbf{u}\,|} \cdot \Psi\, d\mathbf{w}' \tag{1}$$

under these assumptions has the form

$$\Psi_{a,\nu,m}(Z,\ \mathbf{w},\ \mathbf{u}) = e^{-\Sigma Z/\nu}\psi_{\nu,m}(f,\ \varphi)\frac{\delta(|\,\mathbf{w}-\mathbf{u}\,|-a)}{|\,\mathbf{w}-\mathbf{u}\,|} \equiv e^{-\Sigma Z/\nu}F_{a,\nu,m}(\mathbf{w}); \quad f(\mathbf{w}) \equiv \frac{w\mu}{|\,\mathbf{w}-\mathbf{u}\,|}, \tag{2}$$

where

$$\psi_{\nu_i,0}(f) \equiv \frac{c\nu_i}{2}\cdot\frac{1}{\nu_i - f}; \quad c \equiv \frac{\Sigma_s}{\Sigma}, \tag{3}$$

for discreet values ν_i and

$$\psi_{\nu,0}(f,\ \varphi) \equiv \frac{c\nu}{2}\,\mathcal{P}\frac{1}{\nu - f} + \lambda(\nu)\,\delta(\nu - f); \tag{4}$$

$$\lambda(\nu) \equiv 1 + \frac{c\nu}{2}\ln\left|\frac{\nu-(\gamma+1)}{\nu-(\gamma-1)}\right|, \quad \gamma \equiv \frac{u}{|\,\mathbf{w}-\mathbf{u}\,|}; \tag{5}$$

$$\psi_{\nu,m}(f,\ \varphi) \equiv \delta(\nu - f)\,e^{im\varphi}, \quad m = \pm 1,\ \pm 2,\ \ldots, \tag{6}$$

for continuous values ν.

The eigenvalues a are continuous and lie between 0 and $+\infty$. Under the influence of the motion the continuous spectrum of eigenvalues ν is displaced without deformation by the amount γ to the interval $[\gamma - 1, \gamma + 1]$. For $\gamma < 1$ one of the two discrete values ν_i that satisfies the equation

$$1 + \frac{c\nu_i}{2}\ln\frac{\nu_i-(\gamma+1)}{\nu_i-(\gamma-1)} = 0, \tag{7}$$

increases with increasing u while the other decreases. This corresponds to an increase in the diffusion length in the direction of motion of the medium and a decrease in the opposite direction [3]. For $\gamma > 1$ the neutrons diffuse only forward since (7) has only a single real root:

$$\nu_1 \approx \frac{c\gamma}{1-c} \quad \text{for} \quad \frac{c\gamma}{(1-c)(1+\gamma)} \gg 1.$$

The functions $F_{a,\nu,m}(\mathbf{w})$ form a complete set of eigenvalues that are orthogonal in the whole phase space of velocities **w** with weight function $f(\mathbf{w})$.

The solution of Eq. (1) in an infinite medium in the presence of a source $\delta(z - z_0)\delta(\mathbf{w} - \mathbf{w}_0)$, i.e., the Green's function, is constructed from the eigenfunctions in the usual manner:

Translated from Atomnaya Énergiya, No. 5, pp. 444-445, May, 1971.

$$G(z, \mathbf{w}; z_0, \mathbf{w}_0; \mathbf{u}) = \frac{\delta(|\mathbf{w}-\mathbf{u}|-|\mathbf{w}_0-\mathbf{u}|)}{2\pi|\mathbf{w}-\mathbf{u}|^3} \left\{ \sum_m \int_{\gamma-1}^{\gamma+1} \frac{d\nu X\left[\frac{1}{\nu}, z-z_0\right] e^{-\Sigma(z-z_0)/\nu}}{\nu\left[\left(\lambda^2+\left(\frac{c\nu\pi}{2}\right)^2-1\right)\delta_{m,0}+1\right]} \times \right.$$

$$\left. \times \psi_{\nu, m}(f, \varphi)\psi^*_{\nu, m}(f_0, \varphi_0) + \sum_i \left(\frac{c\nu_i}{2}\left[\frac{c\nu_i^2}{(\nu_i-\gamma)^2-1}\right]\right)^{-1} X\left[\frac{1}{\nu_i}, z-z_0\right] e^{-\Sigma(z-z_0)/\nu_i}\psi_{\nu_i, 0}(f)\psi_{\nu_i, 0}(f_0)\right\}, \quad (8)$$

where X is expressed in terms of the unit step function ϑ

$$X\left[\frac{1}{\nu}, z-z_0\right] \equiv \frac{(z-z_0)}{|z-z_0|}\vartheta\left[\frac{z-z_0}{\nu|z-z_0|}\right]. \quad (9)$$

The equality $|\mathbf{w}-\mathbf{u}| = |\mathbf{w}_0-\mathbf{u}|$ is a consequence of the fact that if the nuclei have an infinite mass the system in which the nuclei rest is simultaneously the center of mass system, in which the modulus of the neutron momentum is conserved in an elastic collision. For $\gamma > 1$ it follows from this equality that the neutron velocities are directed only in the direction of motion of the medium and are contained within the cone $1 \geq \mu \geq \sqrt{1-\gamma^{-2}}$. Thus, if $\gamma > 1$, we have $G = 0$ for all $z < z_0$, i.e., the neutrons are completely entrained by the medium. It should be noted that the eigenfunctions that are found enable one to construct not only the Green's function for an infinite medium (for which there is no need once it has been obtained explicitly) but also to construct the solutions of various problems for a semi-infinite medium [1]. In particular, if the medium moves from a boundary in the albedo problem and $\gamma > 1$ for the incident neutrons, all the eigenfunctions vanish for $z < z_0$ and this means the absence of reflected radiation.

LITERATURE CITED

1. K. Case, Ann. Phys., 9, 1 (1960).
2. E. A. Garusov, A. A. Kostritsa, and Yu. V. Petrov, At. Énerg., 21, 128 (1966).
3. A. A. Kostritsa, At. Énerg., 14, 218 (1963).

STABILITY OF THE DIRECTIONAL DISTRIBUTION OF NEUTRONS IN REACTORS WITH A DISCRETE CONTROL SYSTEM

I. S. Postnikov and E. F. Sabaev

UDC 621.039.515

The stability of the directional distribution of neutrons in power reactors with a discrete control system is considered. The following control algorithm is proposed: a full, instantaneous compensation for the deviation of the power from its stationary value is effected at the end of each adjustment step (the step width is assumed to be constant). A similar problem was considered in [1] for the case of "pointwise" equations of reactor kinetics. The present article is a generalization of the results of [1] to the case of the equations of the diffusion approximation.

With these assumptions, the equations describing the dynamics of a reactcr with feedback derived from the xenon contamination have the form

$$A\varphi + \tilde{b}x + R = 0, \quad r \in \Omega; \quad (1)$$

$$\frac{\partial x}{\partial t} = Px + q\varphi, \quad \tilde{x} = (x_1, \ldots, x_\nu). \quad (2)$$

where φ denotes the derivation of the neutron flux from its stationary value; A is a linear operator whose spectrum is entirely located in the unbounded right semiplane; P is a $\nu \times \nu$ matrix; q, b, and x denote $\nu \times 1$ column vectors; $\tilde{P}$ denotes the transposed matrix; φ is a scalar; and R is the regulating force. According to

Translated from Atomnaya Énergiya, No. 5, p. 445, May, 1971.

the control algorithm selected, it is assumed that the function $R(\mathbf{r}, t)$ is independent of t in the time intervals $(n\tau, (n+1)\tau)$, where $n = 0, 1, 2, \ldots$; it is also assumed that the function changes at $t = \tau, 2\tau, \ldots, n\tau R(\mathbf{r}, t)$ by an amount such that $\varphi(\mathbf{r}, n\tau) = 0$ for all $\mathbf{r} \in \Omega$. It follows from Eq. (1) that the function $R(\mathbf{r}, t)$ in the time interval $(n\tau, (n+1)\tau)$ is

$$R = -\tilde{b}x(\mathbf{r}, n\tau). \tag{3}$$

It was shown with the second Lyapunov method and with the Yakubovich matrix-inequality technique [2] that for small widths τ of the adjustment step, the stability of the zeroth solution of the system of Eqs. (1)-(3) is reduced to the determination of the conditions under which the smallest eigenvalue of the boundary problem

$$\frac{1}{2}(A + A^*)\psi - \varkappa(\mathbf{r})\psi = \mu\psi,$$

is positive, where

$$\varkappa(\mathbf{r}) = -\inf_{\omega \in [0, \infty)} \operatorname{Re} \frac{\tau}{2} (j\omega)\tilde{b}(j\omega E - P)^{-1} q;$$

and A* is the operator conjugated to the operator A. The applicability of the stability condition was considered for the particular case in which $A = A^*$ in Eqs. (1)-(3) and in which the system coefficients are independent of $\mathbf{r}$.

The critical width of the adjustment step for a one-dimensional model of a power reactor was calculated as an example in which the feedback derived from the xenon contamination was taken into account. It was shown that the critical width of the adjustment step amounts to several hours and increases considerably when a control system for the average power is used.

LITERATURE CITED

1. O. B. Ronzhin and E. F. Sabaev, At. Énerg., 24, 269 (1968).
2. V. A. Yakubovich, Avtomatika i Telemekhanika, 26, 577 (1965).

HYDRODYNAMICS OF FISSIONABLE MATERIALS

I. ACOUSTIC VIBRATIONS AT CONSTANT NEUTRON FLUX

V. M. Novikov

UDC 621.039.515

A theory of reactor criticality has been developed [1] in which oscillations in the density of the fuel are excited in the reactor. The reciprocal effect of the neutron flux on the hydrodynamics of the fissionable gas can be neglected, according to the underlying assumptions. This assumption would be valid when the amplitude of the neutron flux is not too large. At the present time, the possibility of utilizing gas-fueled reactors for MHD generators is being discussed in the literature. In pulsed MHD generators of this type, the neutron flux would have to reach levels of $\sim 10^{17}$ neutrons/cm^2·sec. In such a case the effect of the neutron flux on the hydrodynamics of the fissionable gas could no longer be ignored safely.* It is demonstrated in the article that the extent of this effect can be assessed from the value of the dimensionless ratio $\alpha = \beta(qNH/c_p c)$, where H is the reactor dimension; N is the neutron flux; β, c_p, c are respectively the volume expansion coefficient, specific heat, and the speed of sound traversing the fissionable material; q is the

*This could bring about reactor instability. The problem is discussed from the standpoint by Goryachenko [2].

Translated from Atomnaya Energiya, No. 5, p. 446, May, 1971. Abstract submitted June 19, 1970.

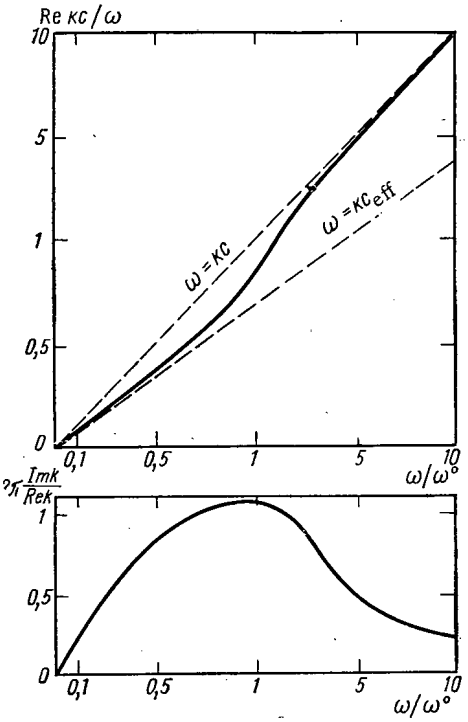

Fig. 1. Dispersion of acoustical oscillations in heat removal through the lateral surface of the channel, according to Newtonian law.

rate of heat generated per unit mass due to unit neutron flux. In the case of an ideal gas $\alpha = (\gamma - 1)qNH/c^3$, where $\gamma = c_p/c_v$. In the case of UF_6, when $H \sim 1$ m, the critical neutron flux ($\alpha(N_{cr}) = 1$) would be $\sim 10^{15}$ to 10^{16} neutrons/cm^2·sec. The law of dispersion of acoustic oscillations in a fissionable gas subjected to a constant neutron flux of sufficiently great intensity is derived for different heat conduction mechanisms. The diagram shows the dispersion of acoustic oscillations along the channel axis for the case of heat exchanged with the laws according to Newtonian law.

It is clear from the diagram that the speed of sound increases by a factor of $\sqrt{2}$ in the case of slow oscillations. The logarithmic growth rate of the oscillations peaks at the frequency $\omega = \omega^0 \equiv (\gamma - 1)qN/c^2$. Dispersion of acoustic oscillations at a high value of the thermal diffusivity is investigated (for the case of radiative heat transfer). In that case, in the limit as $k \to 0$, $\omega \sim k^{2/3}$. It is demonstrated that there exists a portion of the spectrum where v_g and v_{ph}, the group velocity and phase velocity of sound, satisfy the constraints

$$v_g v \ll c; \quad v_{ph} \gg c \text{ and } v_g v_{ph} \approx c^2.$$

The resulting formulas can be used in order to obtain qualitative assessments of the dispersion of sound in the gas flowing through the reactor core.

LITERATURE CITED

1. V. M. Novikov, At. Énerg., 27, 107 (1969); ibid., 30, 307 (1971).
2. V. D. Goryachenko, At. Énerg., 24, 374 (1968).

ABSORPTION OF γ-RADIATION IN RADIATION-CHEMICAL REACTORS IN PROCESSES CARRIED OUT IN HETEROGENEOUS AGITATED SYSTEMS

L. V. Popova, B. M. Terent'ev,
N. V. Kulikova, S. K. Dubnova,
and A. Kh. Breger

UDC 539.122.173

The Monte Carlo method was applied to calculations of the γ-emission energy distribution of Co^{60} in a radiation-chemical reactor with a heterogeneous medium under irradiation. A test-stand facility used in the synthesis of dibutyl tin dibromide was employed to determine the energy of γ-radiation absorbed in the source, in the structural members, and in the reaction volume of the chemical reactor. The reaction mixture constitutes a heterogeneous system consisting of metallic tin powder and liquid butyl bromide.

The dependence of the integrated absorbed dose in the reaction volume on the dimensions of the reaction volume was investigated with the object of optimizing the performance parameters of the radiation-chemical reactor. It was found that the highest efficiency of the equipment is achieved when the diameter /height ratio of the radiation-chemical reactor is 1.2. Figure 1 shows how the absorbed dose rate varies

Translated from Atomnaya Énergiya, No. 5, p. 447, May, 1971. Abstract submitted March 9, 1970.

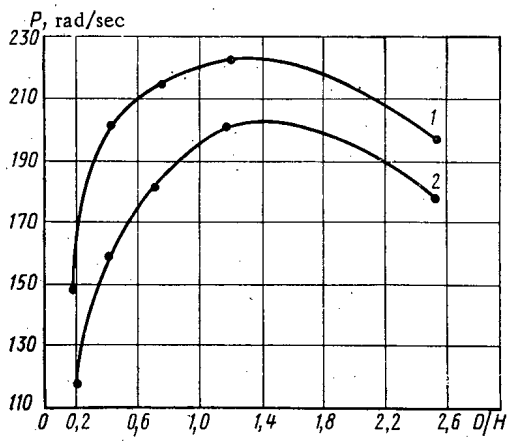

Fig. 1. Relationship between absorbed dose rate and diameter/height ratio (D/H) of radiation-chemical reactor.

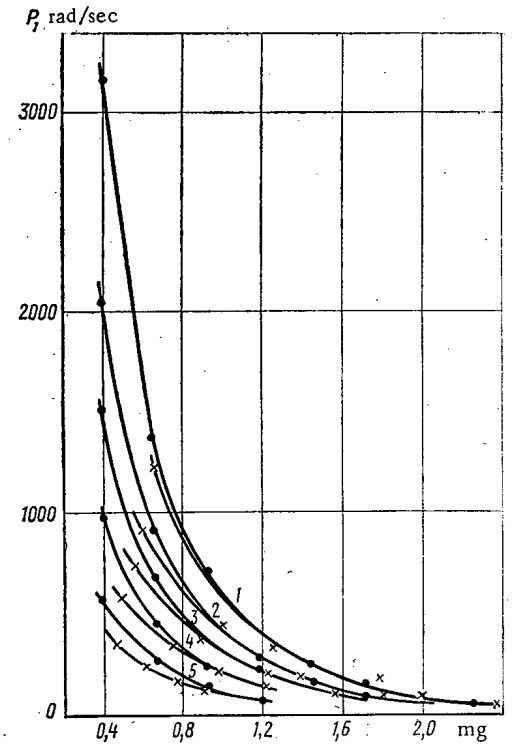

Fig. 2. Dependence of absorbed dose rate on distance in relaxation lengths (μ = 0.133 cm^{-1}) for different D/H values: 1) 2.5; 2) 1.07; 3) 0.65; 4) 0.31; 5) 0.13. •) Engineering physics calculations; ×) Monte Carlo method.

with the diameter/height ratio (D/H) of the radiation-chemical reactor at two values of the weight ratio of tin to butyl bromide, 1:1 and 1.10 (curves 1 and 2, respectively).

Calculations of the efficiency and distribution of the absorbed dose rate along the radius of the radiation-chemical reactor (with an axial irradiator) were carried out. Figure 2 shows the results of calculations carried out by two methods: by the Monte Carlo method and by engineering physics calculations. The maximum discrepancy in the results is 25%.

THE USE OF HIGH-VOLTAGE ALTERNATING CURRENT FOR INDUSTRIAL RADIATION PROCESSES

L. V. Chepel'*

UDC 541.15:621.3.038.624

The use of electron accelerators, primarily those with a constant electron energy in the 300-500 keV range, has recently increased in industrial processes.

However, it may be shown that for industrial accelerators the energy of the emissions generally need not be constant in the given range. On the one hand, every softening of the accelerator's energy spectrum increases the fraction of the beam energy absorbed at the output window; on the other hand, because of the specific nature of the electrons' interaction with the substance, the uniformity of the dose absorbed in the surface layers of the irradiated material is improved.

Therefore, in principle optimal spectral shapes and conditions of irradiation may be found for which, in the final analysis, the efficiency of the electron beam, for a given degree of uniformity of irradiation of a material, will be comparable to the efficiency of a monoenergetic beam.

In this connection it is interesting to consider the possibility of using a high voltage alternating current to feed the accelerator tubes of industrial radiation equipment. Realization of this possibility in the 300-750 keV energy range will simplify the construction of accelerator equipment to a considerable extent and increase reliability through the use of either high voltage power supplies containing no rectifiers or condensers, or electrical transmission lines at a corresponding voltage.

In the article the advantages of using an electron beam with a sinusoidal energy spectrum are evaluated analytically. The corresponding integral curves are obtained by approximating the distribution curve of the deep dose by a sine wave segment. From these curves the energy efficiency of the electron beam and the degree of depth nonuniformity of the dose in the material were determined for irradiation from two sides.

The method of sweeping the sinusoidal-spectrum electron beam by modulating the deviating magnetic field was proposed. The shape of the modulating magnetic field sweep curve and the relationship of its frequency to the electron kinetic energy were found.

A METHOD OF CALCULATING THE BASIC PARAMETERS OF RADIATION INSTALLATIONS IN THE IRRADIATION OF STATIONARY SYSTEMS WITH ACCELERATED ELECTRONS

K. I. Nikulin†

UDC 621.039.83:541.15

In calculating the parameters of radiation installations [1] used for carrying out processes in stationary systems (the cross-linking of polyethylene, the vulcanization of industrial rubber products, etc.), using accelerated electrons, one of the most important problems is to make sure that the absorbed doses are uniformly distributed throughout the volume of the irradiated material.

The initial data for calculating the parameters of radiation installations are the following: the dimensions and shape of the object, the composition and density of the material, the magnitude of the absorbed

*Translated from Atomnaya Énergiya, No. 5, p. 448, May, 1971. Original article submitted May 28, 1970; revision submitted October 2, 1970.

†Translated from Atomnaya Énergiya, No. 5, pp. 448-449, May, 1971. Original article submitted July 10, 1970.

dose, the allowable nonuniformity of the field of absorbed doses in the irradiated object, and the productivity of the installation.

Investigations include the solution of the following problems: choosing the method of equalizing the field of absorbed doses in the object, calculating the field of absorbed dose rates in the object; the nonuniformity of the field of absorbed doses in the material, and the conditions ensuring a prescribed uniformity of irradiation; calculating the energy of the accelerated electrons, energetic efficiencies, the power of the electron source, the velocity of motion of the material in the irradiation zone, and the number of accelerators needed for a prescribed installation productivity. The first systematic investigations along this line were described in [1-4].

The present study gives a method for calculating the magnitudes of absorbed doses throughout the thickness of the material when it is irradiated with a wide beam of monoenergetic electrons. It describes a method for calculating the nonuniformity of the field of absorbed doses throughout the thickness of the material. It proposes irradiation methods which ensure that the absorbed doses will be uniform to within ±5%. It gives equations which can be used to determine the efficiency of utilization of the electronic radiation in various methods of equalizing the magnitude of the absorbed dose throughout the thickness of the material. It describes a method for calculating the basic parameters of radiation installations in the irradiation of stationary systems with a wide beam of monoenergetic electrons.

LITERATURE CITED

1. A. Kh. Breger et al., Fundamentals of Radiochemical Apparatus Design [in Russian], Atomizdat, Moscow (1967).
2. Yu. S. Ryabukhin et al., At. Énerg., 19, 535 (1965).
3. L. W. Chappell et al., in: Electron Accelerators [Russian translation], Atomizdat, Moscow (1966), p. 399.
4. K. I. Nikulin and G. A. Obraztsov, At. Énerg., 23, 50 (1967).

THE MONTE CARLO ALBEDO MONOENERGETIC γ-RAYS NORMAL TO BARRIERS OF VARIOUS MEDIA

D. B. Pozdneev, N. V. Krasnoshchekov, and A. V. Pichugin

UDC 539.122.04

The Monte Carlo method is used for calculating, with a unidirectional source, the spectral-angular and integral characteristics of γ-quanta back-scattered from various media. The study investigates the case of the normal incidence of primary γ-quanta with an energy E_0 of 0.145, 0.279, 0.511, 0.662, 1.0, and 1.25 MeV on barriers made of Be, C, Al, Fe, and Sn, whose thickness in the normal direction measured 0.1, 0.2, 0.4, 0.6, 1.0, and 2.5 times the free-path length of the primary γ-quanta. By means of a scintillation γ-spectrometer an experiment was conducted to investigate the spectral-angular distribution of the reflected "narrow-beam" γ-radiation of Cs^{137} from these media.

An analysis of the resulting data concerning the differential current numerical albedo for the above-mentioned situations showed that its variation as a function of the thickness may be described, with an accuracy of ±10%, by the formula

$$A^{(\theta)}(x) = A^{(\theta)}(\infty)\left[1 - e^{-\alpha(\theta)x}\right], \quad (1)$$

Translated from Atomnaya Énergiya, No. 5, p. 449, May, 1971. Original article submitted July 10, 1970; revision submitted October 21, 1970.

where $A^{(\theta)}(x)$ is the differential numerical current albedo for a barrier of thickness x times the free-path length; $A^{(\theta)}(\infty)$ is the same for the case of a semi-infinite scatterer; $\alpha(\theta)$ is an empirical quantity.

A formula that may be recommended for finding $A^{(\theta)}(\infty)$ is

$$A^{(\theta)}(\infty) = (a - b\cos\theta)\cos\theta, \tag{2}$$

where a and b are empirical quantities depending on E_0 and Z; θ is the exit angle of the photons, measured from the normal.

The study gives recommendations for finding the quantities appearing in formulas (1) and (2).

The variation of the integral numerical current albedo as a function of the thickness can be expressed, to within ±5-10%, by the empirical formula

$$A(x) = A(\infty)(1 - e^{-\alpha x}), \tag{3}$$

where $A(\infty)$ is the integral numerical albedo for a semi-infinite scatterer and α is an empirical quantity.

DEPENDENCE OF THE ELECTRONIC STATISTICAL SUM OF ATOMS ON THE CUTOFF PARAMETER OF ENERGY LEVELS

A. A. Zaitsev and R. A. Kotomina

UDC 539.183.3

The dependence of the electronic statistical sum of the atom (of a monatomic ion) on the cutoff parameter of the energy levels (understood here as ΔE, the maximum energy of an electron present in the electron in the bound state) was studied. The problem of approximate treatment of the contribution made by the highest energy levels to the electronic portion of the statistical sum is also discussed in the article. The assumption entertained in all the calculations is that the highest energy levels of the electron in the atom are similar to the energy levels of a charged particle moving through a central coulomb field. For such a field, the electron distribution is given by the formula

$$d\omega_K = BE^{-5/2}\,dE, \tag{1}$$

where $d\omega_K$ is the number of quantum states of an electron with energy from E to E + dE, and B is a constant.

For convenience in the computations, the concept of the Coulomb statistical sum is introduced, and is understood as the electronic statistical sum of the atom. All the electron levels are assumed to be Coulomb levels in this sum. On the basis of Eq. (1), we proceed to find the explicit dependence of $\ln Q_K$ on ΔE:

$$\ln Q_K(\Delta E) = \ln Q'_K + \varphi(\Delta E), \tag{2}$$

where $\ln Q'_K$ is a part of $\ln Q_K(\Delta E)$ which is independent of ΔE, and

$$\varphi(\Delta E) = 3I_0^{3/2}\exp\left(-\frac{\cdot}{kt}\right)\left[\frac{2}{3}\Delta E^{3/2} + \frac{2}{kt}\Delta E^{-1/2} - \frac{1}{(kT)^2}\Delta E^{1/2} + \ldots\right]. \tag{3}$$

The dependence of the chemical potential I on ΔE and T is obtained in the form

$$I = I_1 + f(\Delta E),$$

where

$$I_1 = I_0\left(1 + \frac{5}{3}y_0 + 6y_0^2 + 4.745y_0^3 + \ldots\right);$$

$$f(\Delta E) = \frac{\varphi(\Delta E, I_1)}{3I_0^{3/2}I_1^{-5/2}(1 + 5.833y_1 + 67.376y_1^2 + \ldots) + \frac{1}{kT}\varphi(\Delta E, I_1)}; \tag{4}$$

$$y_0 = \left(\frac{\pi kT}{2I_0}\right)^2; \quad y_1 = \left(\frac{\pi kT}{2I_1}\right)^2;$$

Translated from Atomnaya Énergiya, No. 5, pp. 449-450, May, 1971. Original article submitted July 1, 1970; revision submitted September 23, 1970.

I_0 is the ionization potential of the atom; k is the Boltzmann constant. In order to find the dependence of the true electronic statistical sum of the atom $Q(\Delta E)$ on ΔE, we break up the entire energy interval of the electron in the atom into two parts such that levels lying above a certain level designated ΔE, may be treated as coulomb levels. On the basis of Eq. (2), it is shown that the formula

$$\ln Q(\Delta E) = \ln Q(\Delta E_1) + \varphi(\Delta E) - \varphi(\Delta E_1) \tag{5}$$

will be valid for ln $Q(\Delta E)$. The lower energy levels are known for most atoms, to sufficient accuracy; these can be used to compute ln $Q(\Delta E_1)$ by direct summation. Accordingly, Eq. (5) can be used to compute the electronic statistical sum of the atom for any cutoff parameter ΔE however small, provided the lowermost energy levels of the atom and the ionization potential of the atom are known. The article cites the results of computations of the electronic statistical sum of indium atoms and lead atoms, using the method proposed, for temperatures up to 14,000°K. The data are compared to values of Q_{el} of those atoms reported in the literature.

EFFECT OF PRESSURE ON ELECTRONIC STATISTICAL SUMS OF ATOMS AT HIGH TEMPERATURES

A. A. Zaitsev and R. A. Kotomina

UDC 539.183.3

An approximate method is proposed for limiting the electronic energy levels of an atom present in a weakly ionized plasma at high temperatures. The atom is treated as a system consisting of a nucleus and the electron gas surrounding the nucleus. The effect of the remaining atoms and ions surrounding the atom in question and perturbing its outer electronic levels reduces to the fact that the electron gas is acted upon by a certain external pressure of p equal to the total pressure exerted by the gas. That distance ΔE from the nucleus at which the pressure exerted by the electron gas becomes equal to the external pressure p is represented by the radius of the sphere confining the atom in question.

Assuming that the higher-lying energy levels of any atom are Coulomb levels, and applying to the electron gas the familiar thermodynamic relations

$$p = -\left(\frac{\partial F}{\partial v}\right)_T; \qquad F = -kT \ln Q, \tag{1}$$

we can obtain a formula linking the cutoff parameter ΔE of the energy levels and the pressure and temperature of the monatomic gas in the form

$$p = \frac{m^{3/2}kT}{\sqrt{2}\,\pi\hbar^3} \ln\left[1 + \exp\left(\frac{\Delta E - J}{kT}\right)\right] \Delta E^{3/2}, \tag{2}$$

where m is the mass of the electron; k is Boltzmann's constant; J is the absolute value of the chemical potential (the dependence of J on T, ΔE, and on the ionization potential of the atom J_0 is obtained).

For practical applications, formula (2) is applied through the expansion of $\ln[1 + \exp(\Delta E - J/kT)]$ in a series in powers of $(\Delta E/kT)$, so that Eq. (2) can be transformed to the form

$$\Delta E^{3/2} \exp\left(\frac{\Delta E}{kT}\right) = \frac{p}{1{,}687 \cdot 10^4 kT} \exp\left(\frac{J}{kT}\right), \tag{2a}$$

where (kT), J, and ΔE are expressed in electron-volts; and p is expressed in atmospheres. ΔE is calculated from specified p and T by a graphical method.

The effective charge does not appear in Eqs. (2), so that ambiguities attendant upon the definition of that parameter can be avoided, and Eqs. (2) can be applied to monatomic ions as well with no modifications.

Translated from Atomnaya Énergiya, No. 5, p. 450, May, 1971. Original article submitted July 1, 1970; revision submitted September 23, 1970.

The example of the lead atom is used over a broad range of temperatures and pressures in this method for calculating the cutoff parameter ΔE, and comparing it to methods developed elsewhere in the literature.

The procedure outlined is applied to calculations of the cutoff parameter of the energy levels of the uranium atom for temperatures to 10,000°K and pressures from 0.01 to 100 atm. These data then provide a basis for obtaining values of the natural logarithm of the electronic statistical sum and the reduced thermodynamic potential of monatomic uranium in the ideal gas state, for the indicated range of temperatures and pressures. It is pointed out that $\ln Q_{el}$ of uranium obeys a marked pressure dependence at T = 10,000°K.

PARTICLE TRAJECTORIES IN AN ISOCHRONOUS CYCLOTRON IN THE PRESENCE OF ACCELERATION. II

Yu. K. Khokhlov

UDC 621.384.611

Time and spatial oscillations of a particle moving in the median plane of a cyclotron are discussed in the article. "Ideal" curves, i.e., trajectories rotating uniformly [1], are used as the coordinate curves. On each portion of the trajectory outside the slits, the position of a particle possessing a momentum p is reckoned from the ideal trajectory belonging to the same momentum p according to the formulas

$$\tau(\vartheta) = t(\varphi) - t_{id}(\varphi); \quad x(\vartheta) = [R(\varphi) - R_{id}(\varphi)]\cos\psi(\varphi).$$

Here t is the time; R, φ are polar coordinates; $\vartheta = \vartheta(\varphi)$ is the generalized azimuth; $\tan\psi(\varphi) = R_e'(\varphi)/R_e(\varphi)$; $R_e(\varphi)$ is the equilibrium (closed) orbit. The linearized equations of motion outside the slits and the boundary conditions on the slits acquire the form

$$\frac{d}{d\vartheta}\mathbf{X}(\vartheta) = \hat{G}(\vartheta)\mathbf{X}(\vartheta); \quad \Delta\mathbf{X}(\vartheta_j) = -p_j^{-1}\varepsilon_j\hat{\Gamma}(\vartheta_j)\mathbf{X}(\vartheta_j). \tag{1}$$

Here $\hat{G}(\vartheta)$, $\hat{\Gamma}(\vartheta)$ are three-row matrices all of whose elements are defined on the corresponding equilibrium orbit $R_e(\varphi)$; $\mathbf{X}(\vartheta)$ is a vector with the components $\tau(\vartheta)$, $x(\vartheta)$, $x'(\vartheta)$; $\Delta\mathbf{X}(\vartheta)$ is the jump increment of the vector $\mathbf{X}(\vartheta)$ upon traversing the j-th slit; $\varepsilon = \omega_c^{-1}[d\Delta W(t)/dt]_{t-t_{id}}$ is the "varying acceleration" parameter; ω_c is the frequency of revolution of the particle; $\Delta W(t)$ is the increment in the kinetic energy W on the slit at time t.

The system (1) is solved in terms of generalized amplitudes and phases in Floquet theory extended to the case of quasiperiodic motion. The resulting formulas describe the behavior of the vector $\mathbf{X}(2\pi n)$ as a function of the number of revolutions n when the azimuth of observation is fixed. The vector $\mathbf{X}(2\pi n)$ moves with a frequency $\mu = 2\pi(\nu_x - 1)$, where ν_x is the frequency of radial betatron oscillations over the surface of a three-dimensional ellipsoid whose parameters in turn vary smoothly with increasing n.

In the case of a cyclotron of the type described in [2] with two dees, all the effects related to ε are divided into proportional parts $|\varepsilon_I| + |\varepsilon_{II}|$ and $|\varepsilon_I| - |\varepsilon_{II}|$ (I, II are numbers assigned to the slits in the semirevolution $0 \le \varphi \le \pi$). Under rigorously isochronous acceleration conditions we have $|\varepsilon_I| = |\varepsilon_{II}|$, i.e., effects of the second kind are absent. Effects of the first kind are manifested specifically in an appreciable inclination of the axes of the ellipsoid, the shift of the center of the ellipsoid relative to the origin of coordinates, "smearing" of the boundaries of the bunch, and of the energy distribution. The sufficient condition for energy separation of bunches of adjacent n values takes the form $|W_n(\mathbf{X}_{n_0}) - W_n(0)| \ll N_s\Delta W_{id}$, where $W_n(\mathbf{X}_{n_0})$ is the energy of the particle making its n-th revolution; $\mathbf{X}_{n_0}$ is the initial deviation from the ideal trajectory; $N_s\Delta W_{id}$ is the energy increment on the ideal trajectory in a single revolution; N_s is the number of slits. In the formula derived for $W_n(\mathbf{X}_{n_0}) - W_n(0)$, special interest attaches to the logarithmically growing term equal, according to estimates, to

Translated from Atomnaya Energiya, No. 5, p. 451, May, 1971. Abstract submitted June 9, 1970.

$$W_n(X_{n_0}) - W_n(0) \approx 4\Delta W_{id}\, 0{,}726 \cdot 10^{-4} \cdot 2\omega_c \tau_{n_0} \ln \frac{n}{n_0} \approx \pm 4\Delta W_{id} \cdot 1{,}67 \cdot 10^{-3}. \quad (2)$$

Here $2\omega_c \tau_{n_0} = \pm 5°$ is the initial phase of the particle; $\ln (n/n_0) \approx \ln 100 = 4.6$. The estimate (2) shows that the growing term has, under real conditions, a shift comprising about 0.1% of the energy step. This satisfies with above condition with a wide margin to spare.

LITERATURE CITED

1. Yu. K. Khokhlov, At. Énerg., 29, 39 (1970).
2. I. Ya. Barit et al., FIAN Preprint [in Russian], No. 15 (1969).

CRITICAL CURRENT IN AN ACCELERATING WAVEGUIDE WITH RADIAL SLITS PROVIDED IN DISCS

A. K. Orlov

UDC 621.384.644.3.01

The maximum charge which can be accelerated in a conventional linear accelerator is limited by the "current-pulse contraction effect" which results from the excitation of a hybrid EH_{11} mode in the waveguide. The hybrid mode can be suppressed with the aid of radial slits provided in discs [1]. Experiments have shown that this method helps to increase several times the accelerated charge [2].

The present article outlines the results of a theoretical investigation of the properties of the EH_{11} wave in a waveguide provided with slits in discs. The critical current was calculated. The electrodynamic properties of the waveguide were analyzed with the method of partial areas, which leads to the following dispersion equation:

$$\sum_{m=-\infty}^{\infty}{}' \left(\frac{\sin n_m \Delta}{n_m \Delta}\right)^2 \frac{1}{\Lambda_{nm}} = \frac{D}{t} \sum_{m=-\infty}^{\infty}{}' \frac{\sin n_m \Delta}{n_m \Delta} \cdot \frac{C_{nm}}{\Lambda_{nm}} + \frac{2\pi}{pks} \operatorname{ctg} kl;$$

$$\Lambda_{nm} = n_m - \frac{(ka)^2}{n_m + 1} - \frac{ka Z'_{n_m}(ka)}{Z_{n_m}(ka)} \cdot \frac{(kD)^2}{2(1 - \cos kD)};$$

$$C_{nm} = \frac{n_m}{Z_{n_m}(ka) \sin kl} \int_{ka}^{k(a+l)} \frac{Z_{n_m}(x)}{x} \sin [x - k(l + a)]\, dx,$$

where k denotes the wave number; D is the period of the structure; t is the thickness of the disc; a is the radius of the center opening; $s = 2a\Delta$; l is the width and the length of the slits (total number of slits p); and Z_{n_m} is a combination of Bessel functions with the number n_m.

It was shown that the dispersion curve is shifted into the low-frequency range when l increases. The quality factor Q of the system was determined.

It was shown in an example that Q decreases 30 times when l is rather large (approximately 20 mm). The strong attenuation of the hybrid mode can be explained by losses of the high-frequency power in the slits along which high-intensity currents flow.

The results were used to determine the critical current in the sections of a 2 GeV accelerator [3] ($I_{cr} \approx 7$ A). The value $I_{cr} = 0.14$ A holds for sections without slits in the discs.

LITERATURE CITED

1. V. M. Levin and V. L. Smirnov, Author's Certificate No. 197785, Byull. Izobret., No. 13 (1967).

Translated from Atomnaya Énergiya, No. 5, pp. 451-452, May, 1971. Abstract submitted July 10, 1970.

2. V. M. Levin, V. L. Smirnov, and L. P. Fomin, Proceeding of the International Conference on High-Energy Accelerators, Cambridge, USA (1967), p. A39.
3. G. D. Kramskoi et al., Zhur. Tekh. Fiz., 39, 2054 (1969).

MAGNETIC SYSTEM OF A SUPERCONDUCTING 50 MeV ISOCHRONOUS PROTON CYCLOTRON

L. A. Sarkisyan

UDC 621.384.633:537.312.62

Research conducted in recent years with the object of developing superconducting accelerators with a time-constant guide magnetic field has been reported in the literature. A synchrocyclotron in a superconducting variant accelerating protons to 100 MeV with a magnetic field intensity of 50 kOe has been discussed at the Radiotechnical Institute of the USSR Academy of Sciences. Superconducting ring synchrocyclotron projects in sectored and spiral variants have been developed at the Physics Institute of the USSR Academy of Sciences, and at Brookhaven, Illinois, and Argonne (USA).

Topics relating to the development of a magnetic system for a superconducting isochronous cyclotron accelerating protons to 50 MeV at a field level $H_0 = 50$ kOe at the center, and beam extraction features, are discussed in the article. The salient features of the accelerator are: 1) dependence of superconductor current on external field in cross section of the coil which will bring about current limitations; 2) relatively low fill factor of the coil cross section enclosing the superconductor (~20%); 3) difficulties in shaping a field to within $\pm 5 \cdot 10^{-4}$ error, since the transition to superconductivity brings about a reduction mainly in the radial dimensions of the machine; 4) presence of internal windings, in addition to the external winding, thereby limiting the current flowing through the windings. When these requirements are taken into account, the shaping of the center field and of the fundamental harmonic of the field can be achieved with the aid of nine concentric windings (basic winding and eight correction windings) and a flat harmonic winding (NbTi conductor). All the windings are placed within a single cryostat.

Analysis showed that spatial field variation with high helicity should be used in order to achieve axial stability of the particles in the accelerator, rather than azimuthal field variation. The basic accelerator parameters assigned were: $H_0 = 50$ kOe, number of spirals 3, parameter of Archimedean spiral 4 cm, frequencies of betatron oscillations $0 \leq Q_Z \leq 0.2$, $1 \leq Q_2 \leq 1.066$, final acceleration radius 20 cm (radius for field shaping 22 cm). When the field is shaped in the median plane of the accelerator, attention is given to the field distribution throughout the cross section of the windings, so that the calculated current values will not exceed the critical values.

The beam power in the accelerator may be ~50 kW at the final radius. A method involving introduction of a local inhomogeneity of the magnetic field at a finite radius is discussed as a means of maximizing beam extraction efficiency, and makes it possible to lower the frequency of radial betatron oscillations $Q_r = 1.066$ to unity. The frequency Q_Z increases to 0.33 in the process. The parameters of the flat superconducting (Nb_3Sn) winding shaping the required gradient of ~3000 Oe/cm were determined.

This projected superconducting isochronous cyclotron will constitute a compact low-cost source of multiply charged ions and polarized particles with smooth energy control, and the use of high magnetic fields ($H_0 \geq 50$ kOe) in accelerators at low energies and medium energies will make it possible to increase beam intensity several times.

Translated from Atomnaya Énergiya, No. 5, p. 452, May, 1971. Abstract submitted September 30, 1970.

LETTERS TO THE EDITOR

PHYSICAL PROPERTIES OF URANIUM DODECABORIDE

V. V. Odintsov and Yu. B. Paderno

UDC 669.822.5

Practically no work has been done on the physical properties of dodecaborides of metals with a UB_{12} structure, particularly UB_{12} itself.

A study of the phase diagram of the system U–B [1] established that the melting point of UB_{12} is 2235°C. According to [3], the microhardness of this compound exceeds 2000 kg/mm^2.

Uranium dodecaboride powder was obtained by reducing uranic oxide by boron in vacuum at 1500°C by the method in [2, 4]. To avoid contamination of the product, the process was performed in zirconium diboride crucibles, using tungsten heaters and removing the surface layer of ~0.5 mm.

X-ray and metallographic analysis showed that the product contained only one phase; the lattice constant of 7.472 Å agrees exactly with [2, 5].

Specimens for this investigation of the physical properties were obtained by sintering pressings in a charge of the same material. The porosity of the specimens was 20-25%; its effect on their physical characteristics was taken into account by methods in [6, 7].

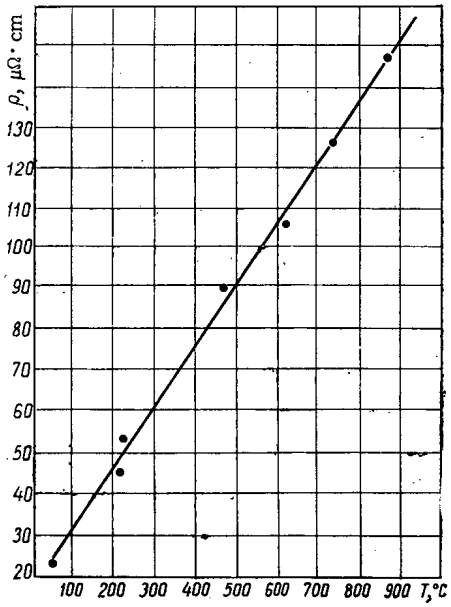

Fig. 1. Resistivity of uranium dodecaboride versus temperature.

As a result of this investigation of UB_{12}, the following were determined: the resistivity 23 $\mu\Omega \cdot$ cm (see Fig. 1); the thermal resistance coefficient $2.3 \cdot 10^8$ deg^{-1}; the Hall coefficient $-0.24 \cdot 10^{-4}$ cm^3/C; the coefficient of thermal expansion $\alpha_{-177+20°C} = 2.55$; $\alpha_{20°C} = 4.6$; $\alpha_{20-300°C} = 5.8$; $\alpha_{300-1000°C} = 6.5 \cdot 10^{-6}$ deg^{-1}; the coefficient of radiation $\varepsilon_\lambda = 0.75$–$0.60$ (900-1700°C); the characteristic temperature, assessed from [8], is 980°K and the mean-square amplitude of elastic vibrations 0.044 Å.

An assessment of the criterion δ [9], indicating the predominant type of conductivity, revealed (in contrast to dodecaborides of trivalent rare earths) the inapplicability of the single-band model for this compound.

These results enable us to draw the conclusion that uranium dodecaboride is a metalloid compound with typical metallic properties. The low values of the coefficient of thermal expansion and the mean-square amplitudes of elastic vibrations confirm the determining role of the boron skeleton in its structure. By analogy with borides of trivalent metals, the electrical conductivity is apparently effected in bands formed by the metal atoms.

LITERATURE CITED

1. B. Howlett, J. Inst. Metals, 88, 91 (1959).
2. Yu. B. Paderno, At. Énerg., 10, 396 (1961).
3. R. Kieffer and F. Benezovskii, Hard Materials [Russian translation], Metallurgiya, Moscow (1968).
4. G. V. Samsonov, Yu. B. Paderno, and T. I. Serebryakov, Kristallografiya, 4, 542 (1959).
5. F. Bertaut and P. Blum, Compt. Rend., 229, 667 (1949).
6. V. V. Skorokhod, Inzh. Fiz. Zh., 11, No. 2 (1959).

Translated from Atomnaya Énergiya, No. 5, p. 453, May, 1971. Original letter submitted May 25, 1970.

7. H. Juretschke and R. Steinitz, J. Phys. Chem. Solids, 4, 118 (1958).
8. V. S. Neshpor, Fiz. Metallov i Metallovedenie, 7, 559 (1959).
9. S. N. L'vov, V. F. Nemchenko, and G. V. Samsonov, Dokl. Akad. Nauk SSSR, 135, 577 (1960).

ASYMPTOTIC BEHAVIOR OF A NEUTRON PULSE IN A "HARD" BREEDER SYSTEM

Yu. A. Platovskikh and I. V. Sergeev

UDC 621.039.51.12

It is known that in a homogeneous system there can be no discrete neutron flux decay constants λ, greater than $(v\Sigma)_{min} = \alpha$. The quantity α determines the boundary of the continuous spectrum. In experiments with "hard" installations, it is sometimes actually observed that exponential decay of a neutron pulse does not occur at sufficiently great subcriticality (5-20%). In other cases exponential decay is observed when $\lambda > \alpha$ [1].

In this paper an attempt is made to determine the asymptotic behavior of fission chamber responses m(t) when there are no discrete decay constants. We shall consider that the system is homogeneous and "hard" enough that there are no thermal neutrons in it. It is shown in [1] that if a Laplacian transformation is applied to the equation

$$\frac{\partial n}{\partial t} + Ln = \chi(v) \int_0^\infty v\Sigma_f n(v')\, v'\, dv' + S(v)\,\delta(t), \tag{1}$$

then the Laplacian transformation $\bar{m}(s)$ of the fission chamber responses may be written in the form

$$\bar{m}(s) = \frac{k_S(s)}{1 - k_\chi(s)}. \tag{2}$$

In Eqs. (1) and (2), n = n(v, t) is the neutron density; L is an operator which describes neutron moderation and accounts for leakage in the form DB^2; $\chi(v)$ is the fission spectrum; S(v) is the spectrum of the pulse source; and

$$\bar{m} = \int_0^\infty v\Sigma_f \bar{n} v\, dv; \quad \bar{n} = \int_0^\infty n e^{-st}\, dt;$$

$$k_S = \int_0^\infty v\Sigma_f \bar{n}_S v\, dv; \quad k_\chi = \int_0^\infty v\Sigma_f \bar{n}_\chi v\, dv,$$

where $\bar{n}_S$ and $\bar{n}_\chi$ are solutions to the equations

$$(s + L)\,\bar{n}_S = S, \qquad (s + L)\,\bar{n}_\chi = \chi.$$

Characteristic values (poles of $\bar{m}(s)$) are determined from the equation $k_\chi(s) = 1$. When $s = -\alpha$, $\bar{m}(s)$ has a branch point. In our case $\bar{m}(s)$ is monotonic on the real axis when $-\alpha < s < \infty$, and so there is only one characteristic value (or none). The equation $k_\chi(-\alpha) = 1$ determines the boundary size of the system at which the discrete characteristic number reaches the bounds of the continuous spectrum. The quantity $k_\chi(-\alpha)$ is equal to the effective neutron multiplication coefficient in a system without 1/v absorption.

In Wigner's approximation

$$Ln = v\Sigma n - \frac{2}{\xi} v^\delta \int_v^\infty \Sigma_s(v')\, v'^{-\delta} dv'; \quad \delta = \frac{2}{\xi} - 1. \tag{3}$$

If we consider that $v\Sigma = vDB^2 + v\Sigma_S + \alpha$ and $v\Sigma_f = \beta$, where D, Σ_S, α, and β are constant, then for a system boundary size corresponding to B_0^2 the following equation may be found:

Translated from Atomnaya Énergiya, No. 5, pp. 454-455, May, 1971. Original letter submitted June 21, 1970.

$$DB_0^2=\beta\nu\int_0^\infty\frac{\chi\,d\nu}{\nu}+\frac{\xi\Sigma_s}{2-\xi}. \tag{4}$$

When $B > B_0$, there are no discrete characteristic numbers.

Suppose that both sources are monoenergetic: $\chi(\nu) = \delta(\nu - \nu_0)$, $S(\nu) = \delta(\nu - \nu_S)$. Then in Wigner's approximation we obtain

$$k_\chi(\omega)=\frac{\nu_0\beta\nu}{\Sigma_0(\nu_0+\omega)}+\frac{2\Sigma_s\nu_0\beta\nu}{\xi\Sigma_0^2(\delta+1)}(\nu_0+\omega)^{\delta-\rho}\omega^{-\delta+\rho-2}\,{}_2F_1\left(\delta-\rho+2,\ \delta+1;\ \delta+2;\ -\frac{\nu_0}{\omega}\right);$$

$$\Delta k=1-k_\chi(-\alpha)=1-\frac{\beta\nu}{\nu_0\Sigma_0}-\frac{2\beta\nu\Sigma_s}{\xi\Sigma_0^2\nu_0(\rho-1)};$$

$$\Sigma_0=\Sigma_s+DB^2;\quad \rho=\frac{2DB^2}{\xi\Sigma_0}; \tag{5}$$

$$\omega=\frac{s+\alpha}{\Sigma_0}.$$

If $\nu_S \gg \nu_0$ and $1 < \rho < 2$, then for small values of ω corresponding to large t, we obtain the approximation

$$\overline{m}(\omega)\approx\frac{1}{\Delta k+c\left(\frac{\omega}{\nu_0}\right)^{\rho-1}};\quad c=-\frac{\beta\nu\Sigma_s\Gamma(\delta+2)\,\Gamma(1-\rho)}{\Sigma_0^2\nu_0\Gamma(\delta-\rho+2)}, \tag{6}$$

in which $\Delta k \geq 0$ when there are no discrete characteristic numbers, and $\Delta k < 0$ when there are. A discrete characteristic value near the boundary of the continuous spectrum is determined by the expression

$$\frac{\omega_0}{\nu_0}=\frac{\alpha-\lambda}{\nu_0\Sigma_0}=\left(\frac{|\Delta k|}{c}\right)^{\frac{1}{\rho-1}}, \tag{7}$$

which is analogous to the formula for the reciprocal numbers when the subcriticality is great (λ close to α). The residue of $\overline{m}(\omega)$ when $\omega = \omega_0$, i.e., the amplitude of the exponential part of m(t), approaches zero when $\lambda \to \alpha$. When there are no discrete characteristic values, the inverse Laplacian transformation of expression (6) yields a real integral, and the asymptotic behavior of m(t) is represented as follows:

$$m(t)\approx e^{-\alpha t}\left(t^{-\rho}+A\,\frac{e^{-\Lambda_0 t}}{t}\right), \tag{8}$$

where $\Lambda_0 = \Sigma_0\omega_0$.

If $\rho > 2$, then $\omega_0 \sim \Delta k$, and m(t) is also represented by expression (8) when there are no discrete characteristic numbers, but the second exponent is proportional to $-\Delta kt$. Equation (8) also describes m(t) when $\chi(\nu) = \nu^2 e^{-a\nu^2}$ (actual fission spectrum). The limits show that, for not very large t, large ρ, and Δk, the second term of expression (8) will be important, i.e.,

$$m(t)\approx\frac{e^{-(\alpha+\Lambda_0)t}}{t}, \tag{9}$$

which corresponds to nearly exponential behavior of m(t) outside the continuous spectrum with a time constant of $\alpha + \Lambda_0$. For large times ($t \to \infty$) the first term of Eq. (8) will predominate, and $m(t) \approx t^{-\rho}e^{-\alpha t}$, where the exponent no longer depends on the subcriticality. Thus, outside the continuous spectrum three types of detector indications are possible, depending on the system parameters and time.

1) There is no definite exponent when both terms of m(t) are about equally important at the time of observation. In this case m(t) will be a concave function.

2) The behavior of m(t) is nearly exponential, with a time constant $\alpha + \Lambda_0$ which depends on the subcriticality. This time constant may be considered a characteristic of the system, even when there is a discrete time constant. The quantity $\alpha + \Lambda_0$ is related to the effective multiplication constant in the same way a discrete characteristic number is [see Eq. (7)].

3) The behavior of m(t) is nearly exponential, with a time constant α, which does not depend on the subcriticality.

At least the first two types of behavior in m(t) are observed in experiments with "hard" installations [1, 2]. For other energy functions of the cross section, the asymptotic behavior of m(t) remains the same, but the exponents change in the preexponential factors.

LITERATURE CITED

1. F. Storrer, Pulsed Neutron Research, Vol. 2, IAEA, Vienna (1965).
2. W. Patterson et al., Pulsed Neutron Research, Vol. 2, IAEA, Vienna (1965).

SCATTERING OF 14 MeV NEUTRONS BY IRON

M. E. Gurtovoi, E. P. Kadkin,
A. S. Kukhlenko, B. E. Leshchenko,
V. M. Neplyuev, G. Peto,
and L. S. Sokolov

UDC 539.171.4

The characteristics of excited states of the Fe^{56} nucleus have been comparatively closely studied. The first 2^+ state (0.85 MeV) and the 3^+ state (4.51 MeV) are strongly excited in inelastic scattering of electrons, protons, dueterons, and α-particles [1-5]. These states are satisfactorily represented by the collective (vibration) model in cross-section calculations by the distorted-wave method, and in the formalism of linked channels. The deformation parameters β_l are in the following ranges: $\beta_2 = 0.18 + 0.29$; $\beta_3 = 0.10 + 0.23$. It was found that β_l depends very little on the type and energy of the bombarding particles, but does depend on the method of analysis. The scatter in the values of β_l is fairly great, and this introduces indeterminacy into the interpretation of the results.

The aim of our present work was to study inelastic scattering of neutrons by Fe^{56} with excitation of the level at 0.85 MeV, to determine whether or not this obeys the laws following from the collective nature of the 0.85 MeV state, and to estimate as accurately as possible the value of β_2 obtained from an analysis of the data by the method of linked channels.

We measured the differential cross sections of elastic and inelastic scattering of 14 MeV neutrons by iron nuclei. We used a time-of-flight spectrometer with a pulsed neutron source. Pulses of deuterons were obtained from a low-voltage neutron generator by grouping the deuteron beam before acceleration [6]. The pulse duration was about 1 msec, the repetition frequency 7 MHz, and the pulse current about 3 mA. The neutrons were generated by the reaction T(d, n)^{4}He with a standard tritium–titanium target. With a flight base of 10 m, the energy resolution of the spectrometer was 3% (about 450 keV). Time marks for the convertor were obtained from an induction electrode placed near the target. The neutron detector was a plastic scintillator, 80 × 80 mm in size, connected to an FEU-36 photomultiplier. The registration threshold was 7.5 MeV. We used annular geometry. The mean diameter of the iron toroid was 33 cm, and the diameter of the cross section was 3 cm.

The measurement results are plotted in Fig. 1 [1], together with the results of other authors [7-9].

The cross sections were analyzed by the method of linked channels [10, 11] on the assumption that the 0.85 MeV level is collective. We used an optical potential with surface absorption. Calculations were performed with and without the spin-orbit term.

TABLE 1. Optical Potential Parameters used in Calculation

Number of curve	V, MeV	W, MeV	U_{LS}, MeV	a, F	r_0, F	a_W, F	r_W, F	β_2
1	43.9	4.35	0	0.515	1.25	0.7	1.2	0.18
2	43.9	2.7	9	0.39	1.25	0.7	1.25	0.23

Note: The parameters V, r_0 and a characterize the depth, radius and blurring of the boundary for the real part of the potential; the parameters W, r_W, and a_W represent the imaginary part; and the parameter U_{LS} denotes the depth of the spin-orbital potential.

Translated from Atomnaya Énergiya, No. 5, pp. 455-456, May, 1971. Original letter submitted September 22, 1970.

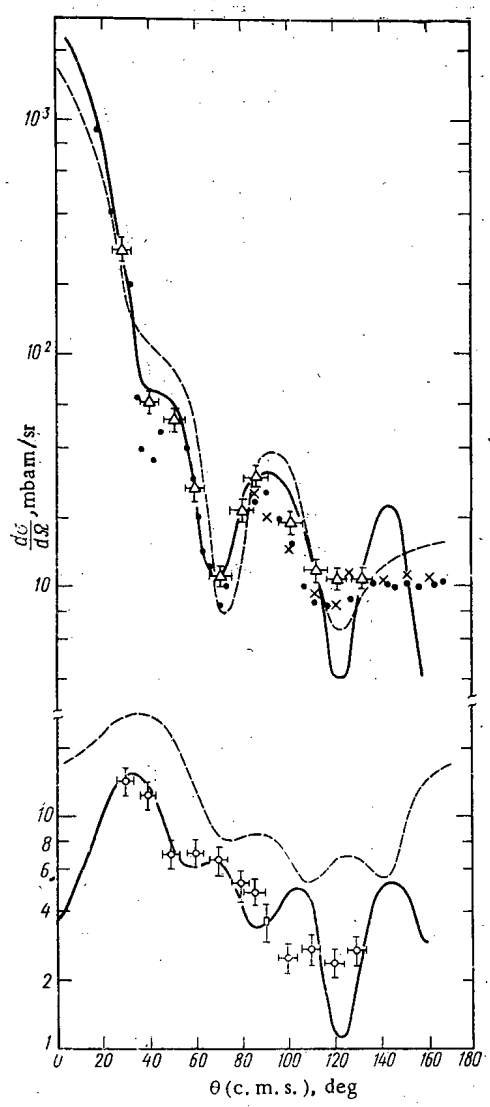

Fig. 1. Differential cross sections of elastic and inelastic scattering of 14 MeV neutrons by iron. Δ) Elastic scattering; ○) inelastic scattering with excitation of 0.85 MeV level; ●) [7]; ×) [8]; □) [9].

As initial potential parameters we used parameters taken from the paper of Rosen et al. [12]. Then the calculated cross sections were fitted to the experimental values by varying all the parameters except r_0 and a_W. The quadrupole deformation β_2 was taken to 0.23 and was also varied during fitting. The optimal theoretical curves are plotted in Fig. 1, and the corresponding values of the optimal potential parameters are listed in Table 1.

As we see from Fig. 1, the collective (vibrational) model gives a satisfactory description of the cross sections for elastic and inelastic scattering of neutrons by Fe^{56} nuclei. The parameter β_2, found as a result of our analysis, is equal to 0.21 ± 0.03, which agrees with the corresponding values of β_2 in [1-5].

LITERATURE CITED

1. R. Peterson, Ann. Phys. (USA), 53, 40 (1969).
2. H. Tjin a Djie et al., Nucl. Phys., A106, 85 (1968).
3. A. Majumder and H. Sen Gupta, Nucl. Phys., A118, 151 (1968).
4. C. Fulmer et al., Phys. Rev., 165, 1218 (1968).
5. S. Fulling and G. Satchler, Nucl. Phys., A111, 81 (1968).
6. M. E. Gurtovoi et al., Pribory i Tekhnika Éksperimenta, No. 4, 24 (1970).
7. J. Coon et al., Phys. Rev., 111, 250 (1958).
8. J. Anderson et al., Phys. Rev., 110, 160 (1958).
9. V. Jacques, C. R. Acad. Sci., 267, B733 (1968).

10. T. Tamura, Rev. Mod. Phys., 37, 679 (1965).
11. E. V. Korbetskii, O. F. Nemets, and L. S. Sokolov, Abstracts of Reports to Twentieth Yearly Conference on Nuclear Spectroscopy and the Structure of the Atomic Nucleus [in Russian], Part 2, Nauka, Leningrad (1970), p. 140.
12. L. Rosen et al., Ann. Phys., 34, 96 (1965).

THE USE OF THE NUCLEAR REACTION $O^{18}(p, \alpha)N^{15}$ TO STUDY THE OXIDATION OF METALS

N. A. Skakun, A. P. Klyucharev,
O. N. Khar'kov, V. F. Zelenskii,
and V. S. Kulakov

UDC 620.197.5.539.17

Data on nuclear reactions have recently been used for the study of the processes that occur in the surface layers during the oxidation of metals and alloys [1, 2]. Recording the reaction products during irradiation of the investigated material with charged particles permits a determination of the content of the element to be studied simultaneously with a localization of it with respect to depth without destruction of the sample.

The essence of one of the methods proposed in this work is the recording and analysis of the energy spectrum of α-particles from the reaction $O^{18}(p, \alpha)N^{15}$ in bombardment of a sample containing the isotope O^{18} with a beam of monoenergetic protons. If the reaction takes place at some depth x, then the α-particle energy E_α depends on the energy losses of the proton that has reached a depth x and the energy lost by the α-particle during its escape from the sample. With an accuracy determined by the energy resolution, the energy E_α indicates the depth at which the reaction takes place. The yield of α-particles $N_\alpha(E_\alpha)$ is proportional to the product of the concentration C(x) of the isotope O^{18} by the cross section of the reaction at a proton energy $E_p(x)$. Thus, the energy spectrum of α-particles permits establishment of the distribution of oxygen according to depth of the sample, if the stopping power of the investigated substance for protons and α-particles and the cross section $\sigma(E_p)$ of the nuclear reaction are known.

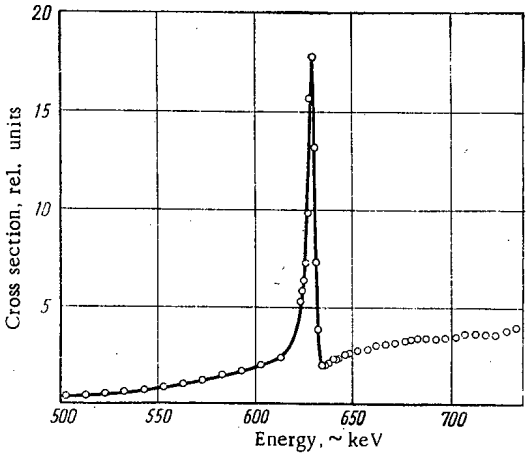

Fig. 1

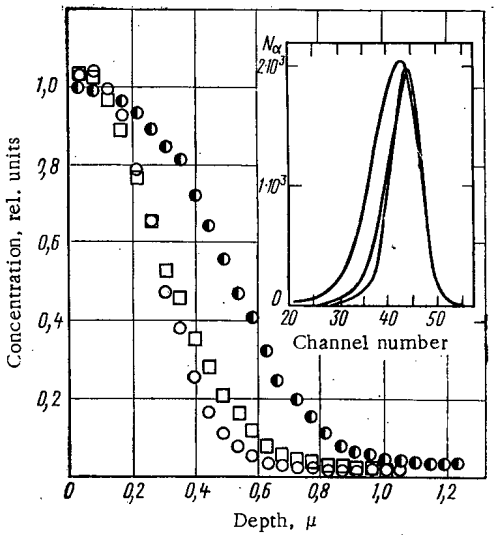

Fig. 2

Fig. 1. Excitation functions of the reaction $O^{18}(p, \alpha)N^{15}$ at an angle $\theta_{ls} = 150°$.

Fig. 2. Distribution of oxygen in samples of zirconium oxidized for 30 (○), 50 (□), and 120 (○) min. The corresponding spectra of α-particles at $E_p = 730$ keV are shown in the insert. Energy scale 16.7 keV/channel.

Translated from Atomnaya Énergiya, No. 5, pp. 456-458, May, 1971. Original letter submitted July 14, 1970.

A sample with a constant concentration of the isotope O^{18} with respect to depth (standard) permits a determination of the profile of the oxygen concentration in the investigated sample by comparison of the α-particle spectra from the sample studied and the standard. In this case the value of C(x) is determined according to the function

$$\frac{N_\alpha(E_\alpha)}{N_\alpha(E_\alpha)_{st}} = \frac{C(x)}{C_{st}}, \quad (1)$$

where C_{st} = const is the concentration of O^{18} in the standard; $N_\alpha(E_\alpha)$ and $N_\alpha(E_\alpha)_{st}$ are determined experimentally. In this case the dependence $\sigma[E_p(x)]$ is considered automatically, if the energy losses of protons (ε_p) and α-particles (ε_α) per unit path in the investigated sample and standard are the same. The values of ε_p and ε_α were calculated using the data of [3].

The excitation function of the reaction $O^{18}(p, \alpha)N^{15}$ was measured experimentally in the interval of proton energies 500-730 keV (Fig. 1). A target Ta_2O_5, produced by anodic oxidation of tantalum in an electrolyte enriched with the isotope O^{18}, was used. The source of accelerated protons was a 4 MeV electrostatic generator from the Physicotechnical Institute of the Academy of Sciences of the Ukrainian SSR. α-Particles were recorded with a silicon surface-barrier counter at an angle $\theta = 150°$ and were analyzed according to energy with an AI-100-1 analyzer.

In the interval of the energy E_p indicated above, only one group of α-particles, corresponding to a value of Q = 3.97 MeV (ground state of the N^{15} nucleus) is emitted in the reaction $O^{18}(p, \alpha)N^{15}$ [4]. Elastically scattered protons were absorbed with a mylar film 1.16 mg/cm^2 thick, placed directly in front of the detector. The surfaces of the irradiated targets were established perpendicular to the axis of the proton beam.

The investigated targets had dimensions 20 × 20 × 0.5 mm and represented samples of iodide zirconium, remelted by an electron beam method, oxidized at 500°C and a pressure of 1 atm in water vapors containing 69% O^{18}. A sample of the alloy Zr – 2% Nb, oxidized for a long time under the same conditions, was used as the standard. A comparison of the α-particle spectrum from a standard obtained at E_p = 600 keV with the excitation function in the region of $E_p \leq 600$ keV, where the cross section $\sigma(E_p)$ obeys an exponential law, indicated that the concentration $C_{st}(x)$ remains practically constant down to a depth of ~1.2 μ.

It has been suggested that ε_p and ε_α in the oxide film formed on a sample of Zr – 2% Nb do not differ significantly from the corresponding energy losses in oxidized zirconium.

The calculated stopping powers of zirconium oxide for protons and α-particles are equal to ε_p = 83 keV/μ at E_p = 730 keV and ε_α = 310 keV/μ at E_α = 3.38 MeV. Using these data and the procedure outlined earlier for comparison of the spectra of α-particles from the investigated samples and the standard, irradiated with protons with an energy E_p = 730 keV, we can obtain profiles of the distribution of oxygen in oxidized samples of zirconium (Fig. 2). The error in the determination of the relative concentration, related to the statistical errors of count, is an average of no more than 3%. From the curves of Fig. 2 we estimated the diffusion coefficient of oxygen in zirconium, the value of which was ~$7.5 \cdot 10^{-14}$ cm^2/sec. The resolving power of the metal with respect to depth, determined by the experimental energy distribution of the α-particles, is equal to ~0.2 μ. In the presence of a standard, the time expenditures necessary for determining the profile of the oxygen concentration in each sample (including the time for irradiation) did not exceed 10-15 min.

The possibility of conducting analogous investigations using the narrow resonance of the reaction $O^{18}(p, \alpha)N^{15}$ at E_p = 639 keV (see Fig. 1) was also considered. Figure 3 presents the curve of the resonance yield of α-particles, obtained as a result of irradiation with monoenergetic protons in the interval 615-650 keV of a sample of tantalum, subjected to anodic oxidation in an electrolyte enriched with the isotope O^{18}. In this case, for each fixed value of E_p we recorded the summary yield of α-particles, from which the contribution of the α-particles due to the nonresonance cross section of the reaction was deducted. The thickness of the oxide film was determined from the curve obtained in this way with the aid of the expression

$$\Gamma^2 = \Gamma_{res}^2 + \Gamma_i^2 + \Gamma_t^2, \quad (2)$$

where Γ is the width of the curve of the resonance yield at half the height (13.6 keV); Γ_{res} is the natural width of the resonance (2.1 keV); Γ_i is the energetic inhomogeneity of protons in the beam (1.7 keV in our case); Γ_t is the thickness of the target (keV).

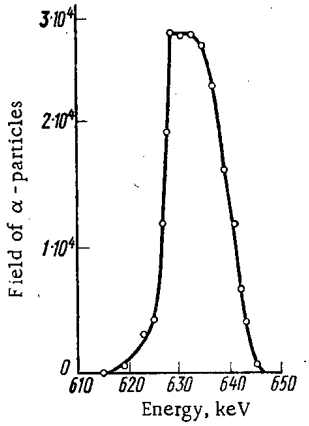

Fig. 3

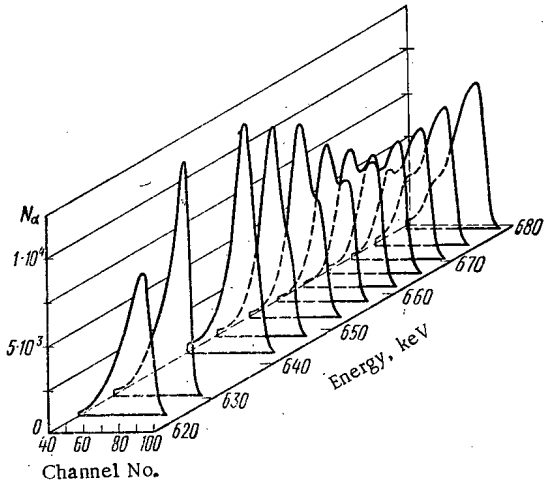

Fig. 4

Fig. 3. Resonance yield of α-particles from a target of Ta_2O_5 1530 Å thick.

Fig. 4. Spectra of α-particles obtained from a sample of zirconium oxidized for 120 min.

The stopping power of tantalum oxide Ta_2O_5 for protons in the energy interval used is 98 keV/μ. Consequently, the value Γ_t = 13.2 keV, obtained from function (2), corresponds to a thickness of the oxide film of 1300 Å.

The process of anodic oxidation was analogous to that outlined in [5]. The sample of tantalum was oxidized at a voltage of 100 V in a 1% solution of KCl in water with enrichment with 12 atomic % O^{18}.

In accord with the results of [5] it was assumed that the oxide has a stoichiometric composition corresponding to the chemical formula Ta_2O_5 with density 8.74 g/cm^3. The increase in the film thickness was 15.3 Å/V. Thus, the oxide film obtained on the investigated sample had a thickness of 1530 ± 30 Å (the error is associated with inaccuracy of the establishment of the voltage and current density of oxidation). Such agreement can be considered satisfactory, considering the possibility of error in the determination of the energy losses of protons in tantalum oxide.

We should also note the promise of the use of the resonance of the reaction $O^{18}(p, \alpha)N^{15}$ for the investigation of thick surface layers of metals. Figure 4 presents the spectra of α-particles from a sample of zirconium oxidized in water vapor for 120 min. At E_p > 629 keV, a peak due to the resonance space of α-particles distinctly appears. The successive increase in the energy of protons bombarding the target leads to an increase in the depth at which the protons have an energy close to the resonance value. From the spectra obtained in this way, according to the change in the contribution of the "resonance" α-particles, we can establish the nature of the change in the oxygen concentration with the depth. The use of resonance permits high resolution with respect to depth to be obtained, which is associated chiefly with the width of the resonance and the nonmonoenergeticity of the protons in the beam. In our case the resolution was ~320 and ~270 Å for zirconium and tantalum, respectively. The methods outlined permit an investigation of the interaction of oxygen with various solids, in particular, with most metals and alloys used in reactor construction.

The authors would like to thank G. K. Khomyakov, A. G. Strashinskii, and P. P. Matyash, for their aid in the experiments.

LITERATURE CITED

1. A. Choudhury et al., Solid St. Communications, 3, 119 (1965).
2. G. Amsel and D. Samuel, J. Phys. Chem. Solids, 23, 1707 (1962).
3. C. Williamson, J. Boujot, and J. Picard, Tables of Range and Stopping Power of Chemical Elements for Charged Particles of Energy 0.05 to 500 MeV, Rapport CEA-R 3042 (1966).
4. F. Ajzenberg-Selove and T. Lauritsen, Nucl. Phys., 11, 1 (1959).
5. G. Amsel et al., J. Phys. Chem. Solids, 30, 2117 (1969).

COMPUTER SIMULATION OF RADIOACTIVE DECAY PROCESSES

G. G. Akalaev

UDC 543.53

Mathematical methods of treating experimental results are beginning to be widely employed in activation analysis [1, 2].

The possibilities of these methods are checked with the aid of synthetic mixtures, i.e., mixtures of known qualitative and quantitative constituents. The preparation of synthetic mixtures of different concentrations often gives rise to technical difficulties. In the measurement of the radioactive decay characteristics of a mixture in a natural experiment there are introduced, in addition to the error associated with the probabilistic nature of the decay process and of the processes whereby the radiation interacts with the detector material, additional errors associated with the operation of the specific electronic-physical recording apparatus. Computer simulation of radioactive decay processes permits elimination of the additional errors and is less time consuming.

Using the terminology of [3], we consider in this article the computer simulation of the radioactive decay of a mixture of isotopes.

Simulation of Radioactive Decay Curve

Quantitative Description of Process. At moments of time $t_k (k = 1, 2, \ldots, m)$ separated by an interval Δt_k the quantity of disintegrated nuclei N_k is recorded; the resulting numbers N_k constitute the radioactive decay curve.

Mathematical Model of Process. We consider a mixture of radioactive isotopes (n isotopes in all) which differ from one another in the parameter λ_i, the decay constant. At the initial moment of time t_0 the number of radioactive nuclei of the i-th isotope $(i = 1, 2, \ldots, n)$ equals N_{0i}. Each nucleus of any isotope decays at some moment of time $t (0 < t < \infty)$. The probability $f_i(t)$ that a particular nucleus of the i-th isotope will decay during a time t, t + dt is given by the radioactive decay law:

$$f_i(t) = \lambda_i e^{-\lambda_i t}. \quad (1)$$

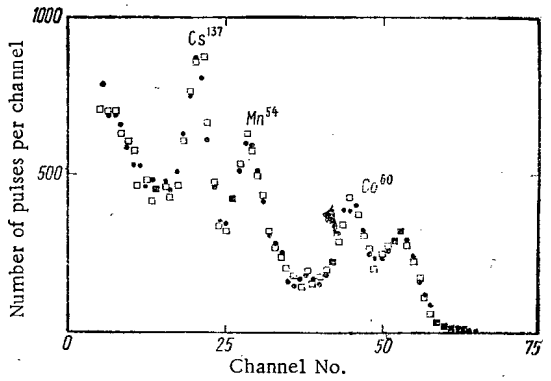

Fig. 1. Computer simulation of γ-spectrum of a three-component mixture. •) denotes experiment; and □) simulation.

Algorithm. We determine the decay time of each nucleus of the mixture by selecting random numbers from a set of random numbers distributed according to law (1). We fix those cases when the nucleus decays in the interval t_k, $t_k + \Delta t_k$. The resulting set of numbers N_k will constitute the required decay curve.

To realize the simulation algorithm on a computer we thus require a generator which can generate random numbers with the above distribution. Several methods are known for the computer production of so-called pseudo-random numbers with an arbitrary distribution law [4]. Since any computer can be employed to generate pseudo-random numbers uniformly distributed in the interval [0, 1] and satisfying the statistical criteria for randomness and uniformity, the best method of obtaining random

Translated from Atomnaya Énergiya, No. 5, pp. 459-460, May, 1971. Original letter submitted January 4, 1970; revision submitted July 23, 1970.

numbers with an arbitrary distribution law in our case is the method of change of variables (the inverse function method). In this method a random number ξ from the set of random numbers uniformly distributed in the interval [0, 1] is placed into correspondence with a random number η from the set of random numbers distributed according to the law (1) by the formula:

$$\eta = -\frac{1}{\lambda_i} \ln \xi. \tag{2}$$

A detailed discussion and statistical analysis is given in [4] of the computer production of pseudo-random numbers. By varying N_{0i} and the duration of the measurement Δt_k, we can obtain the decay curves of a mixture of radioactive isotopes of arbitrary concentration with the requisite statistical accuracy.

Simulation of γ-Spectrum of a Mixture of Radioactive Isotopes Using a Spectrometer with a Multichannel Analyzer

Quantitative Description of Process. The γ-quanta emitted by the isotope mixture are distributed over the analyzer channels. The measurements result in a set of numbers N_k, the spectrum of the mixture or the number of pulses in the k-th channel of the analyzer ($k = 1, 2, \ldots, l$, where l is the number of channels).

Mathematical Model of the Process. We consider a mixture of radioactive isotopes emitting γ-quanta. The total number of radioactive isotopes equals n, and the activity of the i-th isotope we denote by A_i. The probability that a γ-quantum from the i-th isotope will be recorded in the k-th analyzer channel is completely determined by the distribution $f_i(k)$. The distribution function $F_i(k)$ expresses the probability that a γ-quantum from the i-th isotope will be recorded in any of the analyzer channels from 1 to k:

$$F_i(k) = \sum_{j=1}^{k} f_i(j). \tag{3}$$

Algorithm. The number of γ-quanta emitted by the i-th isotope in a time t equals

$$N_i = A_i t.$$

From the inversion method the number k of the channel into which a γ-quantum from the i-th isotope passes is given by the inequality

$$F_i(k-1) < \xi \leqslant F_i(k). \tag{4}$$

By repeating the operation N_i times, we obtain the spectrum of the recorded γ-quanta from the i-th isotope. The γ-spectrum of a multicomponent mixture is obtained by summing over all isotopes.

The distribution function is obtained from the so-called reference spectrum or standard. To this end we record with good statistics the γ-spectra of the individual isotopes and then normalize to the total area of the spectrum:

$$f_i(k) = N_i(k) / \sum_{j=1}^{l} N_i(j). \tag{5}$$

Clearly, the possible errors arising upon simulation in accordance with the above formulas are determined by the qualities of the particular pseudo-random number generator. For example, if the aperiodicity segment L is comparable with the quantity of random numbers selected during simulation ($L \approx \sum_{i=1}^{n} N_{0i}$ for simulation of a decay curve, or $L \approx \sum_{i=1}^{n} N_i$ for simulation of a γ-spectrum), a systematic error will be present in the results obtained.

The Minsk-22 computer was programed in accordance with the above algorithms. The figure shows the simulated γ-spectrum of a three-component mixture and the spectrum obtained experimentally using a scintillation spectrometer with an AI-100 amplitude analyzer and a 70 × 70 crystal.

LITERATURE CITED

1. E. M. Lobanov, N. V. Zinov'ev, and A. G. Dutov, in: Activation Analaysis of Pure Materials [in Russian], Fanlar, Tashkent (1968), p. 26.

2. B. G. Egiazarov et al., Program and Theses of Reports of 19th Annual Conference on Nuclear Spectrometry and the Structure of the Atomic Nucleus [in Russian], Nauka, Leningrad (1969), Part 1, p. 203.
3. N. P. Buslenko, Mathematical Simulation of Industrial Processes [in Russian], Nauka, Moscow (1964).
4. D. I. Golenko, Simulation and Statistical Analysis of Pseudo-Random Numbers on Electronic Computers [in Russian], Nauka, Moscow (1965).

ESTIMATE OF EMERGENCY DOSES AT HIGH-POWER γ-FACILITIES

E. D. Chistov, I. F. Sprygaev,
I. P. Korenkov, A. V. Terman,
and A. V. Sedov

UDC 621.039-78

Experience has shown that the operation of high-power γ-facilities may lead to accidents or to emergency situations. One way in which emergencies arise is from failure of the interlock system on the protective entrance door of the facility and the malfunction of the system signaling the condition of the radiator and the dose rate levels [1, 2]. The serious consequences of such accidents make it necessary to estimate and predict the external radiation dose received by a victim.

A typical high-power γ-facility has a working chamber and a labyrinth. If the interlocking and signaling systems are defective the victim can open the door to the labyrinth and approach the radiator along the path shown in Fig. 1.

The total radiation dose received by the victim can be found from the relation

$$D = D_1 + D_2 + D_3, \tag{1}$$

where $D_1 = \int_{t_1}^{t_2} P \cdot dt \approx \sum_{i=1}^{n} P_i t_i$ is the dose received during the time $t_2 - t_1$ the victim is approaching the radiator, D_2 is the dose received during the time $t_3 - t_2$ the victim is in the vicinity of the radiator, and $D_3 = \int_{t_3}^{t_4} P \cdot dt \approx \sum_{i=1}^{n} P_i t_i$ is the dose received during the time $t_4 - t_3$ the victim is moving away from the working chamber. It is necessary to know the dose distribution along the path of the victim through the labyrinth in order to determine these doses.

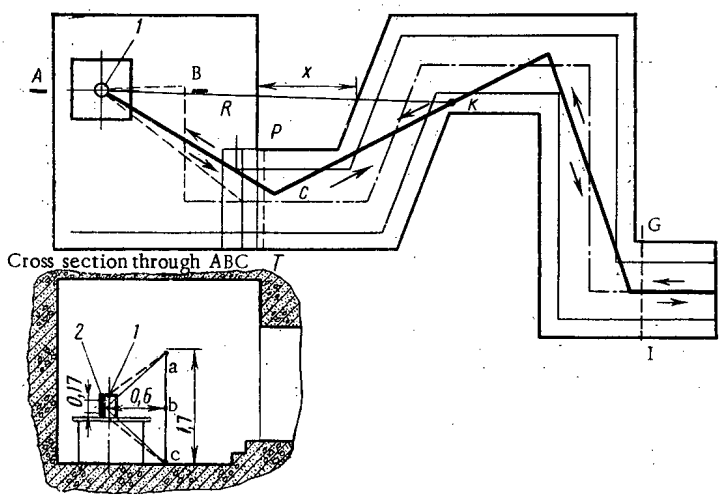

Fig. 1. Typical plan of chamber in a high-power γ-facility: —·—·—) axial line; ⇄) most probable path of victim; a, b, c) levels of head, abdominal cavity, and bottoms of feet; 1) radiator; 2) holder with source.

Translated from Atomnaya Énergiya, No. 5, pp. 460-462, May, 1971. Original letter submitted May 11, 1970.

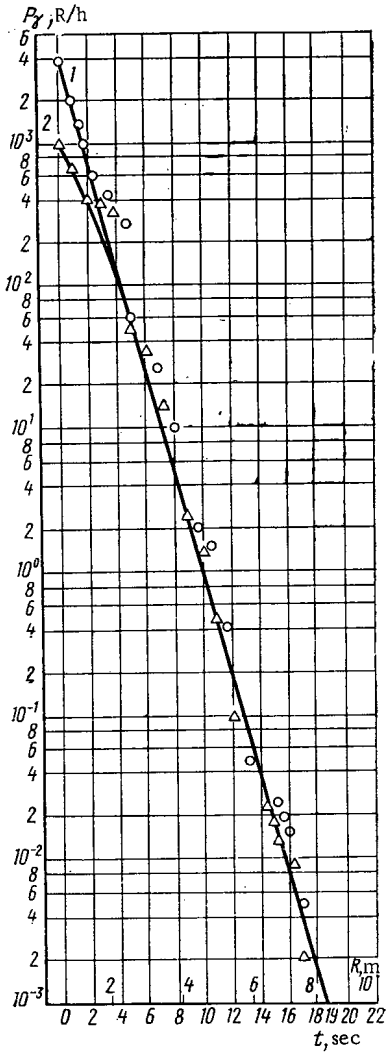

Fig. 2. γ-Dose rate P_γ as a function of path length R from radiator through labyrinth.

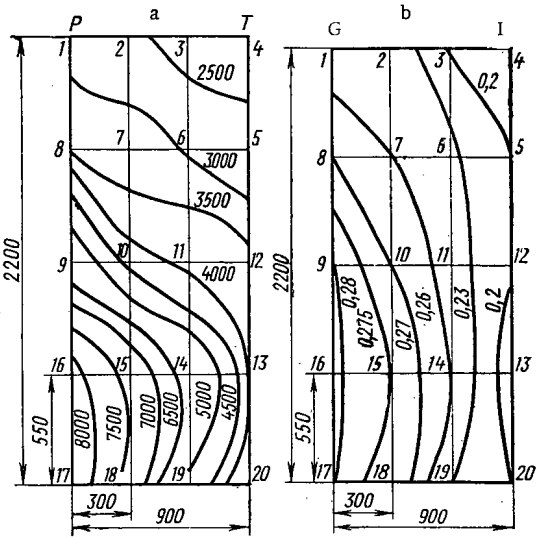

Fig. 3. Distribution of γ-dose rate over vertical cross sections of labyrinth from measurements at 20 points. Cross sections (in mm) as shown on Fig. 1: a) PT plane; b) GI plane. Figures on curves are values of P_γ in R/h. Activity of source 40,000 g-eq Ra.

The dose at any point in the labyrinth can be found as the sum of the doses from direct and back-scattered (reflected) radiation [3]

$$D_{\text{lab}}=\frac{8.4At}{R^2}e^{-\mu x}B(h\nu,\ \mu x,\ z)+\frac{8.4A\cdot t}{(2\pi)^n R_1^2}\prod_{i=1}^{n}\frac{S_i\cos\Theta_i\, d_i(\Theta,E)}{R_{i+1}^2}, \qquad (2)$$

where A is the γ-equivalent of the radiator in mg-eq Ra; R is the distance from the radiator to the dose point (e.g., point K of Fig. 1) in cm; the R_i are the distances from the radiator or the principal scattering planes to the dose point in cm; x is the thickness of the concrete shield in cm; $B(h\nu, \mu x, z)$ is the dose buildup factor; S_i is the area of a scattering surface in cm^2; Θ is the angle between the normal to the scattering surface and the direction of the incident radiation; t is the duration of the exposure in hours, and $\alpha(\Theta, E)$ is the albedo for γ-radiation.

The total dose received by the victim while he is approaching the radiator is given by the relation

$$D_1=0.88\sum_{i=1}^{n}8.4\cdot A\left[\frac{e^{-\mu x}\cdot B(h\nu,\ \mu x,\ z)}{R^2}+\frac{1}{(2\pi)^n R_1^2}\sum_{i=1}^{n}\frac{S_i\cos\Theta_i d_i(\Theta,E)}{R_{i+1}^2}\right](t_2-t_1), \qquad (3)$$

where t_2-t_1 is the time in hours the victim spends in moving from the labyrinth entrance to the radiator, and 0.88 is the conversion factor from roentgens to rads. The dose D_3 is given by an expression similar to (3) for the time in hours t_4-t_3 spent by the victim in moving from the radiator to the labyrinth exit.

The total dose is found from the relation

$$D=0.88D_2+7.4\,[(t_2-t_1)+(t_4-t_3)]\,A\sum_{i=1}^{n}C, \qquad (4)$$

where C is the expression in square brackets in Eq. (3).

We have performed calculations and experiments to determine emergency doses for a facility having an entrance labyrinth with three bends. The dose distribution in the labyrinth is shown in Fig. 2. Curve 1 characterizes the distribution at foot level (20 cm above the floor) and curve 2 at 1 m above the floor. Investigations of the dose distribution in various vertical cross sections of the labyrinth show that after the first bend the distribution is practically uniform, i.e., it is unaffected by the orientation of the radiator in the working chamber (Fig. 3a, b).

TABLE 1. Calculated and Measured Absorbed Doses in Model of Human Body

Place of measurement	Dose, rads		Place of measurement	Dose, rads	
	calculated	experiment		calculated	experiment
Head	10.0	8.2	Gonads	37.0	23.0
Neck	16.2	16.0	Thigh	38.0	28.0
Chest	24.0	18.0	Shin	27.0	20.0
Abdomen	29.0	20.0			

To check the calculations experiments were performed with a phantom under conditions simulating an emergency situation at a radiation facility having a Co^{60} radiator with an activity of 4000 g-eq Ra. The phantom was a wooden model of the human body, had a density of 0.72 g/cm^3, and closely simulated soft human tissue in composition. The phantom had a mass of 57 kg, was 170 cm high, and the sizes of its individual parts corresponded to the parameters of the "standard" man. The phantom had 22 holes 30 mm in diameter filled with wooden plugs having cylindrical cavities 12 mm long and 1.2 mm in radius for aluminum phosphate dosimeters. The emission of the thermoluminescent dosimeters was measured in a special heating device of the DTM-2 type. The intensity of luminescence was recorded with a type FEU-33 photomultiplier. The calculated and experimental results are shown in Table 1.

The appreciable divergences between calculation and experiment in many cases can be explained by the shielding of certain parts of the phantom by structural members. Calculation showed that a dose of 1.2 rads is accumulated in moving through the labyrinth to the radiator and back. This quantity should be added to the total dose.

Our calculational procedure gives results which are adequate for practical purposes and can be used to estimate radiation doses at high-power γ-facilities during emergency situations.

LITERATURE CITED

1. E. D. Chistov et al., in: Scientific Papers of Institutes of Work Safety VTsSPS [in Russian], No. 51, Profizdat, Moscow (1968), p. 39.
2. L. L. Sokolina et al., in: Data from a Conference on Theoretical and Applied Radiation Safety (November 23-29, 1966) [in Russian], VTsNIIOT, Moscow (1968), p. 242.
3. E. D. Chistov and A. V. Larichev, in: Scientific Papers of Institutes of Work Safety VTsSPS [in Russian], No. 3 (29), Profizdat, Moscow (1964), p. 49.

USE OF SEMICONDUCTOR DETECTORS WITH A p – n JUNCTION FOR THE DOSIMETRY OF X-RAYS AND γ-RADIATION IN THE LOW-ENERGY RANGE

V. K. Lyapidevskii and Yu. B. Mandel'tsvaig

UDC 539.12.08

Diffusion-drift silicon or gallium arsenide semiconductor detectors with p–n junctions are widely used for recording various types of radiation. The strong dependence of the sensitivity of these detectors upon the energy of the radiation, particularly in the low-energy range (below 40 keV) has imposed limitations on their use in dosimetry. Figure 1 shows the relative spectral characteristics of silicon detectors having various thicknesses of the sensitive region; Fig. 2 shows similar characteristics for gallium arsenide detectors. The solid lines indicate the dependence of i/P_e upon the energy E of the radiation quanta, where i denotes the signal at the detector output (this signal is proportional to the energy absorbed by the sensitive region) and P_e denotes the dose rate received. The functions i/P_e were calculated with the formula

$$\frac{i}{P_e} = A\frac{(1-e^{-(\mu_k)_{mZ}h})}{(\mu_k)_{mB}h},$$

where h denotes the thickness of the sensitive layer; $(\mu_k)_{mB}$ denotes the overall energy transfer coefficient for air; and $(\mu_k)_{mZ}$ denotes the overall energy-transfer coefficient for a material with the atomic number Z.

The μ_k values for GaAs were calculated with the data obtained with Cu^{29} [1, 2] and with the technique described in [3]. The μ_k values for silicon were calculated with the data of [4, 5].

The position of the maximum depends strongly upon the thickness of the sensitive layer.* The form of the curves undergoes only slight changes and the energy dependence of the sensitivity is very strong in every case in the low-energy range. One must bear in mind that a compensation for the energy losses by means of filters or semiconductor-luminophor combinations which give improved results in the range 40-100 keV [6-9] is not very efficient in the low-energy range considered.

The dose of monoenergetic γ-radiation or of a single-parameter x-ray radiation (i.e., a radiation which depends upon a single parameter only, e.g., upon the attenuation coefficient μ) can be measured by simultaneous determinations of two quantities [5]. We used two semiconductor detectors with p–n junctions, namely a silicon detector and a gallium arsenide detector. The relative spectra characteristics $i/P_e = f(E)$ of these detectors are shown in Fig. 3.

The same characteristics are indicated in Figs. 1 and 2 by dashed lines. A comparison of the experimental curves with the calculated curves leads to the conclusion that the thickness of the sensitive layer of the silicon detector is close to 100 μ, whereas the thickness of the sensitive layer of the gallium arsenide detector is several times smaller and amounts to 20-30 μ.

*The strong dependence of the position of the maximum of the $i/P_e = f(E)$ curve upon the thickness of the sensitive layer makes it possible to determine the layer thickness of a particular photodetector by comparing the experimental curve with a series of calculated curves. One can estimate the diffusion length L of the charge carriers in the base material when $h \approx L$ (this occurs, e.g., in the Si used in solar batteries).

Translated from Atomnaya Énergiya, No. 5, pp. 462-464, May, 1971. Original letter submitted February 20, 1970.

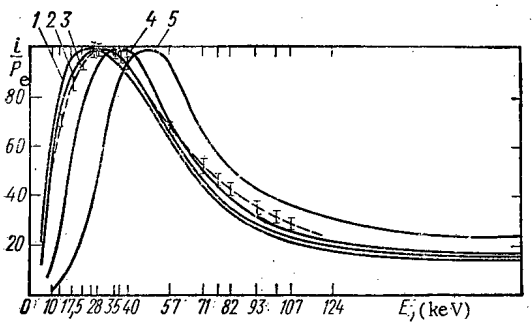

Fig. 1

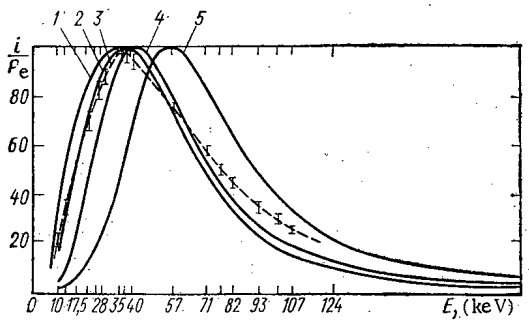

Fig. 2

Fig. 1. Relative spectral characteristics of diffusion-drift silicon detectors with various thicknesses of the sensitive layer: 1, 2, 4, 5) calculated curves for sensitive layer thicknesses of 0.01, 0.1, 1, and 10 mm, respectively; 3) experimental curve.

Fig. 2. Relative spectral characteristics of diffusion-drift gallium arsenide detectors: 1, 2, 4, 5) calculated curves for sensitive layer thicknesses of 0.01, 0.03, 0.1, and 1 mm, respectively; 3) experimental curve.

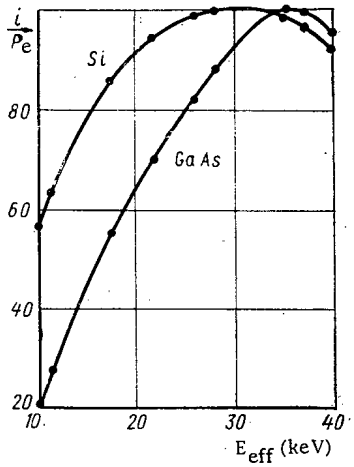

Fig. 3

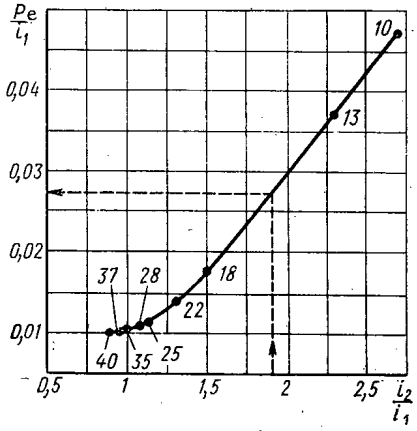

Fig. 4

Fig. 3. Relative spectral characteristics of silicon and gallium arsenide detectors at a radiation energy $E_{eff} < 40$ keV.

Fig. 4. Diagram for the determination of the dose rate from simultaneously measured currents of two detectors, a silicon detector (i_2) and a gallium arsenide detector (i_1).

In accordance with [5], we indicate the ratio P_e/i_1 on the vertical axis of a rectangular coordinate system and the ratio i_2/i_1 on the horizontal axis, where i_2 and i_1 denote the output current of the Si and GaAs detectors, respectively. Figure 4 shows the relations obtained. (The detectors were operated in a short circuit at t = 20°C.) In order to measure the exposure dose rate, the two detectors were placed in a beam of the radiation to be measured and P_e/i_1 was determined from the measured i_2/i_1 value as shown by the arrows in Fig. 4. The P_e/i_1 value obtained was multiplied with the current i_1 measured in this experiment and thus, the exposure dose rate P_e could be determined. The sensitivity of the detectors to x-ray radiation with E_{eff} = 100 keV amounted to $(0.7\text{-}1.3) \cdot 10^{-9}$ A/R/min · cm^2. The relation $i = f(P_e)$ is linear in the range 0.5-400 R, under these conditions.

The method of simultaneously measuring two quantities can also be used for the dosimetry of a radiation with an unknown spectrum. However, in this case (contrary to the previously considered case) errors can be made in the dose determination and the magnitude of the errors depends upon the radiation spectrum. The greatest possible error in the P_e determination can be graphically estimated with Fig. 4 [5]. In the energy range considered, an error is made when the radiation spectrum consists of two lines with quantum energies of 40 and 10 keV. The relative error $\delta = (P_{max} - P_e)/P_e$ in the P_e determination is less than 35% in this case.

It can be shown that the maximum error which is made in exposure dose measurements of a homogeneous radiation with the aid of the setup of [10] (the quantity $\alpha_1 i_1 \pm \alpha_2 i_2$ is measured at the output of this setup) is greater than or equal to the maximum error δ determined from Fig. 4.

When the above method is used, the error is usually much smaller than that determined from Fig. 4. The error vanishes in the case of single-parameter spectra. One can therefore hope that the above-described method of simultaneous measurements of two quantities will be widely used in dosimetry.

LITERATURE CITED

1. H. Jones, Physics of Radiology [Russian translation], Atomizdat, Moscow (1965).
2. G. V. Gorshkov, Penetrating Radiation of Radioactive Sources [in Russian], Nauka, Leningrad (1967).
3. A. M. Gurvich et al., Transactions of the All-Union Scientific Research Institute for Medical Instruments and Equipment [in Russian], No. 5, 40 (1962).
4. Yu. K. Akimov et al., Semiconductor Detectors for Nuclear Particles and Application of these Detectors [in Russian], Atomizdat, Moscow (1967).
5. N. G. Volkov and V. K. Lyapidevskii, Pribory i Tekh. Éksperim., No. 5, 86 (1968).
6. L. Hollander, Rev. Sci. Instrum., 28, 322 (1957).
7. N. Bailey and G. Kramer, Radiation Res., 22, 53 (1964).
8. A. N. Krongauz et al., Meditsinskaya Radiologiya, No. 9, 78 (1970).
9. Yu. B. Mandel'tsvaig and V. G. Epishev, Novosti Meditsinsko Tekhniki, No. 2, 123 (1966).
10. S. P. Vershinina, A. Ya. Berlovskii, and Yu. A. Tsirlin, Atomnaya Énergiya, 24, 262 (1968).

PROTON CURRENT FOR EQUILIBRIUM PHASE DECREASE ALONG A LINEAR ACCELERATOR

A. D. Vlasov

UDC 621.384.64.01

Calculations of the proton current in a linear accelerator for stable and neutral equilibrium of the accelerated bunches showed that the current increases from hundreds of milliamperes to about 10 Å [1, 2] when the equilibrium phase is increased from 35-45° to 85-90°. However, an increase in equilibrium phase requires an increase in the accelerating field and in the length of the accelerator, and can be tolerated only over a limited section. This paper discusses a linear accelerator with an equilibrium phase which is initially 85-90° and which gradually decreases along the accelerator.

The changes in particle energy, equilibrium phase, and other parameters along the accelerator are assumed to be so slow that the bunches at each energy can be considered in a stationary approximation. The state of a bunch at various energies is tied in with stability and charge conservation conditions and also with the corresponding relation for the variation of the phase area of the bunch.

Only beams and bunches of constant density are discussed in the following. Of course, the velocity spread in an injected beam must correspond rather well to the distribution of velocities in the bunches discussed in order to avoid marked loss of particles.

The potential function of an accelerating field has the form

$$\Phi_0(\varphi)=\frac{\varphi\cos\varphi_{s0}-\sin\varphi}{\sin\varphi_{s0}},$$

where φ is the phase of the accelerating wave; $\varphi_{S0}=\arccos(dW/eE_m dz)$ is the nominal equilibrium phase; e and W are the particle charge and energy; E_m is the amplitude of the accelerating wave; and z is the longitudinal coordinate.

Using the well-known disc model of a bunch, we shall represent it in the form of a cylinder of fixed radius r with a charge density ρ (in the laboratory system) which depends only on φ. Then the potential of the intrinsic charge of the bunches, which follow one another with a spacing $\Delta z=\beta\lambda$, is expressed by [2]

$$U(\varphi)=aG\int_{\varphi_f}^{\varphi_i}\left[e^{-\frac{|\varphi-\varphi'|}{a}}+\frac{e^{\frac{\varphi-\varphi'}{a}}+e^{\frac{\varphi'-\varphi}{a}}}{e^{\frac{2\pi}{a}}-1}\right]\rho(\varphi')\,d\varphi'.$$

Here, φ_i and φ_f are the boundaries of the bunch; $a=2\pi\sqrt{1-\beta^2}/k\beta\lambda$ is the reduced radius of the bunch, $G=\beta\lambda/4\pi\varepsilon_0 E_m\sin\varphi_{S0}$; λ is the wave length; $\beta=v/c$; v is the particle velocity; c is the velocity of light; and k is a factor of the order of one which depends on the ratio of the bunch and aperture radii to the quantity $\beta\lambda$. We set $\varphi_{i,f}=\varphi_c\pm a\varepsilon$.

Setting $\rho(\varphi)=\rho_0=\text{const}$ and performing the integration, we express the total potential of the accelerating and bunch fields as

$$\Phi(\varphi)=\Phi_0+U=\frac{\varphi\cos\varphi_{s0}-\sin\varphi}{\sin\varphi_{s0}}-2a^2G\rho_0\frac{\operatorname{sh}\left(\frac{\pi}{a}-\varepsilon\right)}{\operatorname{sh}\frac{\pi}{a}}\operatorname{ch}\frac{\varphi-\varphi_c}{a}+\text{const}. \quad (1)$$

We write the condition for the conservation of the current I and of the bunch charge $Q=I\lambda/c$:

Translated from Atomnaya Énergiya, No. 5, pp. 464-466, May, 1971. Original letter submitted May 25, 1970.

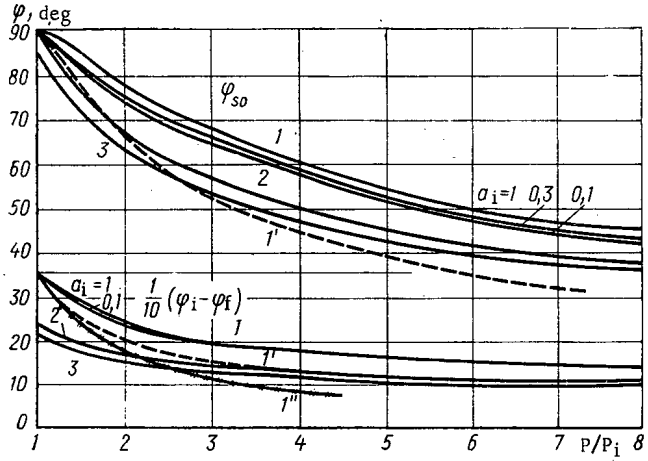

Fig. 1. Lower boundaries of allowed regions of variation of equilibrium phase and of bunch phase length for various cases.

$$\rho_0 \pi r^2 \cdot 2a\varepsilon \frac{\beta\lambda}{2\pi} = \frac{I\lambda}{c} = \text{const.} \tag{2}$$

We substitute in Eq. (1), expressions for G and ρ_0 based on condition (2):

$$\Phi(\varphi) = \frac{\varphi \cos\varphi_{s0} - \sin\varphi}{\sin\varphi_{s0}} - \frac{60a\lambda I}{E_m r^2 \sin\varphi_{s0}} \times \frac{\operatorname{sh}\left(\frac{\pi}{a} - \varepsilon\right)}{\varepsilon \operatorname{sh}\frac{\pi}{a}} \operatorname{ch}\frac{\varphi - \varphi_c}{a} + \text{const.} \tag{3}$$

For stability of phase oscillations, it is necessary that $\Phi'(\varphi_f) \leq 0$ at the trailing edge of a bunch, or, considering Eq. (3),

$$\cos\varphi_{s0} - \cos(\varphi_c - a\varepsilon) + \frac{60\lambda I}{E_m r^2} \cdot \frac{\operatorname{sh}\left(\frac{\pi}{a} - \varepsilon\right)}{\operatorname{sh}\frac{\pi}{a}} \cdot \frac{\operatorname{sh}\varepsilon}{\varepsilon} \leqslant 0. \tag{4}$$

The bunch boundaries are also related through the equation $\Phi(\varphi_f) = \Phi(\varphi_i)$. Hence,

$$\cos\varphi_{s0} = \frac{\sin a\varepsilon}{a\varepsilon} \cos\varphi_c \tag{5}$$

The area occupied by the image of the bunch on the φW phase plane is expressed in the form $V \approx 0.7 (\varphi_i - \varphi_f) \times 2(W - W_s)_c$. But

$$W - W_s = \frac{dW}{d\beta} \cdot \frac{\beta\lambda}{2\pi c} \dot{\varphi} = \frac{m_0 c\lambda}{\pi\sqrt{2}} \cdot \frac{\beta^2\Omega_0}{(1-\beta^2)^{3/2}} \sqrt{\Phi_f - \Phi(\varphi)},$$

where $\Omega_0^2 = 2\pi e E_m (1-\beta^2)^{3/2} \sin\varphi_{s0}/m_0\lambda\beta$; m_0 is the rest mass of the particles; and $\Phi_f = \Phi(\varphi_f) = [\Phi(\varphi_f) + \Phi(\varphi_i)]/2$. Thus

$$V = 2.8a\varepsilon \sqrt{\frac{eE_m\lambda \sin\varphi_{s0}}{\pi m_0^2 c^4}}\, p^{3/2} \sqrt{\Phi_f - \Phi(\varphi_c)}.$$

Here, and subsequently, $p = m_0 c\beta\sqrt{1-\beta^2}$ is the particle momentum and $p_1 = p/p_i$.

As is well known, the phase area in the φW plane is an invariant, but the effectively filled phase area gradually increases because of random small errors in the accelerator with $V \sim \psi^2(p_1)$. Calculating $\Phi_f - \Phi(\varphi_c)$ by means of Eq. (3), we obtain

$$\frac{V^2}{\psi^4} \sim \frac{a^2\varepsilon^2 E_m p^3}{\psi^4} \left[(1 - \cos a\varepsilon) \sin\varphi_c - \frac{60\lambda I}{E_m r^2} \cdot \frac{a \operatorname{sh}\left(\frac{\pi}{a} - \varepsilon\right)}{\operatorname{sh}\frac{\pi}{a}} \cdot \frac{\operatorname{ch}\varepsilon - 1}{\varepsilon} \right] = \text{const.} \tag{6}$$

Let the variation of the parameters along the length of the accelerator be

$$\frac{V}{V_i} = \psi^2(p_1), \quad \frac{r}{r_i} = \chi(p_1), \quad \frac{E_m}{E_{m\,i}} = F(p_1), \quad \frac{k}{k_i} = f(p_1) \tag{7}$$

and let us define

$$I_1 = \frac{\pi r_i^2 E_{m_i}}{60\lambda}. \tag{8}$$

Considering (5), the inequality (4) and Eq. (6) then take the form

$$\frac{I}{I_1} \cdot \frac{\pi a_i \operatorname{sh}\varepsilon \operatorname{sh}\left(\frac{\pi}{a} - \varepsilon\right)}{a\varepsilon \operatorname{sh}\frac{\pi}{a} \sin a\varepsilon \left[\sin\varphi_c - \left(\frac{1}{a\varepsilon} - \operatorname{ctg} a\varepsilon\right)\cos\varphi_c\right]} \leqslant \chi f F p_1, \tag{9}$$

$$p_1^2 F \frac{a^2\varepsilon^2}{\pi^2} (1 - \cos a\varepsilon) \sin\varphi_c - \frac{I a_i^2}{I_1 f} \cdot \frac{a\varepsilon}{\pi} \cdot \frac{\operatorname{sh}\left(\frac{\pi}{a} - \varepsilon\right)}{\operatorname{sh}\frac{\pi}{a}} (\operatorname{ch}\varepsilon - 1) = \frac{2C\psi^4}{p_1}. \tag{10}$$

Inequality (9) and Eq. (10) determine the achievable current I (or I/I_1) and the constant C through the initial values of a, $a\varepsilon$, φ_c.

For fixed I/I_1, the inequality (9) and Eqs. (5) and (10) determine the region of allowed values of p_1, φ_{s0}, which is bounded from below by the curve $\varphi_{s0} = \varphi_{s0}(p_1)$ defined by Eqs. (5), (9), and (10). The allowed p_1, $a\varepsilon$ and p_1, φ_c regions are thereby determined also. The limiting curves are calculated more easily by assigning values to $a\varepsilon$ and finding φ_c and p_1 from the equation system (9), (10) and then φ_{s0} from (5).

Ordinarily $\varepsilon \geq 3$ and $(\pi/a) - \varepsilon \geq 1$ over the greater part of an accelerator so that

$$\frac{\operatorname{sh}\varepsilon}{\operatorname{sh}\frac{\pi}{a}}\operatorname{sh}\left(\frac{\pi}{a}-\varepsilon\right) \approx \frac{\operatorname{ch}\varepsilon-1}{\operatorname{sh}\frac{\pi}{a}}\operatorname{sh}\left(\frac{\pi}{a}-\varepsilon\right) \approx \frac{1}{2}. \tag{11}$$

In the calculation of typical limiting curves below, it is assumed that

$$\psi = p_1^{1/4}, \quad \chi = p_1^{1/3}, \quad f = F = 1 \left(\frac{a}{a_i} = p_1^{-2/3}\right). \tag{12}$$

When Eqs. (11) and (12) are valid, the calculations are significantly simplified.

We consider the injection of a continuous, uniform beam. In such a beam there is no longitudinal repulsion, and the achievable current is determined only by the subsequent separation into bunches. To reduce particle loss to a minimum, it is necessary to set $\varphi_{s0i} = 90°$. Then $2(a\varepsilon)_i = 360°$, $\varphi_{ci} = 90°$, and we find $I = I_1$, $C = 1$ from Eqs. (9) and (10). Figure 1 shows the limiting curves for the variation of the equilibrium phase φ_{s0} and of the bunch phase length $\varphi_i - \varphi_f = 2a\varepsilon$ along an accelerator as a function of p_1, calculated for a_i equal to 0.1, 0.3, and 1.0 (curves 1). Note that $a_i = 0.32$ for our I-2 and I-100 accelerators since $r_i = 4.75$ mm, $\beta_i = 0.0387$, $\lambda = 2.02$ m, and $k = 1.2$. Note also that when $W_i = 0.7$ MeV, the value $p/p_i = 8$ corresponds to $W = 46$ MeV.

For the parameters of the I-100 accelerator (in which $E_m = 1.58$ MV/m), $I_1 = 0.92$ A. This current is low in comparison with the current for neutral initial bunch equilibrium and $\varphi_{s0} = 90°$ [2]:

$$I_n\left(\frac{\pi}{2}\right) = \frac{\beta^2 E_m \lambda k^2 (1+a^2)}{240\pi},$$

which is 10.1 A for the I-100 accelerator. Generally, when $\beta^2 \ll 1$

$$I_1 = \frac{a_i^2}{1+a_i^2} I_n\left(\frac{\pi}{2}\right). \tag{13}$$

The current I_1 approaches $I_n(\pi/2)$ only when $a_i > 1$, i.e., for comparatively large reduced beam radii.

Also shown in Fig. 1 are the curves 1', which were calculated for $a_i = 0.3$ and the same regime as for curves 1 but with $\psi \equiv 1$. It is clear that inaccuracies in the accelerator reduce the allowable regions.

The relative smallness of the current given by Eq. (13) for injection of a continuous beam results from the comparatively large resultant bunch length, which is close to the length of the separatrix. As is well known, the maximum current is achieved with shorter lengths [1] in the case of bunches of constant density.

Equations (5) and (9) make it possible to construct the curve $I = I(a_i \varepsilon_i)$ and to find the maximum I. For example, let $a_i = 0.3$. Then for values $\varphi_{s0i} = 90$ and 85°, we find $(I/I_1)_{max} = 3.86$ and 3.16 respectively for $(a\varepsilon_i) = 117$ and 106°. If $I_1 = 0.92$ A, $I = 3.5$ and 2.9 A. We find $C = 0.251$ and 0.176 from Eq. (10), and plot the limiting curves 2 and 3.

In designing an accelerator with some given variation of equilibrium phase (or of associated parameters), the given variation replaces Eq. (9) and makes up an initial equation system together with Eqs. (5) and (10). The validity of any parameter variation is easy to evaluate by comparing it with the limiting curves. Thus the constant bunch length $(\varphi_i - \varphi_f)\beta\lambda/2\pi$ proposed in [3] is unrealizable for Eqs. (12) because the curve $a\varepsilon\beta = \text{const}$ (curve 1") lies below curve 1. At the same time, the validity of constant equilibrium phase $\varphi_{s0} = \varphi_{s0i} = \text{const}$ and of constant bunch phase length $\varphi_i - \varphi_f = 2(a\varepsilon)_i = \text{const}$ is immediately apparent.

It is necessary to consider the parameters calculated above for $\varphi_{s0i} = 90°$ only as theoretical limits. In practice, we always have $\varphi_{s0} < 90°$.

LITERATURE CITED

1. A. D. Vlasov, At. Énerg., 27, 238 (1969).
2. A. D. Vlasov, At. Énerg., 29, 141 (1970).
3. I. M. Kapchinskii and V. A. Teplyakov, Pribory i Tekh. Éksperim., No. 4, 17 (1970).

POSSIBILITY OF ACCELERATING PROTONS TO ENERGIES ABOVE E_0 IN AN ISOCHRONOUS CYCLOTRON

L. A. Sarkisyan

UDC 621.384.633

Nonlinear effects resulting from the periodicity N of the magnetic field play an important role in isochronous cyclotrons with spatial variation of the magnetic field. Resonance relations between the free betatron oscillation frequencies Q_r and Q_z and the operating focussing harmonic of the field periodicity N lead to the appearance of ideal nonlinear resonances of the form

$$pQ_r \pm qQ_z = N, \tag{1}$$

where p, q = 0, 1, 2. . . ; | p + q| determines the order of the resonance.

Radial nonlinear resonances (q = 0) are the most dangerous because they are of lower order. As is well known, the frequency Q_r of radial betatron oscillations increases in isochronous cyclotrons during acceleration and passes through a series of resonance values $Q_r = N/p$. The lowest value $Q_r = 1$ occurs at the center of an accelerator with a solid structure (in ring cyclotrons, Q_r is somewhat greater than 1 and is determined by the injection energy), and the maximum value of Q_r is determined by the resonance order p. Depending upon the value of p, these resonances ($Q_r = N/p$) may lead to a considerable increase in the amplitude of the radial oscillations of the particles. Thus the particle kinetic energy which can be achieved in an isochronous cyclotron is determined by the resonance values of the radial betatron oscillation frequency and, from linear theory, is approximately

$$W = E_0\left(\frac{Q_r}{\sqrt{1+\frac{3}{2N^2}\left(\frac{\varepsilon r}{N\varkappa}\right)^2}}-1\right), \tag{2}$$

where E_0 is the rest energy of the particles; ε is the variability of the fundamental harmonic of the field; $\varkappa$ is a parameter of the Archimedes spiral; and r is the instantaneous radius of the orbit.

Calculations carried out in [1] showed that for a free radial oscillation amplitude of a few centimeters and the acquisition by the particles of an energy of ~300 keV per turn, the ideal nonlinear resonance of the fourth order (p = 4) leads to practically complete loss of beam, and the maximum energy of protons in isochronous cyclotrons is restricted by the nonlinear resonance $Q_r = 2$. Note that in the electron analog II at Oak Ridge, the resonance $Q_r = 2$ occurred for particles with very small radial oscillation amplitudes (for protons, an amplitude of the order of a few millimeters) [2].

Passage through the resonance $Q_r = 2$ and further acceleration brings with it considerable reduction in beam intensity and the need to overcome difficulties in shaping the magnetic field because the nonlinearity of the average field and the variability increases with radius. In addition, the beam extraction system becomes considerably more complex and its efficiency falls significantly. Therefore, in isochronous cyclotrons designed for maximum energy, the radial betatron oscillation frequency is selected to be $Q_r = N/q = 8/4 = 2$, and the maximum proton energy in the accelerator is somewhat less than the rest energy E_0 depending upon the values of the parameters ε, N, and $\varkappa$.

Thus it is impossible to accelerate protons in an isochronous cyclotron to a kinetic energy above ~E_0, i.e., for $Q_r > 2$. It is therefore necessary to use a cascade method of acceleration where each isochronous cyclotron is the injector for the next one. We shall call such an accelerator a cascade isochronous cyclotron.

Translated from Atomnaya Énergiya, No. 5, pp. 466-468, May, 1971. Original letter submitted May 11, 1970.

TABLE 1. Cascade Cyclotron Parameters

Cascade accelerator	H_0, Oe	N	π, cm	Q_z	Q_r	r_∞, cm	r_i, cm	r_f, cm	ε_i	W, MeV	f_0, MHz
First	6500	8	7	0,2	$1 \leqslant Q_r \leqslant 2$	447	0	385	0,245	823	9,88
Second	3000	12	7	0,2	$\sim 2 \leqslant Q_r \leqslant 3$	1042	902	982	0,157	1670	4,56
Third	1500	16	7	0,2	$\sim 3 \leqslant Q_r \leqslant 4$	2084	1965	2018	0,105	2523	2,28

Note: H_0 is the magnetic field intensity at the accelerator center for $r = 0$; $r_\infty = E_0/eH_0$; r_i and r_f are the initial and final acceleration radii; f_0 is the rotational frequency of the particles.

Note that the concept of cascade acceleration has recently found extensive application for increasing particle energies in accelerators of a different type. In the sub-GeV region of cyclotron acceleration, there is the well-known Zurich design for a ring cyclotron producing ~600 MeV protons in which it is proposed to use a cascade of two accelerators. The first is an approximately 70 MeV, four-sector, "Thomas" cyclotron operating in the radial betatron oscillation frequency range $1.0 \leq Q_r \leq 1.1$, and the second is an eight-sector ring cyclotron operating in the frequency range $1.1 \leq Q_r \leq 1.6$ [3].

In the cascade isochronous cyclotron proposed here, the capability of accelerating protons to an energy above E_0, i.e., $Q_r > 2$, is achieved by the selection of a definite frequency range for the radial betatron oscillations Q_r in each accelerator. The frequency range of the radial betatron oscillations in the first, second, third, etc., isochronous cyclotrons of the cascade is selected to be respectively $\sim 1 \leq Q_r \leq N/p = 8/4 = 2$, $\sim 2 \leq Q_r \leq N/p = 12/4 = 3$, $\sim 3 \leq Q_r \leq N/p = 16/4 = 4$, etc., where the upper value of the frequency Q_r in each cyclotron corresponds to an ideal nonlinear resonance of the fourth order ($p = N/Q_r = 4$), which is determined by the appropriate selection of the periodicity N of the magnetic field.

The first isochronous cyclotron may be either solid or of the ring type (with external injection of the particles); all subsequent cyclotrons are of the ring type.

Transfer of the beam from one accelerator to another is facilitated by the fact that the resonance coupling between radial and azimuthal motion arising through the nonlinear resonance of the fourth order for $Q_r = 2, 3, 4$, etc., will be used in these cyclotrons to achieve high-efficiency beam extraction. Note that with careful optimization of beam characteristics and extraction system, a beam extraction factor of about 95% was achieved with the help of the nonlinear resonance $Q_r = 2$ at the electron analog II at Oak Ridge [4].

The assurance of a large radial increase per turn of the order of 1 cm at the internal radii makes it possible to use an electrostatic or magnetic channel with a central plate for transferring the beam during injection into the ring cyclotrons.

Table 1 gives possible parameters for an accelerator cascade which would make it possible to accomplish cyclotron acceleration of protons to a kinetic energy ~2.5 GeV.

Further increase in proton energy by means of the version of a cascade isochronous cyclotron just discussed will be determined to a considerable extent by economic considerations because each cyclotron provides an increase in proton energy by approximately a constant quantity equal to E_0. In this regard, another version of the cascade isochronous cyclotron is feasible; this is one in which the energy increase in the second cyclotron is not roughly the rest energy of the proton but double or triple it. This can be accomplished if the change in radial betatron oscillation frequency in a cyclotron is not one but two or three.

With an increase in the axial rigidity of an isochronous cyclotron ($Q_z \geq 1$), the average beam current increases by about two orders of magnitude [5, 6].

It is well known that the threshold for the creation of heavy particles by protons on nuclei is 1.1 GeV for K^+ and Λ^0, 1.3 GeV for Σ^+ and Σ^0, and 1.8 GeV for K^- and K^0. With an energy of ~2.7 GeV, therefore, the accelerator just discussed becomes a high-intensity K-meson "factory" which is competitive with linear accelerators.

Note that existing and rebuilt synchrocyclotrons with energies of 600-1000 MeV and 700-1000 MeV linear accelerators under construction can be used as a first stage of the cascade along with an isochronous cyclotron.

LITERATURE CITED

1. V. P. Dmitrievskii, V. V. Kol'ga, and N. I. Polumordvinova, in: Proceedings of the International Accelerator Conference, Dubna, 1963 [in Russian], Atomizdat, Moscow (1964), p. 833.
2. J. Martin and J. Mann, Nucl. Instr. and Methods, 18, 19, 451 (1962).
3. H. Willax, Intern. Cyclotron Conference, Oxford (1969).
4. J. Martin et al., Proc. of the Intern. Conf. on Sector-Focussed Cyclotrons and Meson Factories, CERN (1963), p. 52.
5. V. N. Anosov et al., At. Énerg., 25, 537 (1968).
6. M. Gordon, Nucl. Instr. and Methods, 58, 245 (1968).

TURBULENT HEATING AND CONFINEMENT OF A PLASMA IN A TOROIDAL TRAP OF MULTIPOLE TYPE

B. A. Demidov and S. D. Fanchenko

UDC 533.9.16:621.039.634

As is known, turbulent heating by a current differs from the usual Joule heating in that the former uses strong electric fields for which the plasma resistivity is anomalously large because of the development of very-small-scale instabilities. To facilitate passage of the turbulent-heating current along the circuit of the torus in the "Vikhr'-3" device (Fig. 1), in addition to the field B_φ, a longitudinal field $B_z \leq 2$ kOe was provided. The field B_z was produced by a system of 30 coils 1, placed around a toroidal quartz discharge chamber 2 with major diameter of torus $2R = 150$ cm and minor diameter $2a = 10$ cm. The field B_φ was produced by four opposing ring-shaped conductors 3 that were superimposed on the discharge chamber; a quasistationary current with period 10 msec passed through these conductors. The path of the field lines is shown in Fig. 1 by the usual convention. Each conductor produced a field $B_\varphi \leq 2$ kOe separately on the chamber axis.

The region of space that bounds the ring-shaped conductors is an unusual toroidal mirror machine. The magnetic force lines (with the exception of one central line) emerge at the wall, while the field increases from the center in all directions. For particles coming out of the central region, the mirror ratio is a maximum, and is equal to

$$R_{mir} = \sqrt{1 + 4B_\varphi^2/B_z^2}. \quad (1)$$

By varying the ratio B_φ/B_z, we could vary the mirror ratio within wide limits. For $B_\varphi = B_z$, the mirror ratio $R_{mir} \approx 2.2$.

For a sufficiently large B_φ/B_z ratio, not many of the charged particles succeed in penetrating into the region bounding the conductors in the outer space during the short time of turbulent heating. This situation permitted us to dispense with the large discharge chamber that is usual for multipole machines; instead, in the "Vikhr'-3" device, we used a chamber occupying only the interior region between the conductors.

The discharge chamber was pumped out in advance down to a pressure of 10^{-6} mm Hg. A hydrogen plasma with initial density of approximately 10^{12} cm^{-3} was produced by using six pairs of simultaneously triggered titanium-hydride injectors 5, positioned at 60° intervals around the perimeter of the torus. The current through the injectors flowed for only a few microseconds, after which the "afterglow" plasma gradually decayed, and its density after a time of order 10^{-4} sec fell to 10^{11} cm^{-3}. At a time of 25-60 μsec after the injectors had been triggered, the hf shock circuit was triggered by the four coils 4 in parallel, which served as an inductive element. The circuit produced around the torus a vortex electric field E (Fig. 2a), and the plasma was turbulently heated.

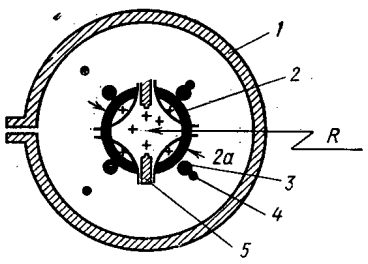

Fig. 1. Diagram of device.

RESULTS

Figure 3 (curves 1-3) presents data on the interferometric measurement ($\lambda = 8$; 30 mm) of the plasma density n for various operational regimes of the device. Curve 1 corresponds to decay of the preliminary plasma in a simple toroidal magnetic field ($B_\varphi = 0$). Switching on the field B_φ (curve 2) increased the confinement time by approximately a factor of five.

Translated from Atomnaya Énergiya, No. 5, pp. 468-470, May, 1971. Original letter submitted May 14, 1970; revision submitted July 23, 1970.

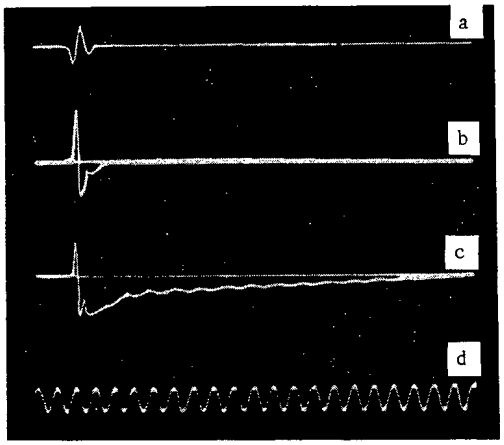

Fig. 2

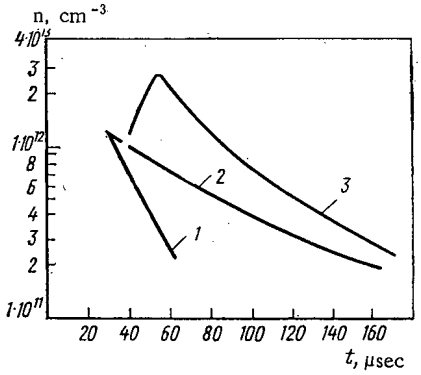

Fig. 3

Fig. 2. Oscillograms: a) vortex electric field; b) diamagnetic signal for $B_\varphi = 0$; c) diamagnetic signal for $B_\varphi = B_z = 1.8$ kOe; d) time markings with period 1 μsec.

Fig. 3. Decay of the plasma density for different operational regimes of the device.

The characteristics of the turbulent-heating phase of a plasma in the "Vikhr'-3" device proved to be in good agreement with the data obtained earlier for the "Vikhr'-1" and "Vikhr'-2" devices [1, 2]. For an electric field E = 60 V/cm, the current amplitude J in the plasma reached 500 A. The current of duration <1 μsec was scattered by the anomalous resistivity of the plasma of energy approximately 10^{16} eV·cm^3. The maximal pressure of the heated plasma, recorded at the instant that the current ceased, was $nT_e = 5 \cdot 10^{14}$-$1 \cdot 10^{15}$ eV·cm^{-3} for a plasma density $(1\text{-}2) \cdot 10^{12}$ cm^{-3}.

The effect of turbulent heating on the behavior of the plasma density for $B_z = B_\varphi = 1.8$ kOe can be seen from curve 3 of Fig. 3. Before the hf circuit was switched on, at the instant t = 35 μsec the plasma decayed. After the turbulent-heating current ceased completely, we observed a smooth increase in density, which passed through a maximum after 15-20 μsec. It is of interest to compare data on the behavior of the density with the time variation of the diamagnetic signal under the same conditions (see Fig. 2c).

In a multipole magnetic field, the diamagnetic signal of the turbulently heated plasma is maintained for approximately 15 μsec, which corresponds well with the time of density increase in curve 3 of Fig. 3.

For $B_\varphi = 0$, a smooth increase in density n after heating was not observed, and the corresponding diamagnetic signal disappeared immediately after the heating ceased (see Fig. 2b). The experimentally measured confinement time of the diamagnetic signal τ_{con} rapidly increased with increasing T_e.

DISCUSSION

Plasma decay in the absence of turbulent heating or prior to it can be explained by ambipolar diffusion along the magnetic field.

The increase in the confinement time of a cold plasma τ_c when the field B_φ is switched on can be explained by an increase in the effective length of magnetic force lines up to their emergence at the wall.

After turbulent heating to $T_e \approx 500$ eV, the electrons should be confined in a magnetic trap of multiple type during the time of Coulomb scattering in a loss cone $\tau_{Coul} \approx 100$ μsec. However, for the selected method of plasma production, the degree of plasma ionization did not exceed 10%, and hot electrons could lose their energy after a shorter time by the ionization of neutral atoms. The density that appears because of the ionization of cold electrons should first increase in time, and then (after the hot electrons disappear) fall exponentially, passing through a maximum at the instant

$$t_0 = \tau_{ion} \frac{T_e}{A} \ln \frac{A}{T_e} \cdot \frac{\tau_c}{\tau_{ion}}. \qquad (2)$$

Here τ_{ion} is the ionization time of atoms by electron impact; A is the ionization value; and T_e is the temperature of the turbulently heated electrons with density n_0 at the instant when the heating ceases. Substituting the values $\tau_{ion} = 1 \cdot 10^{-6}$ sec, $T_e = 500$ eV, A =30 eV, $\tau_c = 7.5 \cdot 10^{-5}$ (according to the data of Fig. 3), we obtain $t_0 \approx 2 \cdot 10^{-5}$ sec, which agrees well with the experimental data.

It is easy to show that the diamagnetic pressure of the plasma for a Maxwellian electron energy distribution is described by the relation*

$$nT = n_0 T_e e^{-\frac{A}{I_a} \cdot \frac{t}{\tau_{ion}}} \qquad (3)$$

Equation (3) sufficiently well describes the oscillograms of the diamagnetic signal observed in the experiment, and the dependence of τ_{con} on T_e.

In the experiments described above, a significant increase in the confinement time for a turbulently heated plasma was reported for a transition from uniform-toroidal to quadrupole magnetic field. It is shown that the confinement time of a turbulently heated plasma after the heating ceases is much greater than the time of toroidal drift, and, when the preliminary plasma is produced by the method of injection, can be explained by the electron losses on ionization of the neutral gas. In spite of the structural differences from the usual closed multipole traps, the "Vikhr'-3" device sufficiently well models the stage of turbulent heating of a plasma in a multipole trap with internal conductors.

In conclusion, the authors thank E. K. Zavoiskii for constant support and D. D. Ryutov for valuable discussions.

LITERATURE CITED

1. S. D. Fanchenko et al., Zh. Éksp. Teor. Fiz., 46, 497 (1964).
2. S. D. Fanchenko et al., Phys. Rev. Letters, 21, 789 (1968).

*Equations (2) and (3) are obtained under the assumption that τ_c, $\tau_{Coul} > (T_e/A)\tau_{ion}$.

NEWS

INTERNATIONAL CONFERENCE ON INSTRUMENTATION IN HIGH-ENERGY PHYSICS

I. A. Golutvin, V. V. Vishnyakov,
N. A. Toropkov, and Yu. A. Shcherbakov

The International Conference on Instrumentation in High-Energy Physics took place at the Joint Institute of Nuclear Research (Dubna) on September 8-12, 1970. The Conference was organized by the State Commission on the Uses of Atomic Energy and the Joint Institute of Nuclear Research (JINR) under the sponsorship of the International Union of Pure and Applied Physics. Nearly 250 leading scientists and engineers of more than 25 countries participated in the proceedings. The program included a wide range of problems associated with the design of new original equipment and with highly efficient methods of research and data processing. More than 150 papers were presented at the Conference.*

The Conference was opened by the Chairman of the Organizing Committee V. P. Dzhelepov. He stressed that the design of new measuring and detection systems and the development of novel research methods underlay all advances in scientific experiments with high-power particle accelerators that at present are the principal sources of fundamental knowledge about nature.

Eighteen plenary sessions dealt with specific problems of experimental high-energy physics and can be roughly grouped into the following basic sections: 1) computer controlled systems; 2) magnetic spectrometers and effective-mass spectrometers; 3) filmless track detectors and streamer chambers; 4) Cerenkov counters, γ-quanta and electron detectors, and semiconductor detectors; 5) bubble chambers and film data processing; 6) polarized targets and application of superconductivity in high-energy physics equipment; 7) particle beams and neutrino detectors; 8) development of certain new techniques for future accelerators and the creation and use of extremely strong magnetic fields.

Computer Controlled Systems. These were discussed in detail in a report by G. Collins (USA) presented at the Conference by M. Fisher (USA) and in other papers. The development of filmless chambers led to an extensive use of computers in experimental high-energy physics. Most widely used are spectrometers composed of multiwire spark chambers and scintillation and Cerenkov counters controlled by digital computers that also perform preliminary data sorting and processing of experimental results. Great interest was aroused by the apparatus developed at the Brookhaven National Laboratory (USA) which consists of three spectrometers and is capable of recording up to ten multiple-track events per one accelerator burst. To reduce processing time the entire information from all detectors is entered into the computer and recorded on magnetic tape. Principal data processing is performed on an SDS-6600 computer. Further advances in computer controlled experimental systems will evidently include multiwire proportional chambers which will allow a radical increase in experimental information. This in turn will require further improvement of computer interfacing methods.

Magnetic Spectrometers. Magnetic spectrometers both with a "small" aperture for the detection of one or two particles and with "large" aperture for analysis of multiple-track events are characterized by ever-increasing resolving powers. W. Panowsky (USA) reviewed equipment for measuring the angle and momentum of particles knocked out of the target.

A new development in this field is the use of particle focusing which allows the use of shorter particle paths and a reduction of the weight and cost of equipment without affecting its performance. Although all

*The presented papers will be published as a collection of the Proceedings of the Conference.

Translated from Atomnaya Énergiya, No. 5, pp. 471-474, May, 1971.

existing 4π spectrometers have at present optical chambers there is no doubt that most of them will be in the near future fitted with filmless detecting devices.

Effective-Mass Spectrometers. These have been discussed by M. Martin (CERN). The author reviewed the fundamental characteristics of three large spectrometers: 1) the boson spectrometer (CERN-IFVE); 2) multiple-particle magnetic spectrometer in Brookhaven (dead time 10 msec, data processing rate 50 events per accelerator pulse, average time of analysis of one event using the SDS-6600 computer 0.025 sec); the CERN Omega spectrometer (dead time 30 msec, average data retrieval rate $5 \cdot 10^4$ events per 24 h, 18 kG magnetic field, the use of filmless spark chambers considered). Other types of special-purpose spectrometers were also discussed.

Filmless Track Detectors and Streamer Chambers. Recent progress in these fields was discussed by I. A. Golutvin (JINR) and Yu. A. Shcherbakov (JINR). The following exchange of information and lively discussion proved that multiwire spark chambers with ferrite-core or magnetostrictive-line readout are most popular in accelerator experiments. However, the most important advance in filmless chamber techniques was the discovery and development of multiwire proportional chambers first proposed by G. Charpak (CERN) and V. G. Zinov (JINR). Recent progress in these devices was discussed by G. Charpak (CERN). Two large facilities using multiwire proportional chambers with $5 \cdot 10^3$ wires each were designed at CERN. Maximum chamber dimension is 2.7 m. The electronics uses integrated circuits. Most popular are multiwire proportional chambers filled with an argon–isobutane–freon bromide mixture and having an amplification of $\sim 10^8$.

J. Fisher (Brookhaven, USA) reported on a so-called hybrid chamber in which a spatial accuracy of 0.25 mm is achieved with small resolving (80 nsec) and dead ($\sim$60 μsec) times. The chamber has a 1.5 mm spark gap with a high detection efficiency obtained by using auxiliary proportional and drift gaps. Notwithstanding its quite complicated construction the hybrid chamber is relatively inexpensive because of the possibility of using magnetostrictive readout.

Some progress has also been achieved in liquid electronic chambers. B. Dolgoshein et al., (USSR), L. Golovanov et al., (JINR), E. Kurishchenko et al., (USSR), and R. Muller (USA) reported new results concerning the spatial resolution ($\sim$0.1 mm), resolution factor ($\sim 10^4$), and detection efficiency ($\sim$100%) of such chambers; these results were the topic of a special discussion. It is to be hoped that further improvement necessary in order to make these chambers useful in experimental practice will be reported already at the next conference.

Of special interest is the work of V. I. Rykalin et al. (IFVE, USSR) on the development of a new hodoscopic photomultiplier operating in crossed electric and magnetic fields. Such a device can be efficiently exploited in the future for a data processing system much faster than conventional television systems used with hodoscopes, spark chambers, Cerenkov chambers, etc.

Streamer chamber techniques have also received much attention. Experience gained in the operation of two large facilities (at SLAK and DESY) proved the high efficiency of this technique. Gas and liquid-hydrogen targets as well as converters (JINR) can be easily located in such chambers. Several papers dealt with the possibility of using ionization measurements in the field of relativistic ionization growth.

The technique of high-pressure helium streamer chambers (JINR) has also been discussed. Further progress in this direction is associated with the development of high-power lasers for creating high-intensity fields (CERN) and with the use of holography for photographing the discharge (FTI, Leningrad).

Favorable characteristics of an instrument with combined target and detector functions stimulated further development of a hydrogen streamer chamber (JINR, CERN). The design of new facilities with large streamer chambers (up to 12 m, Berkeley) has been reported.

Cerenkov Counters and γ-Quanta and Electron Detectors. As noted in a review report by S. P. Denisov (USSR) and in seven original papers, considerable advances have been achieved in the design of Cerenkov counters and chambers. Better models of both threshold and differential Cerenkov counters provide a resolution of nearly 10^{-6} (IFVE, JINR, ITEF). Hodoscopic (multichannel) systems are being designed with such counters that will have an accuracy of an order of magnitude better than the systems now in use for measuring total interaction cross sections in the energy range of tens of GeV/sec. It seems that further developments in Cerenkov chambers will involve the design of wide-aperture high-efficiency counters and the use of high-resolution image converters for recording Cerenkov radiation rings in various magnetic spectrometers. Such facilities have already enabled a velocity resolution of $6 \cdot 10^{-7}$ allowing the measurement of a π meson momentum to within 10^{-3} and of proton momentum to within 10^{-4} (JINR, CERN, etc.).

Sandwich-type avalanche detectors and total-absorption Cerenkov spectrometers were designed for γ-quanta and high-energy electrons detection. A combination of avalanche detectors and spark chambers, Cerenkov-spectrometer hodoscopes, are used for simultaneous measurement of energy and direction of motion of particles. In the field of precision (1%) measurement of γ-quanta energies in the range 10-15 GeV one should mention unique miniature total-absorption detectors using PbF_2 single crystals (density 7.77 g/cm^3, refractive index 1.8) developed by Hoffschtadter (Stanford, USA).

Of great importance for research with future accelerators (hundreds and thousands of electronvolts) is the relatively simple method of finding the energy of γ-quanta from the electron intensity at the shower minimum (A. A. Tyapkin, JINR). As proved by measurements made in Serpukhovo, the technique provides a resolution of 20% at an energy of 30 GeV.

Review reports of A. I. Alikhanyan (experiment) and G. M. Garibyan (theory), as well as several other original reports, were devoted to the investigation of transition x-ray radiation discovered at the Erevan Physical Institute and suitable for particle recording at ultrahigh energies (hundreds of GeV or more). The intensity of transition radiation is proportional to the Lorentz factor of the particle so that both the detection efficiency and measuring accuracy increase with particle energy. Counters of this type are useful for high-energy electrons detection.

The application of semiconductor detectors in high-energy physics has been discussed by C. Vigand (USA). A very effective use of silicon detectors in elastic pp scattering has been made in experiments with the Serpukhovo synchrotron (V. A. Nikitin et al., JINR). The capabilities of semiconductor detectors in the spectrometry of heavy charged particles (K-mesons, protons, deuterons, etc.) at energies of up to 200 MeV and in magnetic systems has also been noted.

Bubble Chambers and Processing of Film Data. Basic developments in bubble chamber techniques have been reviewed by S. Ya. Nikitin (USSR). New-generation bubble chambers (12 ft chamber of the Argonne National Laboratory, USA; Mirabel and Gargamel chambers, France; 30 m^3 chamber of the Batavia accelerator, the Large European Chamber at CERN; SKAT, USSR) are all characterized by large active volumes and high magnetic field intensity. Advances in bubble chamber techniques include high-speed control and comprehensive automation of data acquisition and processing.

P. Huff (USA) reported on new results in film data processing and discussed future prospects of its development. Davey (England) and Douning (USA) discussed high-efficiency measuring systems. A simple readout instrument for semiautomatic film processing has been described by Kitahaki (Japan).

Improvement of data processing systems and the reduction of their cost has been made possible by the application of fast and reliable readout devices together with modern computers for controlling the readout process and for data reduction. According to Huff, the transfer from operator-controlled semiautomatic instruments to computer-controlled systems that read out information along a preset path increased the efficiency by four to ten times per one operator.

Further perfection of programmed scanning made it possible to pass from "road guidance" (RG) to "vertex guidance" (VG) operation used, for example, in helical measuring instrument, and to "minimum guidance" (MG) operation. Such operating modes allow an additional increase of productivity by a factor of two to three. The change from RG to VG and MG operation has been made economic after the IBM-7094 computer has been replaced by the more powerful SDS-6600 computers that reduce the cost of a single run by approximately a factor of four to five.

Systems operating in the VG and MG mode are now widely used in many Western physical centers (Brookhaven National Laboratory, CERN, Berkeley, and others).

One should mention the MG system developed in Oxford (England). This system uses a PDP-6 computer with a memory of 64 k 36-bit words and a 1.75 μsec access time. The input information to this system consists of preliminarily sorted data on the topology and position of the vertex of the investigated event on a given projection in a region of the order of 1-2 mm. The system is capable of processing up to 430 events /h without the intervention of an operator (up to 150 events/h in more complex cases). The control and track searching programs were written almost entirely in Fortran-4 and occupy 34 k words of the PDP-6 memory.

The following basic trends in the development of data processing systems were noted at the Conference:

1. Systems operating in the VG and MG modes are almost universally accepted. Intensive work is conducted on the improvement of the existing and on the design of new more efficient scanning devices. Thus, the Brookhaven Laboratory developed a new automatic scanner capable of processing several thousands of tracks per hour; foreseen is a study of the feasibility of an instrument capable of processing up to 50 thousands events/h.

2. The computers used at present will be replaced by more efficient machines. For example, the Brookhaven Laboratory foresees the introduction of an SDS-7600 computer in the next two years and the use of PDP-101 machines in individual groups.

3. An important new direction in data acquisition and processing is the application of holographic methods.

Polarized Targets and Superconductivity. B. S. Neganov (JINR) noted that recent theoretical and experimental works made it possible to understand the mechanism of dynamic polarization and to select suitable target materials. Most successful proved to be Rubo targets on a basis of ethylene glycol or a mixture of butanol with 5% water and 0.9% ether peroxide that have a 67% polarization for 12 mV of microwave power. The polarized target under development at the JINR is cooled to 0.1°K by means of a special cryostat whose operation is based on the dissolution of He^3 in He^4.

Superconductivity is also gaining firm hold in high-energy physics. As an example one can mention the design of externally-stabilized superconducting magnets for bubble chambers (ANG, NAL, CERN), of an Ω spectrometer, of superconducting resonators for radio-frequency particle beam separators (CERN), etc.

Particle Beams and Neutrino Detectors. A new development in this field is the production of hyperon (Ξ^-, Σ^-, etc.,) beams in several accelerators. This topic has been discussed by Sandweiss (USA). The Brookhaven beam of charged hyperons will have an intensity of 5-10 Ξ^- per sec and 150-1500 Σ^- per sec. Such an intensity should allow total cross sections of hyperon–nucleon interactions to be measured very accurately with the aid of spark chambers.

Another promising development is the production of a beam of tagged photons with an intensity of 2-4 per sec (Morrison, Stanford, USA). The production of tagged photon beams will be greatly facilitated by the introduction of proton accelerators with energies of the order of tens and hundreds of GeV. As follows from several papers presented at the Conference, experiments with tagged photons are being planned at Serpukhovo and several other laboratories (USSR, USA). A growing number of studies is now being conducted with beams of polarized quasimonochromatic γ-quanta (R. O. Avakyan et al., V. G. Gorbenko et al., USSR). This method is now fully developed and is being used also in several Western laboratories.

V. S. Kaftanov (USSR), F. A. Nezrick (USA), and Walker (USA) discussed the already performed and planned (with USSR, CERN, and USA accelerators) neutrino experiments using bubble chambers and detectors consisting of spark chambers and scintillation counters.

Future Accelerator Techniques and Superstrong Magnetic Fields. The most important results in electronic system techniques have been analyzed by A. Roberts (USA) who described their application in the Batavia proton synchrotron. Bubble chamber techniques become ineffective at such energies since the required accuracy and the possible number of channels increase rapidly. Methods based on electronic systems are thus preferable even in the case of very complex events.

A new method of measuring magnetic moments of hyperons and based on the use of superstrong magnetic fields (~1 MG) has been proposed by L. M. Barkov et al. (USSR). The authors expect that ten exposures in the VEPP-3 electron accelerator, having a rated electron energy of 1.35 GeV and a intensity of 10^{12} particles per burst, will suffice to accumulate statistics of about 100 events which will make it possible to measure the magnetic moment of Σ^+ hyperon with an accuracy of 3%.

A lively discussion of the future developments and trends in experimental techniques in high-energy physics was held on the last day of the Conference. Novel original ideas were expressed in papers by G. Charpak (CERN) and B. A. Dolgoshein (USSR) as well as in the following discussion with the participation of B. M. Pontekorvo, A. A. Tyapkin, A. F. Pisarev (JINR), G. Charpak (CERN), and others.

The materials of the Conference prove that all leading laboratories of the world involved in high-energy physics research devote much attention to the development of new experimental techniques and detectors, and to putting all latest achievements in various fields into experimental practice. All this is aimed

at a more efficient utilization of accelerators and experimental equipment as a result of which the flow of scientific data increases and the cost of an arbitrary unit of information decreases.

All papers read at the Conference aroused great interest and lively discussions. The Conference owes its success to the fact that most papers presented at the Conference dealt with new developments and successful solutions of original ideas; to the excellent organization of the Conference; and last but not least, to the excellent work done by all lecturers and reporters and scientific secretaries in organizing the materials of the conference and by all participants.

The Conference noted the progress achieved in the last few years in the design of high-quality equipment and particularly in the discovery and development of new methods of investigation in high-energy physics. The Conference demonstrated the spirit of collective creativity that reigns at present in science and makes important contributions into the consolidation of international cooperation among scientists.

PROBLEMS ENCOUNTERED IN HANDLING OF TRANSURANIUM ELEMENTS

V. N. Kosyakov

An International Seminar on Radiation Protection in Handling Transuranium Elements organized by the European Nuclear Energy Agency in cooperation with Euratom has been held in Karlsruhe (FRG) in September 1970. More than 60 specialists of eleven countries and three international organizations took part in the Seminar. The following problems were discussed at the Seminar: production and application of transuranium elements, hazards encountered in handling transuranium elements, their metabolism, physical and medical survey of personnel, measures to be undertaken in case of emergencies.

One of the most abundant transuranium isotopes is Pu^{238} which can be relatively simply obtained in kilogram quantities from irradiated Np^{237} which is a side product of the processing of irradiated uranium fuel elements of power reactors. The production of Np^{237} and consequently also of Pu^{238} can be organized in any country that has fuel element processing plant. For example, a production of about 5-7 kg/yr is planned in the WAK processing plant (Karlsruhe, FRG) with a yearly productivity of 40 tons of UO_2. Isotopically pure Pu^{238} suitable for biomedical applications including implantation is obtained as a consequence of α-decay of Cm^{242} as a result of irradiation of Am^{241}.

Americium, as well as neptunium, is a side product of the processing of spent nuclear fuel elements. Thus, about 2 kg of Am^{241} and 0.6 kg of Am^{243} can be produced from the highly active wastes of the above-mentioned WAK plant. The possibility of obtaining americium and other transplutonium isotopes will improve with higher degrees of burn-up and with the use of plutonium fuel. Both isotopes of americium can serve as a source of higher transplutonium isotopes Cm^{244}, Bk^{249}, and Cf^{252}.

Cm^{244} is produced by special irradiation of Pu^{242} or americium in reactors with high-density neutron fluxes. The Cf^{252} isotope is obtained by subsequent irradiation of Cm^{244}, as well as Pu^{242} and americium isotopes, in reactors with a neutron beam density of the order of 10^{15} n/cm^2 · sec.

The many different uses of transuranium elements can be divided into two main groups: as energy sources and as direct or indirect radiation sources. Most widely used as an energy source is Pu^{238} with a half-life of 86.4 years and a specific energy density of 0.55 W/g. Electrical generators based on Pu^{238} are used as power supplies in space, in remote radio-navigation and radio-relay stations, in meteorological stations, etc. Such power sources can use up kilogram quantities of plutonium. One of the most important applications of Pu^{238} is as long-lived, reliable, miniature power supplies in heart pacers. As shown by preliminary design, as little as about 200 mg of Pu^{238} is capable of supplying the nearly 100 μW of electric energy needed to power such a pulse generator.

High-intensity α sources can be used in chemical analysis based on α-particle scattering and on (α, p) reactions with matter. The use of Pu^{238}, Am^{241}, and Cm^{242} together with beryllium for the production of neutron sources with a yield of up to 10^8 n/sec is well known. The availability of Cf^{252} made possible the design of still more compact and powerful neutron sources (1 g of Cf^{252} emits $2.3 \cdot 10^{12}$ n/sec). Californium sources can find application in various sorts of measurements based on neutron diffraction, neutron radiography, as trigger sources in reactors and critical assemblies, in neutron activation analysis, in medicine, geology, hydrology, etc.

As compared with the majority of radioactive isotopes commonly encountered in research and isotope laboratories, transuranium isotopes have certain specific features that put them apart not only in respect of their special applications but also from the point of view of safety measures that must be observed in using

Translated from Atomnaya Energiya, No. 5, pp. 474-475, May, 1971.

these isotopes. Radioactive decay of many isotopes of transuranium elements is accompanied by emission of x-ray, γ, and neutron radiation. Even in cases when the fraction of such radiations is not large, handling of significant amounts of these isotopes requires special protection from penetrating radiation and the use of remote control devices. One unique feature of some transuranium isotopes is spontaneous fission with ejection of fast neutrons. For example, the density of the neutron flux at a distance of 1 m from 1 g of Cf^{252} is $\sim 10^7$ n/cm^2 · sec while the maximum permissible level of fast neutrons is 20 n/cm^2 · sec. It is thus evident that the problem of radiation protection in the case of californium becomes an important factor even if microgram quantities of it are involved.

The specific α-activity of transuranium isotopes varies from several units to thousands of curies per gram. It is enough to compare these magnitudes with the average annual allowable concentration (AAC)* of transuranium isotopes in air ($\sim 10^{-15}$ Ci/liter) to realize how dangerous even negligible amounts of these isotopes in the environment are. From the point of view of radioactive contamination of the surrounding space, safety is a function of the degree of air tightness of the protective screens and of the efficiency of the ventilating and filtering systems. Neglect of any one of these conditions is liable to lead to serious consequences not only as a result of external contamination but also of these elements entering the human organism.

Determination of the level of internal contamination by transuranium elements is quite difficult. The content of most transuranium isotopes in the lungs is evaluated by measuring the associated α-decay of soft (17-20 keV) x-rays near the body's surface. This radiation is strongly absorbed also by soft tissue. At the same time, the maximum allowable levels of transuranium-elements activity in the human organism are so low as to be practically close to the sensitivity threshold of the appropriate measuring devices. For this reason a reliable estimation of the level of internal contamination and exposure requires much additional information: the results of radiometric analyses of body eliminations taken during a long time, data on the metabolism of transuranium elements in the human body, information about the actual contamination of the air at the time of entry of transuranium elements into the body, etc.

Radioactive materials can enter the human organism with inhaled air, through the alimentary tract, and through wounds; the first way is the most probable one. Experiments with rodents and dogs proved that the distribution of plutonium in respiratory tracts depends to a large extent on particle size and on the solubility of the compound. Nearly 40% of plutonium introduced in the form of a insoluble compound is concentrated in bronchial lymph nodes. Plutonium introduced into the lungs in the form of a soluble compound spreads easily in the organism and accumulates mainly in the bones and liver. Plutonium and americium entering blood are fixed predominantly by protein molecules and deposited on bone surface. Investigation of the liver of mice proved that plutonium, americium, and curium that enter blood in the form of monomers are fixed by lysosomes. Although this process is relatively slow in the case of plutonium, americium is practically completely fixed one hour after being injected into blood.

Many laboratories study stimulated elimination of transuranium elements from the body under the action of strong chelates, complexing agents such as ethylenediaminetetraacetate (EDTA), diethylenetriaminepentaacetate (DTPA), triethylenetetraminehexaacetate (TTHA), and disferrioxyamine-B (DFOA). Timely administration of chelate complexing agents through the respiratory tract or internally shortens the elimination time of transuranium elements from the body and reduces their accumulation in the lungs, liver, and bones. These reagents are particularly effective for decontamination of wounds.

Fast determination of internal contamination levels in the case of an emergency allows the medical staff to undertake the appropriate therapeutic and surgical measures in order to reduce the accumulation of transuranium elements in the body to a minimum. These measures lose their effectivity if undertaken too late. Examination of victims usually consists of three stages: immediate, preliminary, and final. The two principal ways through which radioactive substances can enter the body are the respiratory tract and damage of the integument (injury).

*The concept of allowable average annual concentration (AAC) has been introduced by "Radiation Protection Norms NRH-69" to replace the incorrectly used term "maximum allowable concentration" (MAC).

TESTING OF THE "STAVRIDA" NAVAL γ-FACILITY

The first in the USSR naval γ-facility "Stavrida," installed on the industrial-research ship "Akademik Knipovich" and intended for developing the technology of γ-radiation preservation of fresh fish and other sea products immediately after catching, has been field-tested in the period from January till July, 1970. The tests proved the feasibility of radiation processing of sea products with the aim of increasing their storage time as well as the reliable and smooth operation of all units of the facility under sea navigation conditions.

The outside view of the facility is shown in Fig. 1. The installation (Fig. 2) consists of a metal body including a base (1), and biological protection screens (2) that reduce the dose rate to 0.25 mR/h and are fitted with internal square wells. Plates (13) in the central portion of the well hold eight tubes (14) that form a flat irradiator containing cans with the radiation sources.

Two slide blocks (16) on both sides of the irradiation yoke form a delivery gate and have, just in front of the irradiator, horizontal shafts that serve as irradiation chambers for boxes (4) with the irradiated product.

The delivery gate with the irradiation chamber and the motion of the irradiated packages into and out of their radiation zone is controlled by an electric block-and tackle mechanism (6) mounted on frame (5) which rest on top of the instrument body. Stops (10), controlled through a system of rods by handle (9), are provided to position the packages in the irradiation chambers. If the packages are stuck in an incorrect position the limit switch (8) disconnects the control circuit and disables the lifting mechanism.

Irradiation is controlled by a timing relay by means of which it is possible to set the desired irradiation dose to any value between 0.005 to 2 Mrad. The facility is provided with an aural and visual signalization system and with radiation monitoring instruments.

The γ-facility is operated as follows. The product to be irradiated is packed in metal boxes which by means of the loading mechanism are placed in delivery gate shafts. Pressing a pushbutton causes the boxes to be placed in the irradiation zone on one side of the irradiator. After being exposed to one half of the desired dose, the boxes are shifted automatically by means of the delivery gate to the other side of the irradiator where irradiation is completed.

Technical Specifications of the Facility:

Radiation source	Cs^{137}
Irradiator activity	85,200 Ci
Bulk average dose rate in water-equivalent medium	207 ± 25% rad/sec
Productivity at 0.25 Mrad dose	100 kg/h
Dose rate at the surface	<0.28 mR/h
Number of irradiation chambers	2
Size of irradiation chamber	400 × 300 × 200 mm
Power consumption	8 kW
Supply voltage of three-phase 50 Hz line	380/220 V
Dimensions:	
diameter	1450 mm
height	3800 mm
Weight	20 ton

Translated from Atomnaya Énergiya, No. 5, pp. 476-478, May, 1971.

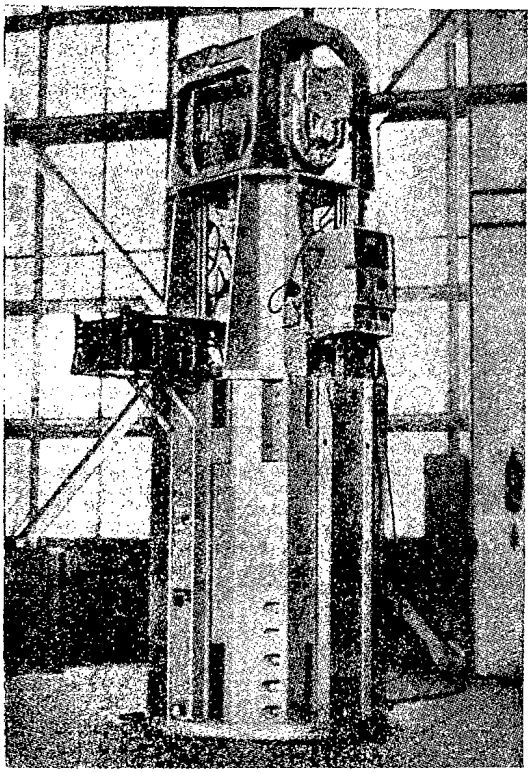

Fig. 1. Outside view of the "Stavrida" γ-facility.

The "Stavrida" γ-facility was designed by the All-Union Scientific-Research Institute of Radiation Technology and its manufacture was completed at the beginning of 1969; at the end of 1969 the facility was assembled, loaded with radiation sources, and passed three months of tests and checkups on the shore. In the course of shore tests all units of the facility operated satisfactorily in all modes.

After passing all shore tests the facility was installed in December 1969 on the large refrigerator trawler "Akademik Knipovich" used for various industrial research works.

From January to July 1970 the ship sailed through nearly 48,000 km from the Black Sea to South Atlantic. During this time we made the following tests: 1) the performance and reliability of the mechanical and electrical units of the facility were thoroughly tested; 2) the active portion of the irradiation chamber was tested dosimetrically using various kinds of fish as the test medium; 3) various species of industrial fish, products, and other sea objects were irradiated in order to develop optimum techniques for radiation preservation. The tests were conducted under the following conditions: a) in various climatic zones of the ocean (subtropics, tropics, Antarctic) with an air humidity of up to 98% and surrounding temperature from +8 to +35°C; b) in conditions of calm; and c) under gale conditions with the ship heeling up to 20°C (rolling) and up to 8°C (pitching). Up to 70% of all tests were made under gale conditions.

Dosimetry of the active volume was conducted with a 20% solution of glucose in distilled water, whose initial concentration was determined from the angle of rotation of the polarization plane (φ_0). After irradiation the angle of rotation (φ) was measured once more and the change ($\Delta\varphi$) due to the reduction of glucose concentration in the irradiated sample was determined.

The development of techniques for γ-irradiation of sea products was conducted under the following conditions:

1. Determination of the optimum preserving dose for various species of fish. The experiments were made with 50 to 70 pieces of fish of each kind. After dressing and vacuum packing into packages wrapped in PTs-2 film, the samples were exposed to 0.1, 0.2, 0.3, 0.4, 0.5, and 0.6 Mrad doses. The test batch was stored at 0 to +5°C together with a control, i.e., not irradiated batch. An organoleptic examination of the nutritive value of the irradiated fish was made immediately after irradiation and after 14 days of storage in order to determine the optimum dose. Samples of fish irradiated with an optimum dose were taken for further chemical and biochemical tests immediately after exposure and after 14, 30, 45, and 60 days of storage. Optimum irradiation conditions were established on the basis of organoleptic and chemical analyses.

2. Biochemical investigation of muscle proteins of irradiated and nonirradiated fish. Two carcasses of each kind of fish of the same age and physiological state were packed in 20 g cans, exposed to 0.1, 0.2, 0.3, 0.4, 0.5, and 2 Mrad doses, and stored for up to two months at 0 ± 5°C. The changes that took place in the fish were then analyzed.

3. Investigation of the microflora of irradiated fish, i.e., of the bacterial semination of freshly caught and irradiated fish as a function of storage time and dose rate. The optimum irradiation doses were determined from the results of bacteriological analyses. The analysis was made with several sorts of industrial fish (Carangidae, nototheniids, sea crucian, putassu) caught on various fishing grounds in the Atlantic and exposed to 0.1, 0.2, 0.3, 0.4, 0.5, 0.6, 1, 1.15, and 2Mrad doses.

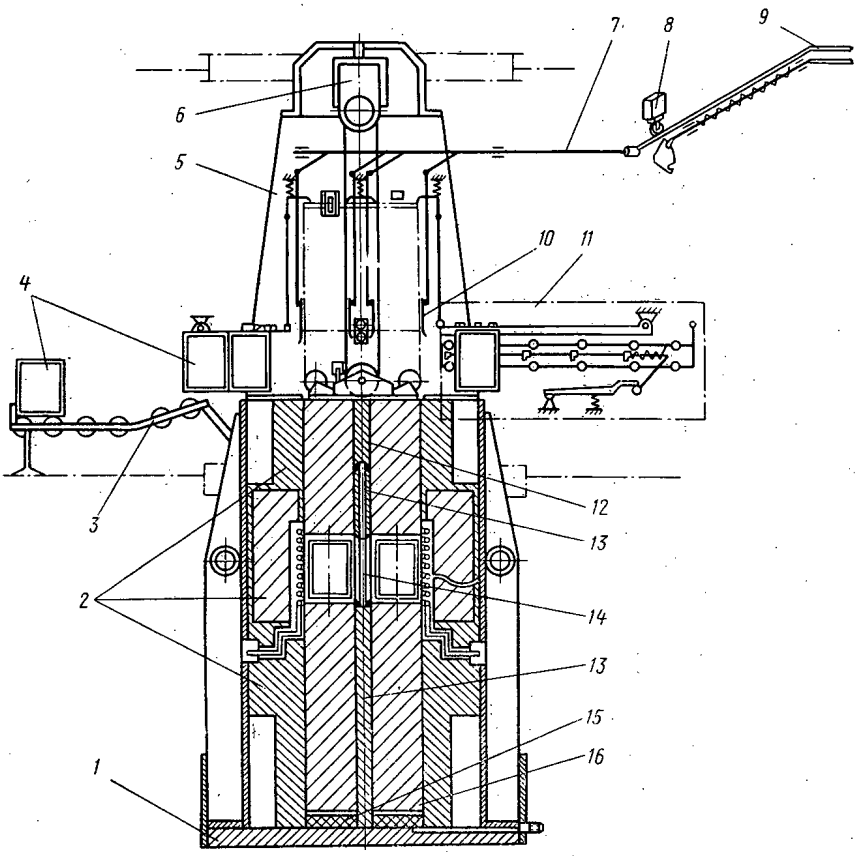

Fig. 2. Schematic drawing of the γ-facility: 1) base; 2) protective screens; 3) transport mechanism; 4) packages; 5) frame; 6) TÉ5-911-380 electric steel; 7) interlock mechanism; 8) VPK-111T limit switch; 9) handle; 10) stop; 11) loading mechanism; 12) loading tackle; 13) plate; 14) tubes; 15) shock absorber; 16) slide block.

Preliminary analysis of the results indicated that from the point of view of the state of muscle proteins and organoleptic indicators the optimum dose for prolonged storage is 0.4 Mrad.

The facility proved its reliability in all sea conditions that allow trawling.

The "Stavrida" γ-facility is simple in operation and can be used in a wide range of investigations.

THE "BETAMICROMETER" RADIOISOTOPIC COATING THICKNESS GAUGE

I. I. Kreindlin, V. S. Novikov,
and A. A. Pravikov

Scientists at the All-Union Scientific Research Institute of Radiation Technology have developed a coating thickness gauge using radioisotopes and called the "betamicrometer" (Fig. 1), designed for on-the-job measurements of the thickness of various metallic and nonmetallic coatings on metallic and nonmetallic backings.

The principle of action of this instrument is based on the method of scattering, in which β-particles emitted by a radiation source are scattered by the object in the opposite direction, to a radiation detector (Fig. 2). The number of particles reaching the detector is proportional to the thickness of the coating. A radioactive source S, placed in a collimator, emits β-particles which hit the object being measured; the reflected β-particles produce flashes of light in a scintillator Sc, and these are converted in a photomultiplier Ph into electrical current pulses, which are transmitted by an amplifier A to a scaler at the input of a pulse counter PC. The pulse counter records the number of pulses arriving within a fixed period of time, measured by a timer T. If the atomic number of the coating material is greater than the atomic number of the backing material and the range of measured thicknesses lies on the linear (initial) segment of the counting characteristic, the measurement will be read directly in microns. For example, for a platinum coating on titanium, a gold coating on nickel, or a gold coating on brass the linear range is between 0 and 10 μ. In this case, by means of a programming device PD, the pulse counter and timer are fed the adjusting data in inverse code (the digits are converted to their decimal complements). The timer is fed the time of measurement, and the counter is fed the number of pulses corresponding to the value of the count received from an uncoated object (from the backing). After the scaler is started, the counter accumulates the number of the pulses corresponding to the readings received from the coated object; the pulse counter overflows and begins counting from zero again. When the measurement time has expired, the timer issues a command to the control trigger CT to stop counting. The digital display of the pulse counter is left with a reading showing the thickness of coating in microns, which is equal to the difference between the number of pulses from the coated object and the number of pulses from the backing.

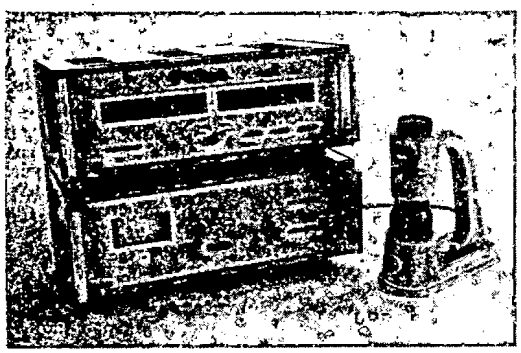

Fig. 1. The "Betamicrometer" radioisotopic coating thickness gauge.

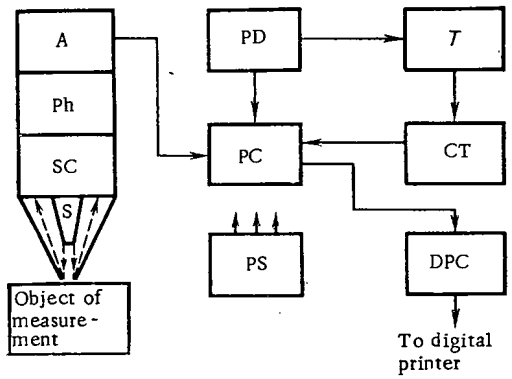

Fig. 2. Block diagram of the "Betamicrometer."

Translated from Atomnaya Énergiya, No. 5, pp. 478-479, May, 1971.

TABLE 1. Calculated Error Characteristics of the "Betamicrometer" for Some Commonly Used Coatings

Coating and backing	Thickness of coating, μ	Calculated error, μ
Silver on copper	Up to 5	± 0.26
The same	5-15	± 0.6
Gold on copper or nickel	Up to 3	± 0.04
The same	3-8	± 0.1
Plastic on steel	Up to 30	± 0.65
The same	30-100	± 1.2
Silver on nickel	Up to 5	± 0.17
The same	5-15	± 0.5
Rhodium on nickel or copper	Up to 2	± 0.14
The same	2-6	± 0.42

In all other cases the thickness of the coating is determined with the aid of a calibration curve.

The digital printer control unit DPC makes it possible to record the readings of the display lights automatically on a B3-15 digital printer. Power to all units of the apparatus is delivered by the power supply PS.

The "Betamicrometer" is constructed in individual units: a DOT-1 sensor, a PU-1 scaler and a BP-1 power supply unit.

The sensor consists of a closed cylinder containing a β-ray source, a stilbene scintillator, and a pulse amplifier. In order to exclude background β-radiation and bremsstrahlung, the source is placed in a tungsten collimator. The sensor is so designed that it can be used for making measurements of coating thickness on structural details of various dimensions. The sensor is aimed at the test point of the object being measured by means of a sighting device.

The scaler contains a pulse counter, a timer, a control trigger, a programming device, and a digital printer control unit. For accurate time measurement, the master oscillator of the timer is stabilized by a quartz resonator. The electronic units are made with transistors and printed circuits.

The coating thickness measurements are carried out over a 10 mm^2 area. A single measurement requires no more than 100 sec. Table 1 shows the calculated error characteristics of the "Betamicrometer" for some commonly used coatings. The operating temperature range is +10 to +35°C, the time required for adjusting to the operating regime is 30 min, the operating regime is continuous for 8 h, the instrument is fed by a 220 ± 10% V AC power supply with a frequency of 50 ± 1 Hz, and the power used does not exceed 150 VA.

MOBILE γ-UNIT "STIMULATOR"

D. A. Kaushanskii

A special γ-unit "Stimulator" has been designed at the Special Design Office of the N. D. Zelenskii Institute of Organic Chemistry of the Academy of Sciences of the USSR for presowing seed irradiation (Fig. 1). The first test model of the facility has been built and put into operation in March 1970. The facility is intended for irradiation of the seed of agricultural plants with a low seeding rate (from 0.05 to 3 kg/ha, as well as for use in strain-testing stations, experimental stations, and in research institutes and farms. The facility can be used for production purposes for industrial crops such as tobacco, etc.

The unit (see Fig. 2) consists of a separable container (body 1 and cover 2). At the center of the container is a cylindrical irradiator 3 in the form of a cartridge consisting of six tubular cells with the radiation sources 4.

The latter are conventional Cs^{137} sources 11 mm in diameter and 84 mm high. The radiation sources are loaded either in a hot chamber or under water. After the sources are loaded the cells are closed shut by plugs 5 in an atmosphere of argon. A rod 6 with the active volume 7 moves in a guide shaft along the container axis. The rod and active chamber are moved through the irradiator by means of a manual lifting mechanism 8. Up and down motion of the irradiation chamber is manual. The unit is mounted either on a GAZ-69 car (Fig. 1) or on a GAZ-704 trailer; the unit is protected from rainfall by a special cover. The trailer has an arrangement which makes possible its transportation by practically any kind of car.

The unit is operated in the following way: the seeds are poured into special 0.2 liter cups that are placed in the active chamber and lowered into the irradiation zone. The unit is operated by one man.

Principal Technical Data of the Unit:

Output at 1000 rad dose	5 kg/h
Total maximum irradiator activity	700-720 Ci
Dose rate at the center of irradiation chamber (in air)	800-1000 R/min
Inhomogeneity of the dose field	±20%
Surface dose rate	$<2.8 \cdot 10^{-3}$ R/h
Irradiation chamber:	
shape	Cylinder
diameter (outside)	60 mm
height	75 mm
volume	0.2 liter
Unit dimensions (container):	
length	550 mm
width	480 mm
height (including lifting mechanism)	1070 mm
Weight	540 kg
Total weight installed on GAZ-69 car	1860 kg
Total weight installed on GAZ-704 trailer	850 kg

The experimental model is loaded with six Cs^{137} radiation sources with a total activity of ~720 Ci.

Translated from Atomnaya Énergiya, No. 5, pp. 479-481, May, 1971.

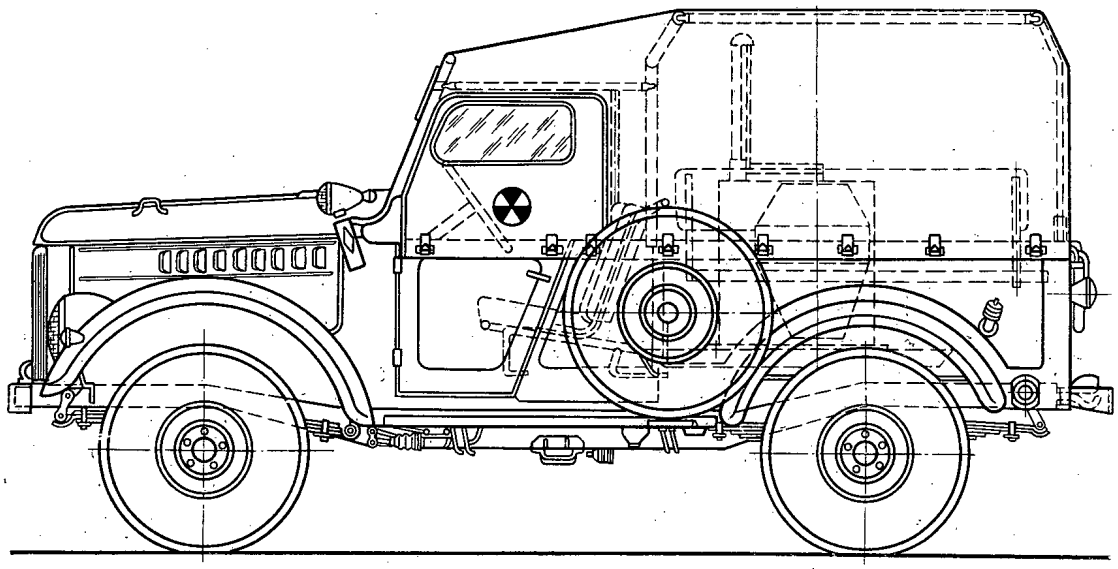

Fig. 1. Mobile γ-unit "Stimulator" mounted on a GAZ-69 car.

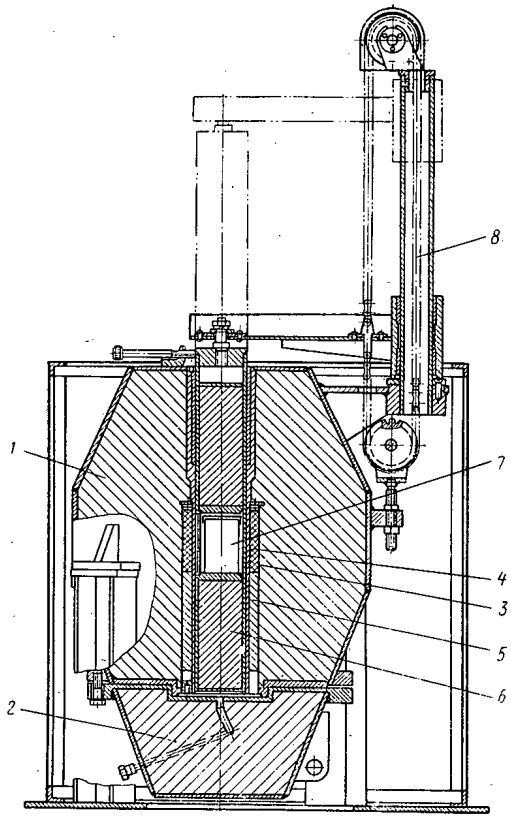

Fig. 2. Cross section through the "Stimulator" γ-unit.

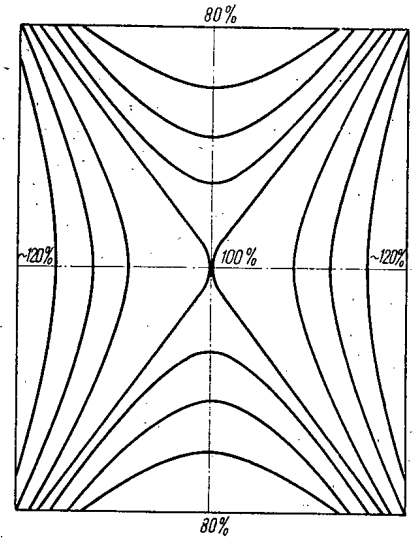

Fig. 3. Dose field in the active chamber (in air).

As shown by measurements conducted at the Institute of Nuclear Physics of the Academy of Sciences of the Belorussian SSR, the surface dose rate does not exceed 0.5 mR/h at any point under operating conditions and 2 mR/h during loading conditions. The measurements were made with an RUP-1 instrument. The calculated dose field in the active chamber is shown in Fig. 3. The dose rate experimentally measured at the center of the active chamber is ~1100 R/min.

AN ATOMIC ENERGY SOURCE FOR ELECTRICAL CARDIOSTIMULATORS

E. B. Babskii, É. E. Geronin,
V. A. Kremnev, and G. M. Fradkin

With the use of various implanted devices – stimulators (especially cardiostimulators), radiotelemetry capsules, and miniature artificial blood circulation devices ("mechanical hearts") – in physiological experiments and clinical practice, the problem of creating miniature long-lasting self-contained electrical energy sources has become quite urgent.

Chemical sources of electrical energy are used to stimulate the heart by means of implanted stimulators. Their basic disadvantage is a limited service life. The stimulators have to be reimplanted every six months to two years to change the chemical batteries.

Compared to chemical ones, atomic batteries differ in unit energy capacity by at least an order of magnitude, and in reserve capability by five times. Because of these advantages and their small size, they may be used in various devices implanted in the organism, such as electrical stimulators.

Development work on atomic electrical energy sources was begun in 1966-1967 in the USA, the USSR, England, and France.

In the development of atomic electrical energy sources, maximum overall efficiency is sought, which at a given level of electrical power should lead to a decrease in the quantity of radioactive "fuel" required and a decrease in the radiation effects on the organism. The technical characteristics of several types of such generators are shown in Table 1.

Experience in the development of radioisotope electric generators in the USSR enabled us to determine the type and basic components needed for creating a source of electrical energy for stimulators implanted in the body. Theoretical and experimental studies were conducted on all aspects of the problem, enabling us to construct a gas-filled plutonium thermoelectric generator with a power of 160-200 μW at 5.5-6.0 V with a guaranteed service life of at least ten years. The generator we used in 1969 weighed 47 g, but there is hope that it will be possible to reduce it to 20-25 g.

TABLE 1. Basic Characteristics of Radioisotope Electric Generators for Powering Implanted Electrical Cardiostimulators

Manufacturer	Information source	Isotope	Converter	Electrical power, μW	Volts*	n†, %	Wt‡, g	Comments
Nuclear Materials and Equipment Corp., USA	[2-3]	Pu^{238}	Thermoelectric	162	6	0.07	97.5*	
McDonnel Douglas Corp., USA	[4]	Pu^{238}	Thermionic	800	0.28	0.3	110	Matching transformer required
		Pm^{147}	p-n junction	212	3.35	0.84	-	
Alcatelle, France	[5]	Pu^{238}	Thermoelectric	200	0.5	0.27	200	The same
Harwell, England	[2, 5]	Pu^{238}	Thermoelectric	300	0.5	-	<140	" "

* Voltage at atomic battery terminals.
†Efficiency of atomic battery.
‡Weight of electrical cardiostimulator together with atomic battery.

Translated from Atomnaya Énergiya, No. 5, pp. 481-482, May, 1971.

On the basis of the work completed, the following conclusions may be drawn:

1. Generator efficiency, whose parameters are given above, may be extended to 1% by using specially constructed semiconducting thermoelectric materials.

2. Of the isotopes used for power purposes, specially purified metallic Pu^{238} will allow the creation of a generator with minimal radiological effects.

3. A gas-filled generator optimized for the working temperatures provides the maximum reliability of all possible variants of such devices.

LITERATURE CITED

1. T. Hursen, Intersoc. Energy Convers. Engng. Conf., Boulder, Colo., 1968, Vol. 1, IEEE, New York (1968), p. 765.
2. Isotopes and Rad. Technol., 7, No. 2 (1969-1970).
3. Nucl. Appl. and Technol., 8, No. 6 (1970).
4. W. Matheson, International Nuclear Industries Fair, Basle, Switzerland (October 6-11, 1969).
5. Newsletter, Informations Bulletin on Isotopic Generators and Batteries, ENEA of the OECD, Paris, 1, No. 1 (1970).

BRIEF COMMUNICATIONS

A conference of specialists from member nations of the Council for Mutual Economic Aid (COMECON) on isotope production was held in Moscow in December, 1970. Discussed at the conference were the results of technical–economic studies of the production of Co^{60}, long-lived decay products (Kr^{85}, Sr^{90}, Cs^{137}, Pm^{147}), C^{14} (barium carbonate), cyclotron isotopes (including generators), and isotopic neutron sources in Council member nations. Also examined were the production requirements of Council member nations for the period 1971-1975, possible volumes of production, and the technical characteristics of the products. Proposals were prepared for specializing production of these products.

An agreement on joint efforts in the field of high-energy physics between the USSR State Committee on the Utilization of Atomic Energy and the US Atomic Energy Commission was signed November 30, 1970, during a visit of a delegation of the USSR State Committee on the Utilization of Atomic Energy to the United States. The agreement provides for joint work on the accelerators of the High-Energy Physics Institute (Serpukhov, USSR) and the National Accelerator Laboratory (Batavia, USA). The agreement is an addition to the presently effective memorandum on cooperation in the field of peaceful uses of atomic energy. The term of the agreement is five years. The topics of concrete experiments will be agreed upon finally by both sides and formulated as additions to the agreement. Results of joint experiments will be published in joint reports.

Translated from Atomnaya Énergiya, No. 5, p. 482, May, 1971.

ORGANIC SEMICONDUCTORS AND BIOPOLYMERS

A Volume in MONOGRAPHS IN SEMICONDUCTOR PHYSICS

By **Leonid I. Boguslavskii** and **Anatolii V. Vannikov**
Institute of Electrochemistry
Academy of Sciences of the USSR
Moscow, USSR

In recent years chemists, physicists, and biologists have made considerable progress in the study of organic semiconductors. While Western scientists have generally worked with molecular crystals, Soviet investigators have concentrated on polymeric organic semiconductors. The present volume brings to the Western scientist, for the first time, a comprehensive survey of Soviet work and provides an excellent introduction to new activities in the field. Within this general review, the authors have placed special emphasis on the mechanism of conduction in organic semiconductors with a detailed analysis of methods which permit the direct measurement of the mobility of the carriers. Biologists and biochemists will find this approach extremely promising as an explanation of many elementary processes in biological systems. These findings will be valuable for physical chemists, biophysicists, medical and industrial researchers, as well as advanced undergraduate and graduate research students. Placing a continuation order will ensure delivery of this and other volumes of the series **immediately** upon publication.

Translated from Russian

Approx. 186 pages Plenum Press 1970 **$18.50**

SBN 306-30433-3

Reviews of earlier volumes:

"... an authoritative work which will stand as a leading reference book on the subject for many years to come."
—CURRENT ENGINEERING PRACTICE

"... a useful library source of data...." *—NATURE*

"... the information presented in this monograph will doubtlessly be of considerable value in the future...."
—SCIENCE

CONTINUATION ORDER PLAN
In order to facilitate the rapid delivery of important research information, a continuation order plan is available for volumes purchased in a series. The plan is of particular benefit to those readers who wish to remain thoroughly informed about the latest developments in their fields of research. Utilization of such a plan will ensure the delivery of each new volume in a series **immediately** upon publication and will eliminate a great deal of paper work on your part. Members of the plan are billed upon shipment of the book. This arrangement is solely for your convenience and may be cancelled by you at any time.

PLENUM PUBLISHING CORPORATION
Plenum Press • Consultants Bureau • IFI/Plenum Data Corporation
227 WEST 17th STREET, NEW YORK, N. Y. 10011

In United Kingdom: Plenum Publishing Co. Ltd., Donington House;
30 Norfolk Street, London, W.C. 2.

16
3650
1990
5640

TOPICS IN CARBOCYCLIC CHEMISTRY

Volume 1

Edited by **Douglas Lloyd**
Senior Lecturer in Chemistry
University of St. Andrews, Fife, Scotland

The appearance of a new series of review volumes often signals a new direction in research. Such is the case with *Topics in Carbocyclic Chemistry*. It is a direct response to the large amount of recent work on non-benzenoid aromatic compounds—work that is breaking down the traditional distinction between alicyclic chemistry and what has commonly been called aromatic chemistry, but is more precisely called the chemistry of benzene derivatives.

In light of these developments, *Topics in Carbocyclic Chemistry* will present review articles on benzenoid compounds, non-benzenoid aromatic compounds, and alicyclic compounds. Naturally, each article will cover recent work, but it will also provide an overall review of the most important information on each topic. In this way, the articles will serve the needs of both specialists and non-specialists and will be invaluable preparation for a detailed search of the primary literature.

Moreover—as the contents of Volume 1 indicate—each volume will contain articles dealing with practical, theoretical, mechanistic, and biochemical aspects of carbocyclic chemistry. This breadth of approach will also be apparent in the widely differing scope of the individual articles, which will range from surveys of broad sections of the subject to detailed accounts of more specific topics.

About the Editor...

Douglas Lloyd is the author of numerous papers in chemical journals and of five books, the two latest being *Carbocyclic Non-benzenoid Aromatic Compounds* (1966) and *Structure and Reactions of Simple Organic Compounds* (1966). He graduated in 1941 from the University of Bristol and then held research posts at the Universities of Sheffield and Bristol. In 1947 he moved to the University of St. Andrews, where he is now Senior Lecturer in the Department of Chemistry.

Contents of Volume 1:

380 pages Plenum Press 1970 **$26.00**
LCC No. 74-80937
SBN 306-37761-0

Available in the United States, its possessions, and Central and South America from Plenum Press exclusively.

PLENUM PUBLISHING CORPORATION
Plenum Press • Consultants Bureau • IFI/Plenum Data Corporation
227 WEST 17th STREET, NEW YORK, N. Y. 10011

In United Kingdom: Plenum Publishing Co. Ltd., Donington House, 30 Norfolk Street, London, W.C. 2.